Fall 2022

Cascadia Subduction Zone Earthquake Vertical Ground Acceleration Investigation and Potential Impact on Bridges in the Pacific Northwest

Rachel Caroline Bassil
Portland State University

Cascadia Subduction Zone Earthquake Vertical Ground Acceleration Investigation and Potential Impact on Bridges in the Pacific Northwest

by

Rachel Caroline Bassil

A research project submitted in partial fulfillment of the requirements for the degree of

Master of Science
in
Civil and Environmental Engineering

Project Advisor:
Dr. Peter Dusicka

Portland State University
2022

Abstract

The effects of vertical ground accelerations during subduction zone earthquakes currently are not sufficiently understood. There are numerous case studies and evidence that effects of vertical ground accelerations can significantly impact the performance of bridges during a seismic event, but most previous research has been focused on shallow crustal earthquakes. Current bridge design codes provide little guidance for accounting for vertical ground accelerations in seismic design, in part because additional information is needed about the characteristics of vertical ground motions during Cascadia Subduction Zone (CSZ) earthquakes in the Pacific Northwest.

For this study, recorded seismic data from recent subduction zone earthquakes was reviewed and compared to predicted CSZ ground motions. Time history data obtained from subduction zone earthquakes in Japan and Chile was used to compute response spectral accelerations for the three axes of motion. These results were then binned based on peak ground acceleration, short period spectral acceleration and 1.0-second period spectral acceleration, and geometric mean results then compared to the geometric mean of the predicted CSZ response spectra from the M9 CSZ Tool. Stations located within deep sedimentary basins were reviewed and compared separately. This study found that recorded subduction zone vertical accelerations and the predicted CSZ earthquake vertical accelerations could impart significant forces and should likely be considered in design of earthquake resistant bridges.

Differences between recorded subduction zone accelerations and predicted CSZ accelerations included magnitude of vertical acceleration, magnitude of vertical to horizontal acceleration ratio (V/H ratio) and spectral period ranges of maximum V/H ratios and decay.

Contents

List of Tables

List of Figures

1 Introduction

This paper aims to investigate subduction zone earthquake vertical ground motions and their potential impact on bridges in the Pacific Northwest. As part of this effort, time history data from recorded subduction zone earthquake events was analyzed and compared to predicted ground motions of the Cascadia Subduction Zone (CSZ) M9 Tool. Subduction zone ground motion records were used from Japan's K-NET and KIK-net Strong Motion Seismograph Networks and Chile's SIBER-Risk Strong Motion Database. Ground motion stations considered were located on soils classified as Site Class B based on V_{S30} shear wave velocity data available. Sites that were located outside of deep sediment basins were investigated and compared separately from sites inside of deep sediment basins in order to compare the effects of deep basin amplification between historical ground motions and predicted ground motions.

2 Background

Research dating back to the 1990's has provided evidence that the effects of vertical ground accelerations have been underestimated and, in some cases, under designed by previous and current bridge design codes. Vertical ground motions can significantly affect the performance of bridges by increasing axial demands at columns, and moment demands at the face of the bent cap and in the middle of the span. Numerous investigations have shown that vertical ground acceleration effects have contributed to observed failures in highway bridges.

But the effects of vertical ground accelerations during subduction zone earthquakes currently are not sufficiently understood. While numerous studies investigating the vertical ground motion effects for shallow crustal earthquakes have been completed, the same is not true for vertical ground motion effects of subduction zone events. This is likely due in part to the more frequent occurrence of shallow crustal earthquakes and the spurred research funding from resulting bridge damage. Because subduction zone earthquakes are less frequent, there are fewer resulting ground motion records and less earthquake damage reconnaissance information available. Subduction zone earthquakes have different characteristics than shallow crustal earthquakes including significantly longer duration (more cycles), stronger motion at longer periods, and larger magnitudes. Because of this, it is possible that vertical ground accelerations could impact structures differently during subduction zone seismic events and therefore merits its own investigation.

3 Bridge Design Guidance

AASHTO Guide Specifications for LRFD Seismic Bridge Design (AASHTO Seismic Guide Specifications) only provides guidance to account for vertical ground accelerations for long flexible spans, eccentric load paths bridges, and critical and essential bridges within 6 miles (near fault) of an active surface or shallow fault (Section 3.4.3.1, Section 3.4.4, Section 4.2.2, Section 4.7.2, Section C3.4).

Section 4.7.2 of the AASHTO Seismic Guide Specifications state that specific recommendations for assessing vertical acceleration effects are not provided in the

AASHTO Seismic Guide Specifications until more information is known about the characteristics of vertical ground motion in those areas affected by subduction zones in the Pacific. The AASHTO Seismic Guide Specifications advise designers to be aware that vertical acceleration effects may be important and should be assessed for essential and critical bridges. The AASHTO Seismic Guide Specifications direct designers to reference Caltrans Seismic Design Criteria (Caltrans 2006).

The Caltrans Seismic Design Criteria guides designers to account for the effects of vertical ground accelerations by applying an equivalent static vertical load to the superstructure. Multi-span girder bridges located at sites with peak horizontal ground accelerations equal to or greater than 0.6g are required to be designed so that moment demands induced by a uniformly applied vertical force equal to 25% of the dead load applied upward and downward do not exceed the nominal flexural capacity of the superstructure (Sections 3.2.1.4 & 7.2.2).

In 2008, a Caltrans study found that only considering vertical accelerations for sites with a PGA of 0.6g and greater is not an adequate basis to determine the significance of vertical effects. The study also found that the application of 25% static dead load in the upward and downward directions to account for vertical acceleration effects resulted in inadequate reinforcement for a significant number of bridges examined.

The Oregon Department of Transportation Bridge Design Manual and the Washington Department of Transportation Bridge Design Manual do not provide specific guidance on consideration of vertical ground accelerations.

Overall, the bridge design guidance consideration of vertical ground accelerations provided by AASHTO, Caltrans, WSDOT and ODOT only contain guidance for bridges located near shallow crustal faults and not subduction zones. Within this limited guidance, even the shallow crustal fault guidelines for near fault effects have been found to be deficient.

4 Recorded Seismic Data Overview

Recorded seismic data from recent subduction zone earthquakes was reviewed and compared to predicted CSZ ground motions. Time history data obtained from Japanese and Chilean events for various stations was converted into response spectral accelerations for the three axes of motion. Vertical to horizontal ratios were compared and binned based on peak ground acceleration (PGA), short period spectral acceleration (S_s) and 1.0-second period spectral acceleration (S_1). Results were then compared to predicted CSZ response spectra from the M9 CSZ Tool.

The intent of this investigation is to review real earthquake records and the CSZ M9 forecasted ground motions to determine if vertical accelerations during a M_w 9.0 CSZ earthquake will be an important component of earthquake accelerations that effect structures.

5 Events

Ground motion data was reviewed for five earthquake events. All events were interplate subduction zone earthquakes with magnitudes greater than 7.0 Mw and with recorded peak accelerations greater than 0.1g. Events were chosen that were sufficiently instrumented with ground motion station recordings located on Site Class B soils; the intent of this was to limit the impacts of acceleration amplification and de-amplification due to site soils. The 8.8 M_w Maule earthquake in Chile (2010) was not included in the reviewed events because data at Site Class B soil stations was not available. See Table 1 for list of reviewed subduction zone earthquake events.

Event Location	(Mw)	Date
Illapel, Chile	8.4	9/16/2015
Iquique, Chile	7.6	3/4/2014
Iquique, Chile	8.2	1/4/2014
Miyagi, Japan	7.1	4/7/2011
Tohoku, Japan	9.0	3/11/2011

Table 1: Subduction Zone Earthquakes Reviewed

6 Stations

Ground motion records from Japan's K-NET and KIK-net Strong Motion Seismograph Networks and Chile's SIBER-Risk Strong Motion Database were obtained for the five earthquake events shown in Table 1. Ground motion stations were selected for use that were located within 300km of the event epicenter with recorded peak accelerations greater than 0.1g. To avoid acceleration amplification due to soft soils, stations were selected for review that were located on Site Class B soils with shear wave velocity data indicating 1500m/s $\leq V_{S30} \leq$ 760m/s. Some

K-NET stations did not have V_{S30} data extending the full 30m depth. At these select stations, it was assumed that the deepest V_{S30} value available extended to a 30m depth (i.e., if the deepest V_{S30} data point available was at 20m depth, it was assumed the same value extended from 20m to 30m depth). See Table 2 for stations reviewed.

Event	Magnitude (Mw)	Station	Max UD (g)	Max V/H (g/g)
Illapel	8.4	VA03	0.14	1.81
Illapel	8.4	C10O	0.54	0.85
Illapel	8.4	CO06	0.59	0.57
Iquique	7.6	TA01	0.21	1.36
Iquique	7.6	T05A	0.41	1.00
Iquique	7.6	T06A	0.28	1.18
Iquique	7.6	PB11	0.33	0.93
Iquique	7.6	GO01	0.48	1.53
Iquique	7.6	T08A	0.54	1.25
Iquique	8.2	TA01	0.25	1.67
Iquique	8.2	T06A	0.42	1.54
Iquique	8.2	T05A	0.68	1.41
Iquique	8.2	GO01	0.37	1.20
Iquique	8.2	T08A	0.88	1.30
Iquique	8.2	PB11	1.06	1.26
Miyagi	7.1	IWTH21	0.91	1.51
Miyagi	7.1	IWTH28	0.71	1.33
Miyagi	7.1	IWTH23	2.04	2.12
Miyagi	7.1	MYGH04	1.84	2.05
Miyagi	7.1	IWTH02	2.35	2.59
Miyagi	7.1	IWT009	1.96	1.35
Miyagi	7.1	MYGH03	1.62	1.02
Miyagi	7.1	MYG012	0.91	1.00
Tohoku	9.0	FKS014	0.66	2.77
Tohoku	9.0	IWTH22	0.55	1.17
Tohoku	9.0	IWT008	0.42	0.98
Tohoku	9.0	IWTH18	0.51	1.33
Tohoku	9.0	IBRH14	2.11	4.08
Tohoku	9.0	IWTH21	1.31	2.36
Tohoku	9.0	FKSH09	0.81	1.63
Tohoku	9.0	MYGH03	0.98	0.93
Tohoku	9.0	IWTH23	1.15	1.60
Tohoku	9.0	MYGH12	1.26	1.16
Tohoku	9.0	MYGH04	1.44	2.07
Tohoku	9.0	IWT009	0.92	1.34
Tohoku	9.0	IBRH16	1.71	1.94
Tohoku	9.0	IWTH02	1.86	2.28
Tohoku	9.0	MYG002	1.43	1.43
Tohoku	9.0	IWTH27	1.08	1.06
Tohoku	9.0	IBRH15	2.32	1.94
Tohoku	9.0	TCGH13	1.00	0.83
Tohoku	9.0	MYG012	1.25	1.07

Table 2: Ground Motion Stations Reviewed. Maximum Vertical Spectral Acceleration and Maximum Vertical to Horizontal RSA Ratio per Station

7 Data Analysis: Recorded Events, Non-Basin Sites

Recorded subduction zone event time history data was converted into response spectra acceleration (RSA) curves using the software SeismoSignal. Both horizontal directions (East/West and North/South) and vertical (Up/Down) data was developed into RSA curves. Vertical to horizontal (V/H) ratio curves were then developed. To avoid skewing the curves at longer period ranges where the accelerations are low, but V/H ratios can be very large, V/H ratio curves are only shown for accelerations that are equal or greater than 0.5*PGA. This cut off point was selected to capture the portion of the response spectra that would significantly impact structure response. See Figure 1 for examples of developed RSA curves for non-basin stations. See Appendix A for all stations.

The maximum recorded vertical spectral acceleration at the reviewed non-basin stations ranged from 0.14g to 2.3g. The maximum V/H spectral acceleration ratios at the reviewed stations ranged from 0.6 to 4.1. See Table 2.

Figure 2, Figure 3 and Figure 4 (left) show the PGA, S_s, and S_1 respectively for each site investigated versus the maximum spectral V/H ratio at that site. These figures indicate that most investigated sites had max V/H ratios between 1.0-2.0. It also shows that there is not a strong correlation between increasing or decreasing V/H ratios and PGA, Ss or S1 magnitude.

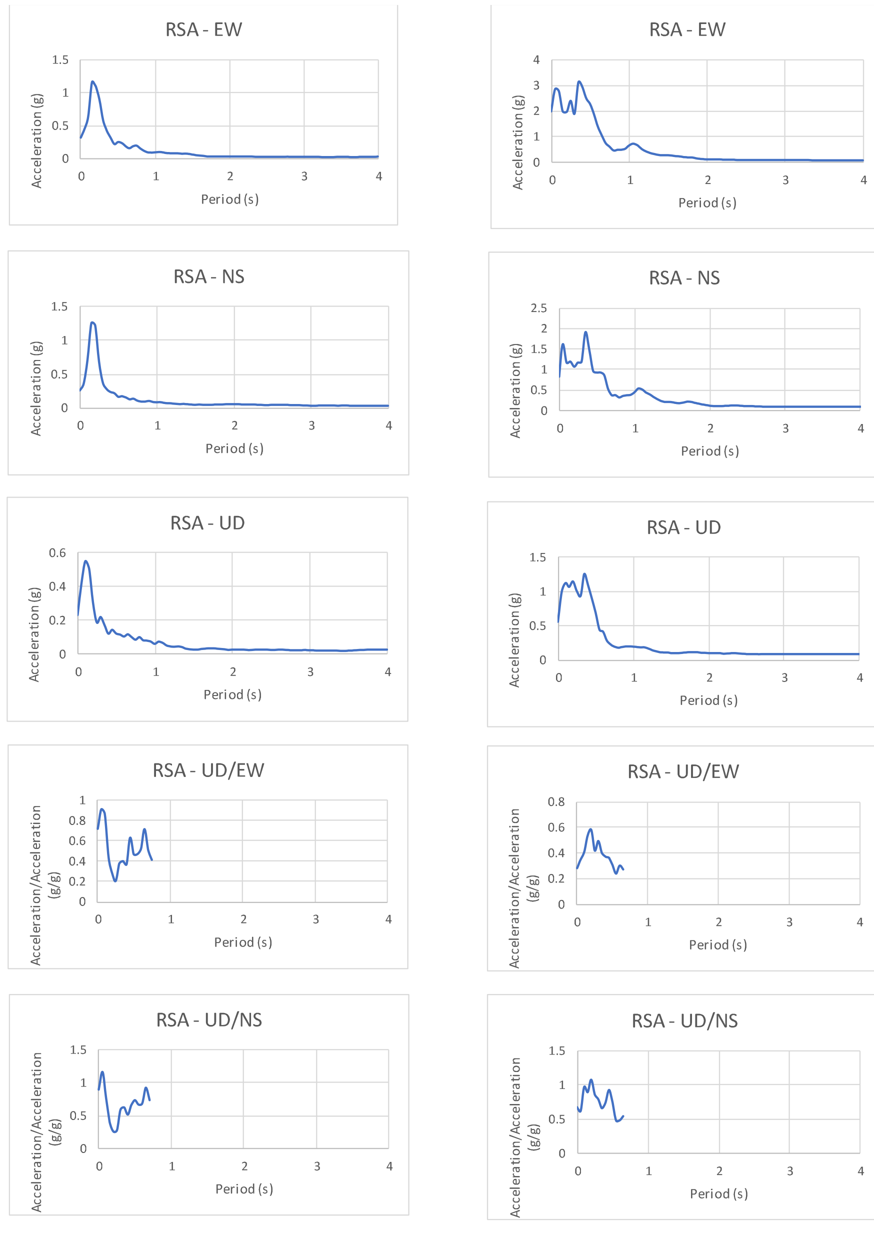

Figure 1: Examples of RSA and V/H Ratio Curves Developed. Great Tohoku Earthquake Mw 9.0.
Stations IWTH22 (left) MYG012 (right). In order from top to bottom: X-direction RSA, Y-direction RSA, Z-direction RSA, X/Z RSA ratio, Y/Z RSA ratio. See Appendix A for RSA curves for all reviewed sites.

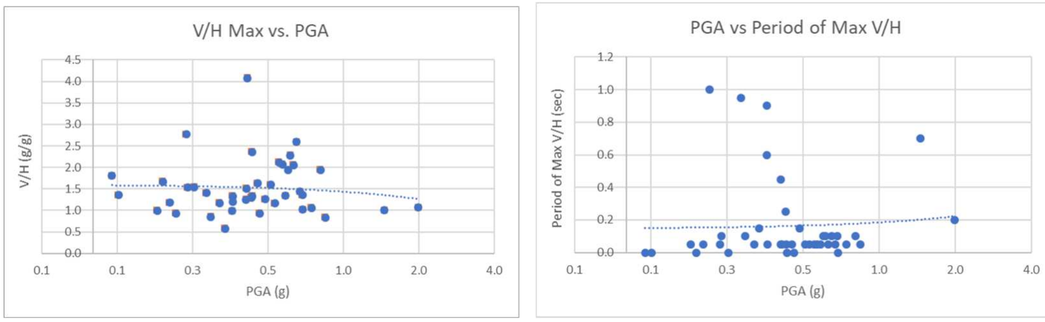

Figure 2: Japan and Chile Non-basin Sites, V/H Max vs SS (left), SS vs Period of Max V/H (right)

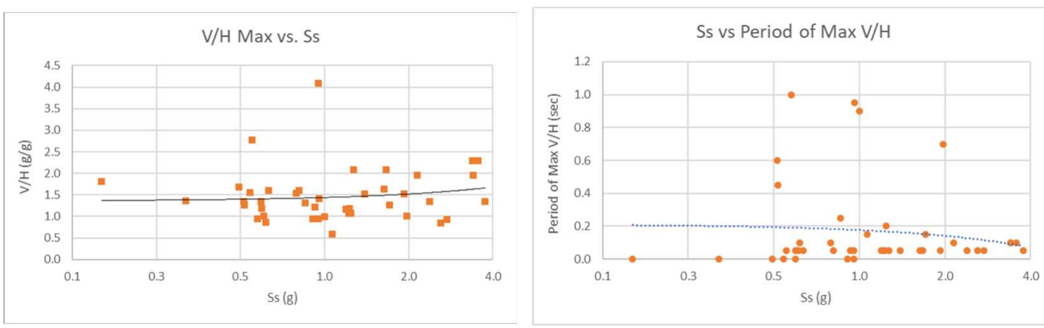

Figure 3: Japan and Chile Non-basin Sites, V/H Max vs SS (left), SS vs Period of Max V/H (right)

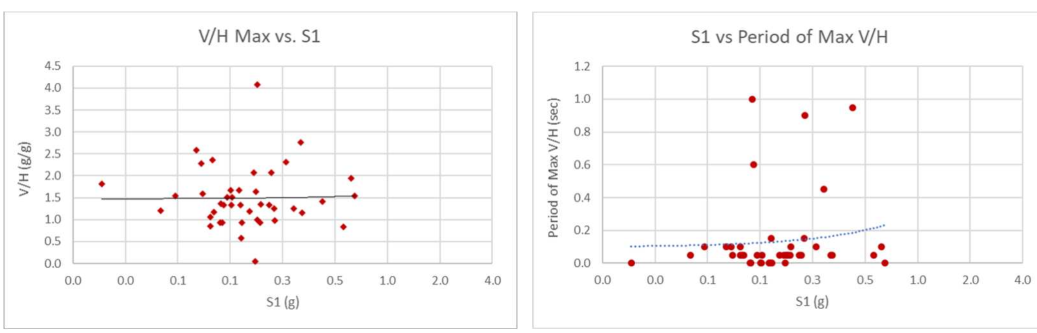

Figure 4: Japan and Chile Non-basin Sites, V/H Max vs S1 (left), S1 vs Period of Max V/H (right)

Figure 2, Figure 3 and Figure 4 (right) show the PGA, S_s, and S_1 respectively for each site investigated versus the spectral period that the maximum spectral V/H ratio occurred. These figures indicate that most sites' max V/H ratio occurred at periods below 0.2 seconds. It also indicated that there is not a strong correlation between the magnitude of PGA, S_S or S_1 and the period where the max V/H ratio occurs.

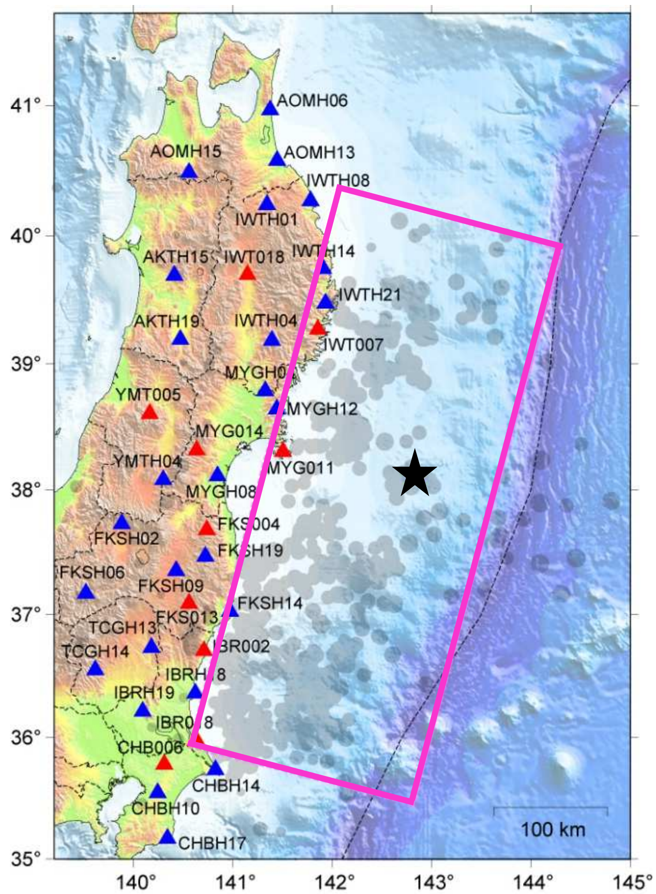

Figure 5: Tohoku Earthquake Rupture Area

Station sites were initially binned based on epicentral distance, but early analysis of the Tohoku data indicated that epicentral distance was not a relevant binning parameter. This is likely due to the earthquake's large rupture area, shown in Figure 5, approximately 200km wide by 500km long. Megathrust earthquakes occur due to slip across large areas of subducting plates. A site could be located 200km away north or south from the epicenter of the Tohoku earthquake and still be located within the rupture area, but if a site was located 200km away east or west of the epicenter it would be well outside of the rupture area. Rupture process information was not readily available for all of the other earthquake events investigated, so for consistency, rupture distance was abandoned as a binning parameter. Rupture distance may be correlated to V/H ratios and should be investigated in the future.

All sites were then binned based on peak ground acceleration (PGA), short period spectral acceleration (S_s) and 1.0-second period spectral acceleration (S_1), see Figure 6. The geometric mean of the V/H ratio for each data bin was graphed verses period. The results are shown in Figure 9 for the investigated Japan and Chile recorded data at non-basin sites

Group	PGA min	PGA max
1	0.0	0.25
2	0.25	0.50
3	0.50	0.75
4	0.75	1.00
5	1.00	2.00

Group	Ss min	Ss max
1	0.0	0.75
2	0.75	1.50
3	1.50	2.25
4	2.25	3.00

Group	S1 min	S1 max
1	0	0.1
2	0.1	0.2
3	0.2	0.3
4	0.3	0.5
5	0.5	0.7

Figure 6: Data bins used for PGA (left), Ss(middle) and S1 right.

Results in Figure 7 indicate that for non-basin sites recorded V/H ratios were greatest at short periods less than 0.2 seconds. V/H ratios were greater than 1.0 at sites where the PGA was between 0.5-0.75g between 0-0.2s periods. V/H ratios were also greater than 1.0 at sites where PGA was between 1.0-2.0g and between 0.6-0.8g. In general for sites with PGAs below 1.0g, V/H ratios decreased as period increased.

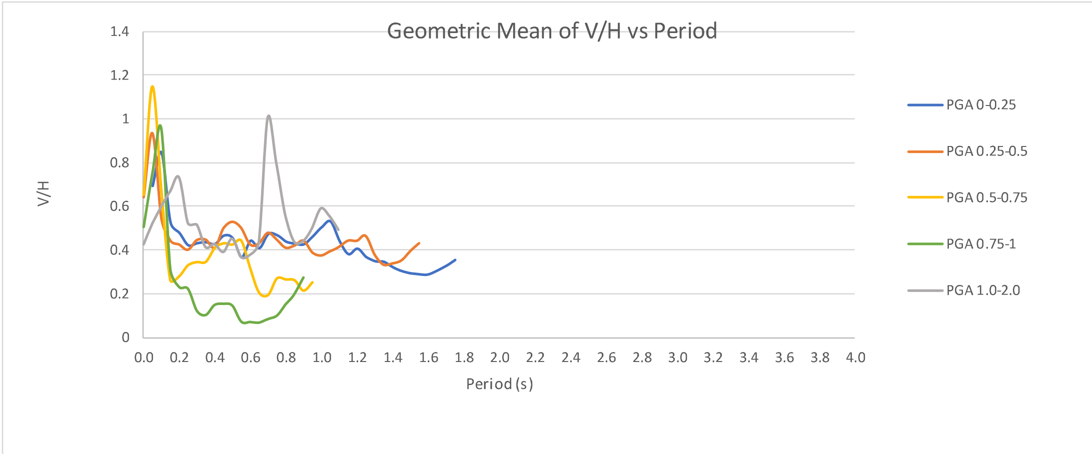

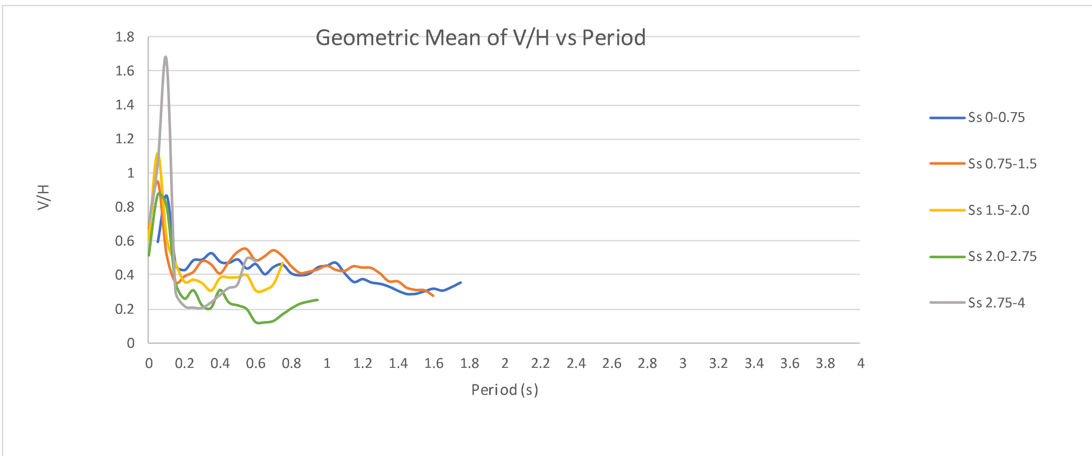

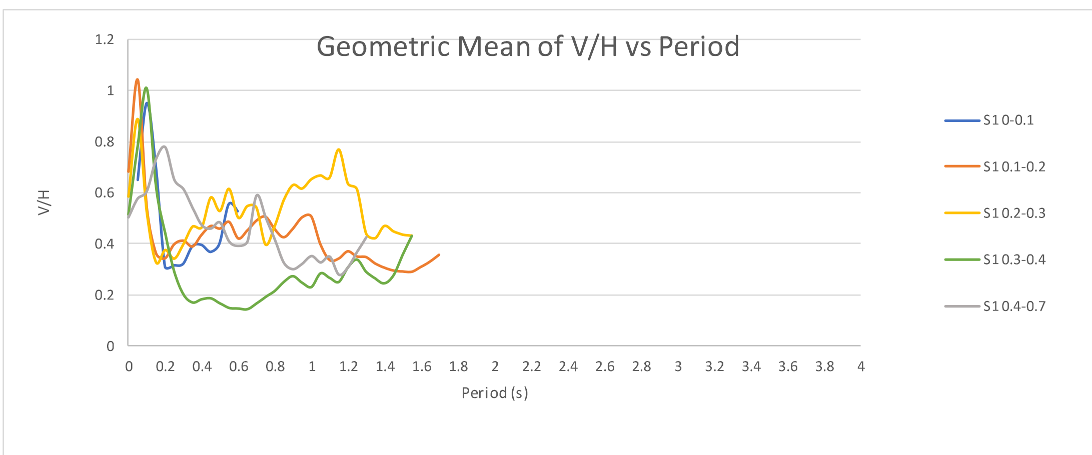

Figure 7: Geometric Mean of V/H vs. Period for Recorded Time History Data of Japan and Chile Subduction Zone Earthquakes, Non-basin Sites.
Binned by: PGA (top), S_s (middle), S_1 (bottom).

Figure 7 also indicates that V/H ratios were greatest at sites with S_s between 1.5-2.0g and 2.75-4.0g; V/H ratios were greater than 1.0 for both of these bins between 0-0.2s periods. Overall V/H ratios decreased as period increased.

Results binned by S_1 showed no clear trends other than V/H ratios being greatest between 0-0.2s periods and decreasing as period increases, similar to results binned by PGA and S_1.

The geometric mean of V/H ratios are graphed for periods ranging from 0.0-1.8 seconds. This is because accelerations beyond 1.8 second periods decayed to a value of less than 0.5*PGA, and were therefore not included, as they would have less significant effects on structures.

8 Data Analysis: CSZ M9 Tool, Non-Basin Sites

The M9 CSZ Tool is being developed to provide data in a visualization format for a full rupture 9.0 Mw earthquakes along the Cascadia Subduction Zone. The tool currently includes 30 different CSZ full rupture scenarios and provides 5% critically damped spectral accelerations for locations across the Pacific Northwest. All of the predicted CSZ ground motion data used for this study was the geometric mean response of the 30 different rupture scenarios. Three general Pacific Northwest (PNW) locations were reviewed in the M9 Tool for comparison with the event data presented in Section 7 above from Japan and Chile. The sites selected in the Seattle, Portland and Medford regions were located onshore and outside of deep sediment basins, See Figure 8.

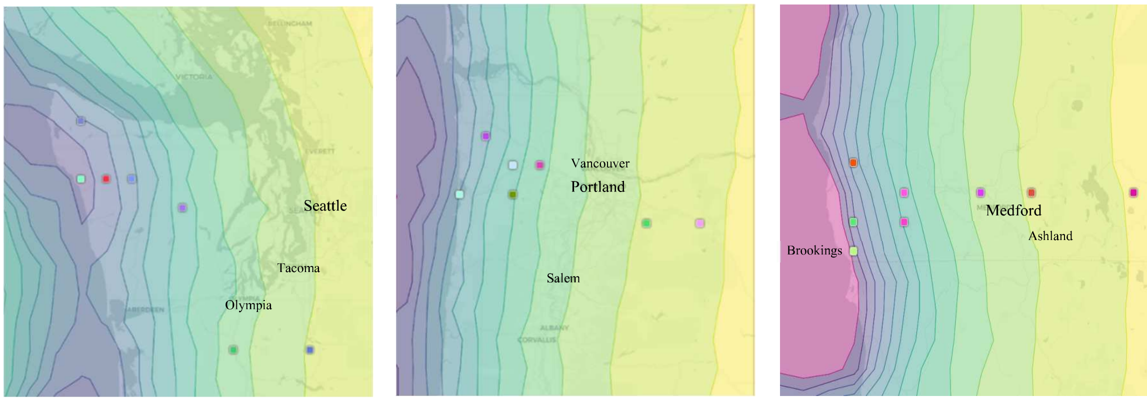

Figure 8: M9 CSZ Tool Non-Basin Sites Reviewed, Seattle (left), Portland (middle), Medford (right)

All M9 Tool acceleration data is for Site Class B soil conditions. The maximum predicted vertical spectral acceleration at the reviewed CSZ non-basin stations ranged from 0.20g to 1.76g. The maximum V/H spectral acceleration ratios at the reviewed non-basin CSZ stations ranged from 0.46 to 2.2. See Figure 9 for examples of RSA curves developed and Appendix B for all data.

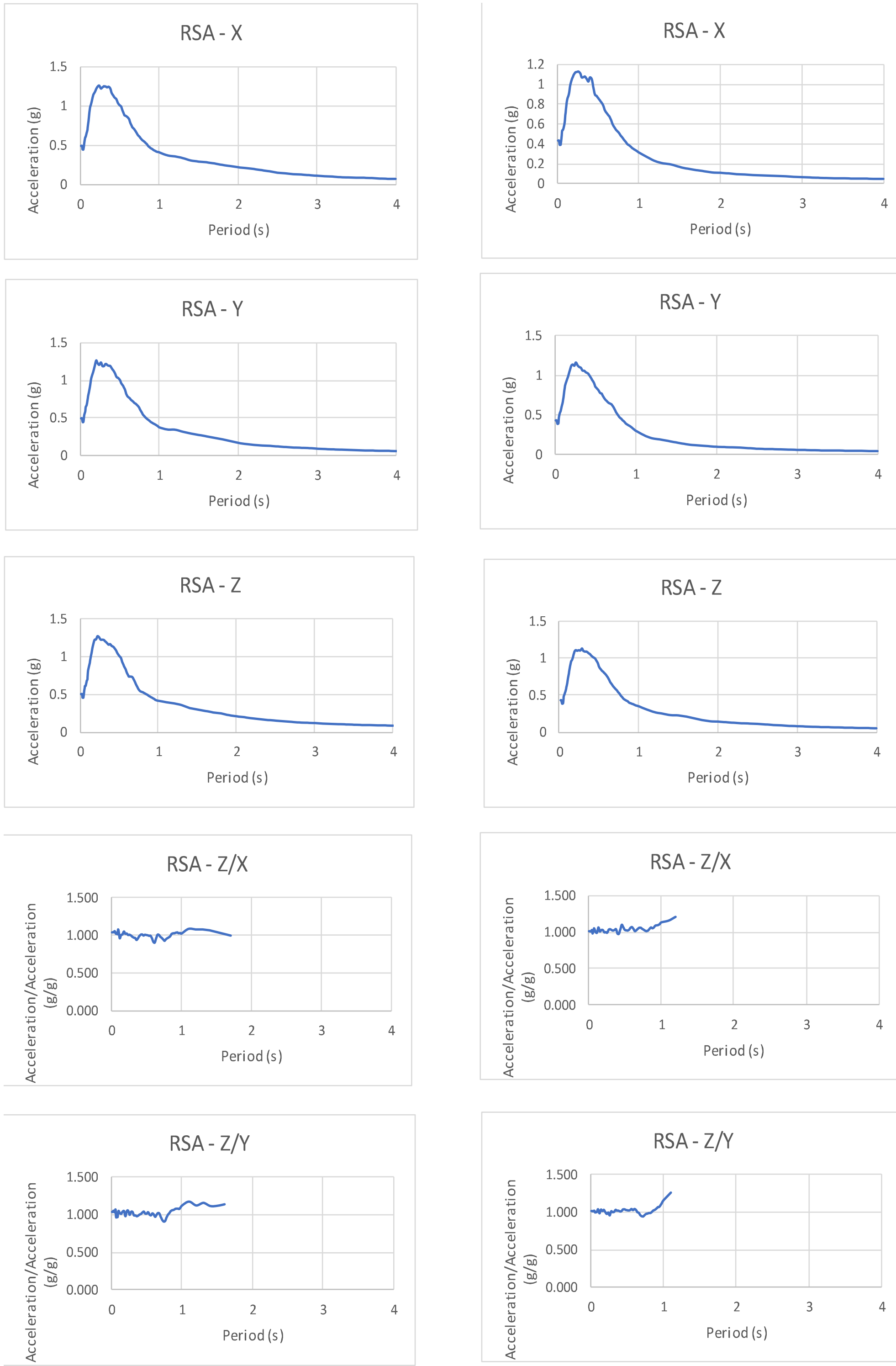

Figure 9: Examples of RSA and V/H Ratio Curves Developed. M9 CSZ Tool. Stations Puget Sound Region (Seattle 8)(left) and Northern Oregon (Portland 8) (right). In order from top to bottom: X-direction RSA, Y-direction RSA, Z-direction RSA, X/Z RSA ratio, Y/Z RSA ratio. See Appendix B for RSA curves for all reviewed sites.

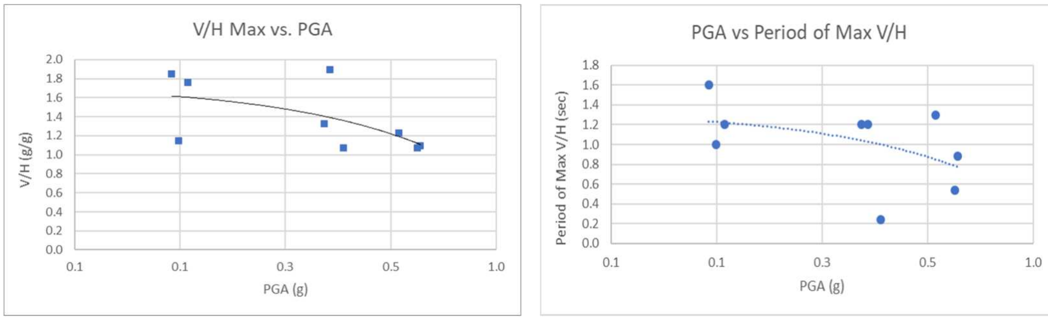

Figure 10: CSZ M9 Tool Non-basin sites, V/H Max vs PGA (left), PGA vs Period of Max V/H (right)

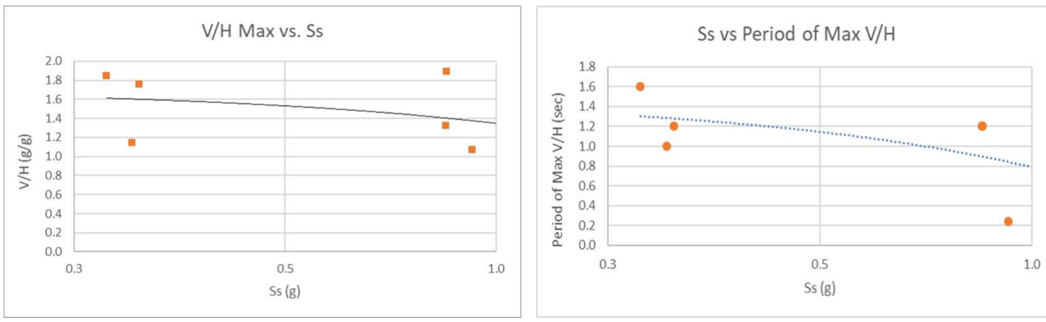

Figure 11: CSZ M9 Tool Non-basin Sites, V/H Max vs S_S (left), S_S vs Period of Max V/H (right)

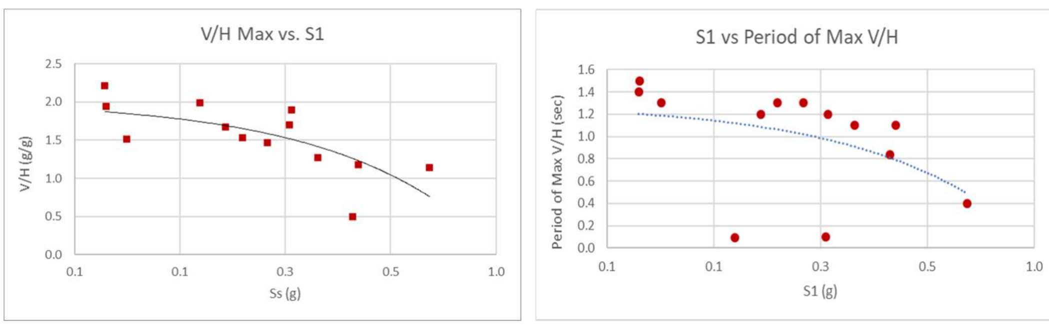

Figure 12: CSZ M9 Tool Non-basin Sites, V/H Max vs S_1 (left), S_1 vs Period of Max V/H (right)

Figure 10, Figure 11 and Figure 12 (left) show the PGA, S_s, and S_1 respectively for each M9 CSZ non-basin site investigated versus the maximum spectral V/H ratio at that site. This figure indicates that most investigated M9 CSZ sites had max V/H ratios between 1.0-2.0. It also shows that there is a slight correlation between increasing PGA and S_s and decreasing V/H ratio. There is not a strong correlation between S_s values and V/H ratios.

Figure 10, Figure 11 and Figure 12 (right) show the PGA, S_s, and S_1 respectively for each M9 CSZ site investigated versus the spectral period that the maximum spectral V/H ratio occurred. This figure indicates that most sites' max V/H ratio occurred at periods greater than 0.8 seconds. It also indicated that there is not a strong correlation between the magnitude of PGA, S_S or S_1 and the period where the max V/H ratio occurs.

RSA data was reviewed and binned for non-basin CSZ sites similarly to the steps outlined in Section 7.

Results in Figure 13 indicate that for non-basin CSZ sites V/H ratios were consistently near 1.0 for periods up to 1.0 seconds for all PGA bins. V/H ratios increased after 1.0 second periods. V/H ratios were greatest for smaller PGAs of 0.1-0.25g.

V/H ratios were consistently near 1.0 for periods up to 1.0 seconds for all S_s bins. Sites with S_s values between 0.1-1.5g V/H ratios increased for periods greater than 1.0 seconds, while site with S_s values greater than 1.5g V/H ratios decreased.

V/H ratios were consistently between 0.75 – 1.25 for all S_1 bins at periods between 0-0.8s. As periods increased greater than 1.0 seconds, V/H ratios increased for all sites with S_1 less than 0.5g and decreased for sites with S_1 greater than 0.5g.

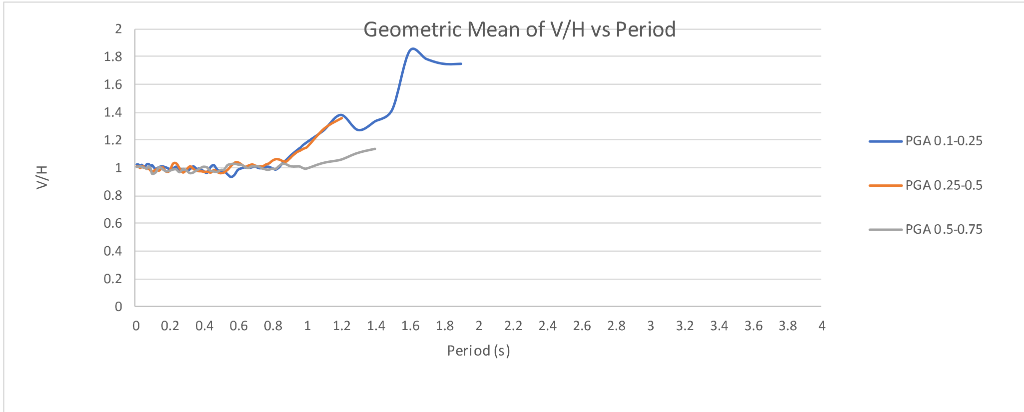

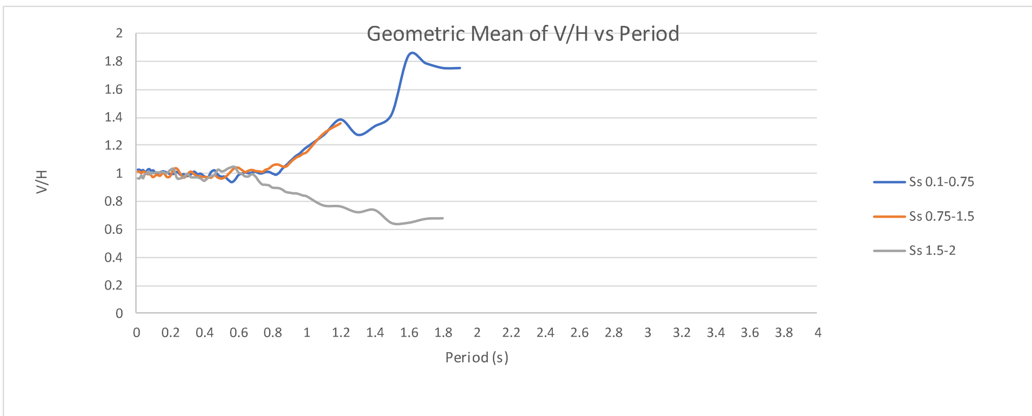

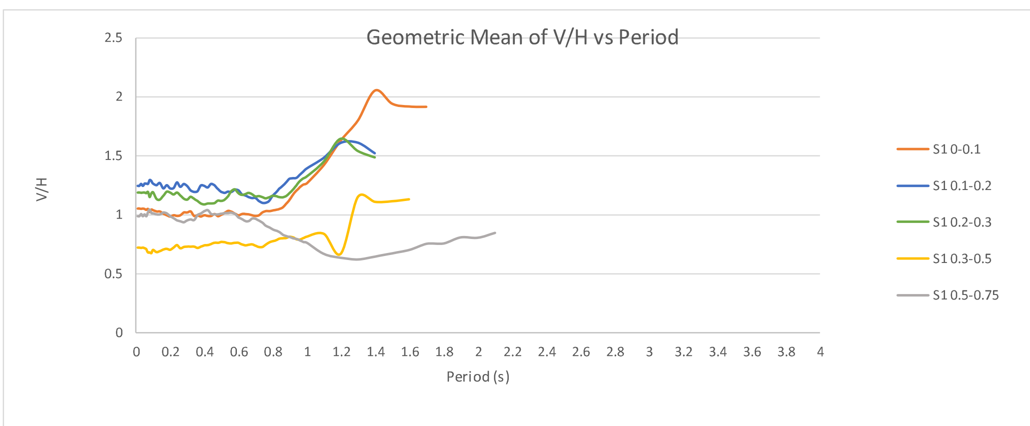

Figure 13: Geometric Mean of V/H vs. Period for CSZ M9 Tool Data, Non-basin Sites. Binned by: PGA (top), S_s (middle), S_1 (bottom).

Geometric mean of V/H ratios are graphed for periods ranging from 0.0-2.2 seconds. This is because accelerations beyond approximately 2.2 second periods decayed to a value of less than 0.5*PGA, and were therefore not included, as they would have less significant effects on structures. This range is similar to the range of significant accelerations for the Japan and Chile stations investigated.

9 Non-Basin Discussion, Japan & Chile Time History Data vs. CSZ M9 Tool Data

Predicted CSZ V/H ratios are on average larger than V/H ratios from the Japan and Chile events. Recorded event data from the reviewed Japan and Chile subduction zone earthquakes indicates that V/H ratios peak at short periods between 0-0.2s and then taper to a V/H ratio of approximately 0.6 and remain consistent as period increases. The predicted CSZ M9 Tool data trends vary from the recorded Japan and Chile subduction earthquake data as the M9 Tool data predicts that the V/H ratios will remain consistently near 1.0 for periods between 0-1.0 seconds and then increase for sites with lower PGA and S_s, while decreasing for sites with higher PGA and S_s. This suggests that the predicted V/H ground motion behavior in a CSZ earthquake has inverse trends when compared to the recorded Japan and Chile even data.

While recorded data sees vertical acceleration ratios decaying at longer periods, the predicted CSZ data anticipates that vertical acceleration ratios will not decay as rapidly, but instead increase at longer periods. The M9 CSZ V/H ratios for periods between 0.0-1.0 seconds are almost consistently 1.0, this is the portion of the RSA curve that contains the bulk of the higher magnitude accelerations, only when the curve starts to decay after 1.0 seconds, do the V/H ratios sharply increase.

The M9 CSZ synthetic seismograms were created using stochastic synthetic seismograms for periods less than 1.0 seconds and an assumed V/H ratio of 1.0. For periods greater than 1.0 seconds, deterministic synthetic seismograms were used from 3D physics based simulations. These assumptions explain why the CSZ predicted V/H ratios are consistently near 1.0 for periods less than 1.0 seconds. The initial 3D model that was used to develop the predicted M9 CSZ synthetic seismograms was limited by the grid size that could be used in the model given the computational resources that were available. This limited the period range that deterministic results could be determined for. A refined 3D model using smaller grid sizing is currently being developed and will allow for deterministic results for periods between 0.0 seconds and 1.0 second. This study recommends re-evaluating and comparing trends between the recorded data and predicted data when refined predicted data becomes available. If the current approach of using stochastic results for periods below 1.0 and using a set V/H ratio, further consideration could be given to the assumed V/H ratio value; this study has shown that the M9 CSZ assumed V/H ratio may be conservative in comparison to V/H ratios observed during other subduction zone earthquakes, but the maximum magnitudes of the vertical accelerations for the M9 CSZ are comparable to the maximum magnitudes of reviewed vertical accelerations from recorded subduction events.

Similarly to the recorded data, the M9 CSZ data also contains sites that are predicted to experience vertical spectral accelerations greater than 1.0g. These large vertical response accelerations could have a significant impact on structures during and event. The predicted M9 CSZ responses reviewed and discussed in this study are the geometric mean of the 30 possible rupture scenarios, so there could be singular rupture scenarios and sites that have larger or smaller maximum responses than what is reported here.

10 Deep Sediment Basins

Basin amplification is a phenomenon in which deep sedimentary basins increase earthquake ground motions. These deep sedimentary basins consist of soils that do not reach a layer of very hard rock for many kilometers depth. Within the Puget Sound Region and the Portland Metro Area there are deep sedimentary basins that could amplify ground shaking during a CSZ event and increase damage to structures. For this study the Portland Metro and Puget Sound Basins were characterized by the depth until soils reached a V_{S30} equal to 2500m/s ($Z_{2.5}$). CSZ V/H ratios in the Portland and Puget Sound Basins were investigated and compared to V/H ratios in the Kanto and Nagata Basins in Japan during the Great Tohoku Earthquake.

Sites in the Kanto and Nigata basins were selected for analysis if they were onshore, with soil V_{S30} greater than 180m/s, and at locations that showed no evidence of liquefaction. Site selection criteria was set to reduce the effects of soft soil amplifications but also to provide a sufficient number of review sites for each basin. Basin depth at selected sites range between 2-5km.

Kanto Basin : Z2.5 = 2.5-5km					Niigata Basin: Z2.5 = 2.5-5km			
Station	V_{S30}	Max UD (g)	Max V/H (g/)		Station	V_{S30}	Max UD (g)	Max V/H (g/)
CHB012	300	0.39	0.89		NIG010	200	0.05	0.75
CHB015	200	0.23	0.97		NIG013	200	0.04	0.72
CHB017	300	0.14	1.08		NIG016	200	0.03	1.63
CHB026	400	0.15	0.92		NIG024	500	0.04	1.62
CHB013	300	0.11	0.81		NIG025	200	0.04	1.04
CHBH10	300	0.29	1		NIG026	300	0.03	1.39
TKY007	300	0.24	0.84		NIG028	400	0.06	1.17

Table 3: Japan Basin Sites Reviewed

For the Portland and Puget Sound Basins, PGA, S_S and S_1 values were not varied enough to bin data based on these values. Instead, each basin is binned together. Puget Sound sites were selected to have similar $Z_{2.5}$ values as the Kanto and Nigata Basins. Portland Basin has a maximum $Z_{2.5}$ value of approximately 2.2km; Portland sites were chosen that had $Z_{2.5}$ values near or greater than 2km.

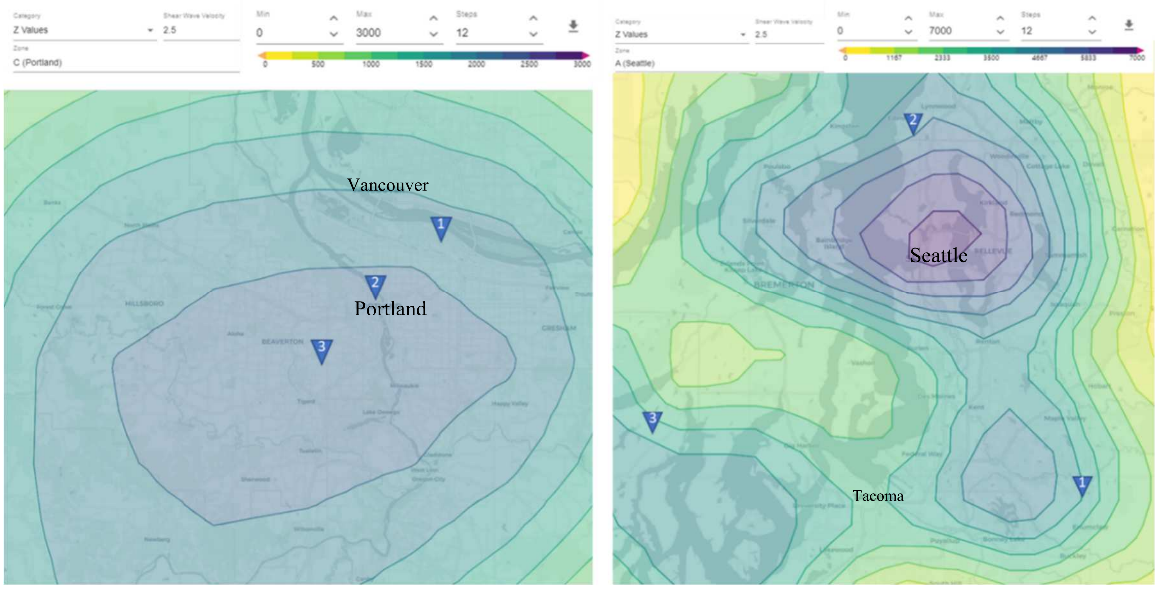

Figure 14: Deep Sedimentary Basin Sites: Portland (left), Seattle (right)

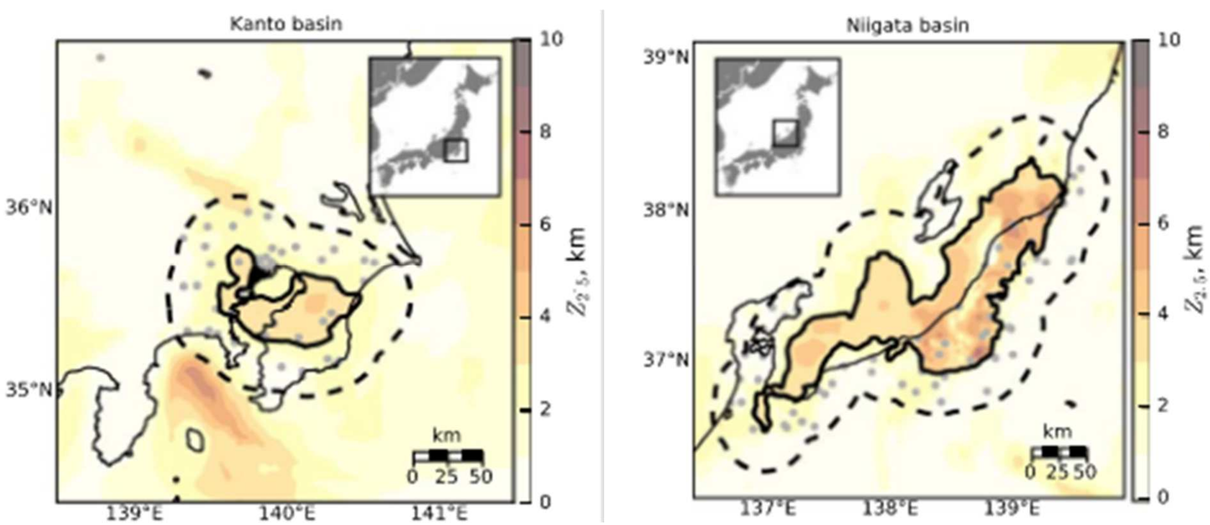

Figure 15: Deep sedimentary Basins in Japan: Kanto (left), Nigata (right)

RSA data for basin sites was reviewed and binned similarly to the steps outlined for non-basin sites in Section 7 and Section 8.

11 Data Analysis: Japan, Kanto and Nigata Basin Sites

The maximum recorded vertical spectral acceleration at the reviewed basin stations ranged from 0.03g to 0.39g. The maximum V/H spectral acceleration ratios at the reviewed basin stations ranged from 0.69 to 1.6.

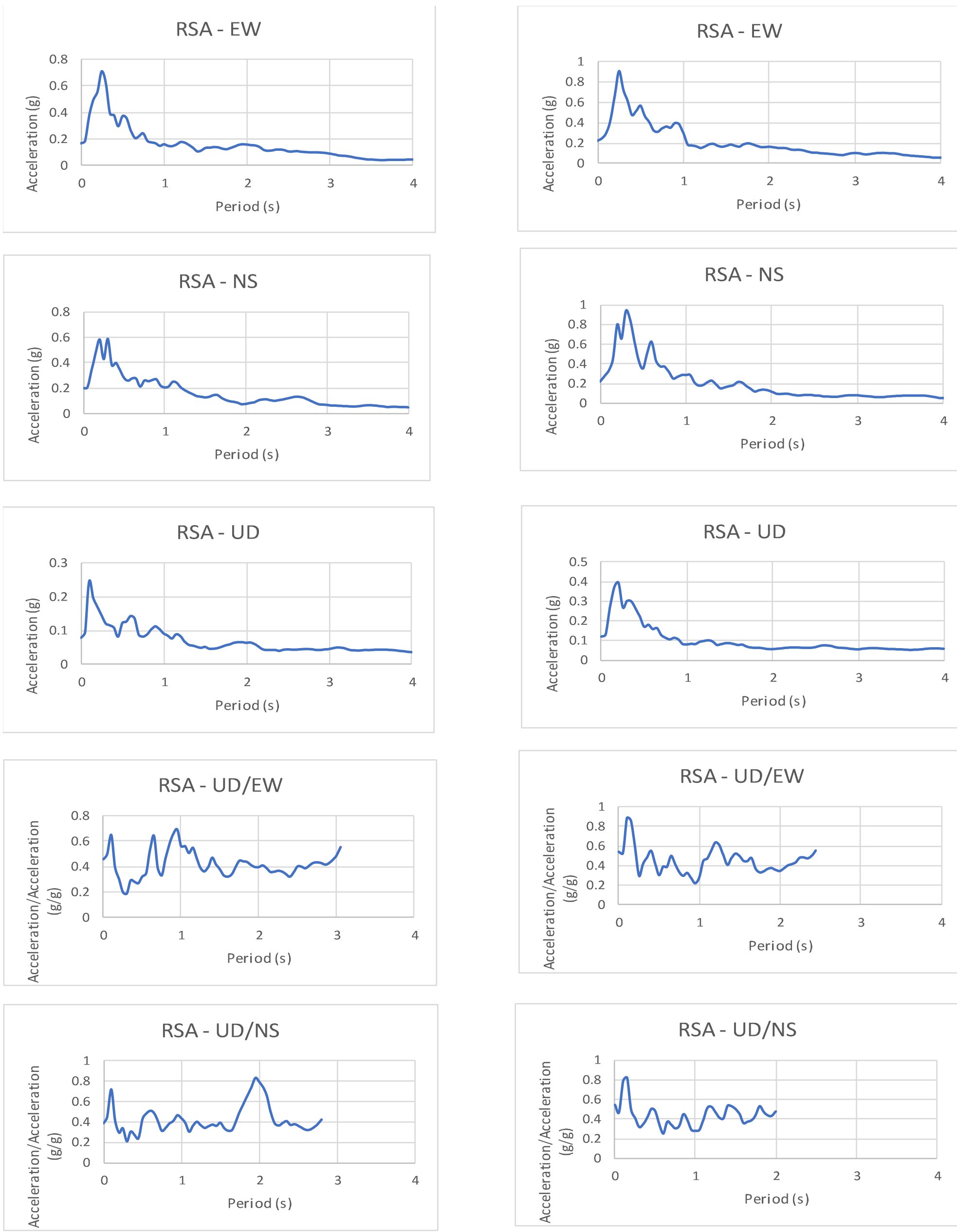

Figure 16: Examples of RSA and V/H Ratio Curves Developed. Kanto & Nigata Basins

Stations:TKY007 (left) and CBH012 (right). In order from top to bottom: X-direction RSA, Y-direction RSA, Z-direction RSA, X/Z RSA ratio, Y/Z RSA ratio. See Appendix C for RSA curves for all reviewed sites.

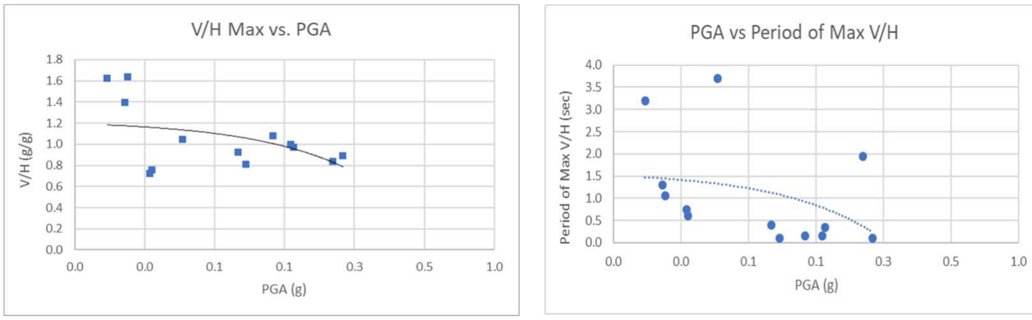

Figure 17: Kanto and Nigata basin sites, V/H Max vs PGA (left), PGA vs Period of Max V/H (right)

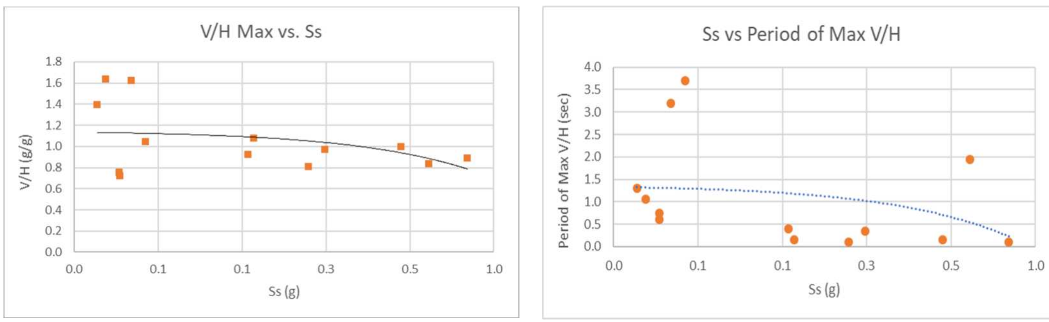

Figure 18: Kanto and Nigata Basin Sites, V/H Max vs SS (left), SS vs Period of Max V/H (right)

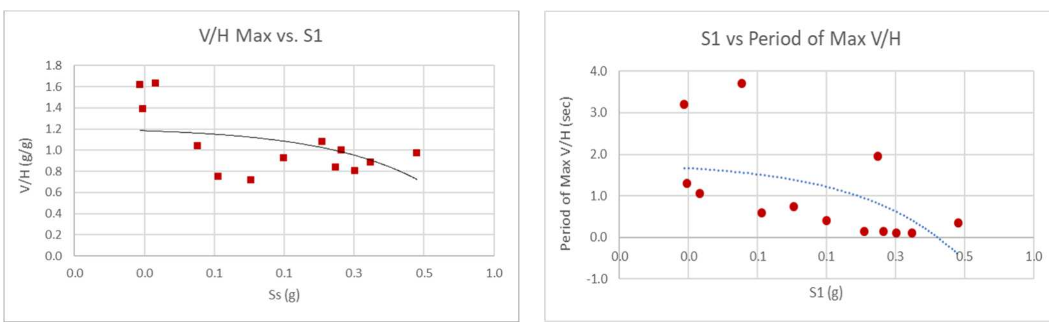

Figure 19: Kanto and Nigata basin sites, V/H Max vs S1 (left), S1 vs Period of Max V/H (right)

Figure 17, Figure 18 and Figure 19 (left) show the PGA, S_s, and S_1 respectively for each basin site investigated versus the maximum spectral V/H ratio at that site. This figure indicates that all investigated basin sites had max V/H ratios greater than 0.6. It also shows that there is a slight correlation between increasing PGA, S_s and S_1 and decreasing V/H ratio.

Figure 17, Figure 18 and Figure 19 (right) show the PGA, S_s, and S_1 respectively for each basin site investigated versus the spectral period that the maximum spectral V/H ratio occurred. This figure indicates that the max V/H ratios occurred at periods of 0-4.0 seconds across sites, with many sites experiencing a maximum V/H ratio at periods below 1.0. This figure also indicated that there is not a strong correlation between the magnitude of PGA, S_S or S_1 and the period where the max V/H ratio occurs.

Results in Figure 20 indicate that for the Kanto and Nigata Basin sites V/H ratios for PGA less than 0.1g were between 0.45-0.65 for all periods. For PGA between 0.1g-0.2g V/H ratios peaked at 0.77 at short periods less than 0.2s and long period greater than 3.6s. For other periods V/H ratios were between 0.3-0.6.

V/H ratios were consistently between 0.5-0.7 for S_s values below 0.1g. Sites with S_s values between 0.1-1.1g V/H ratios peaked at 0.75 at period 0.2s and were between 0.35 and 0.55 for other periods.

V/H ratios were consistently between 0.5 – 0.65 for sites with S_1 less than 0.1g. For sites with values of S_1 between 0.1-1.0g, V/H ratios peaked at 0.2s periods and then were consistently between 0.35-0.5.

On average V/H ratios were larger for lower PGA, S_s and S_1 bins.

Kanto and Nigato Basin V/H ratios were on average smaller for short periods and larger for longer periods than the non-basin Japan and Chile data in Figure 7.

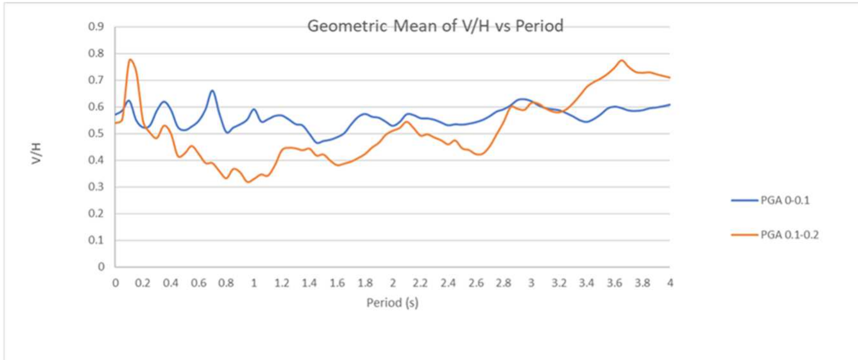

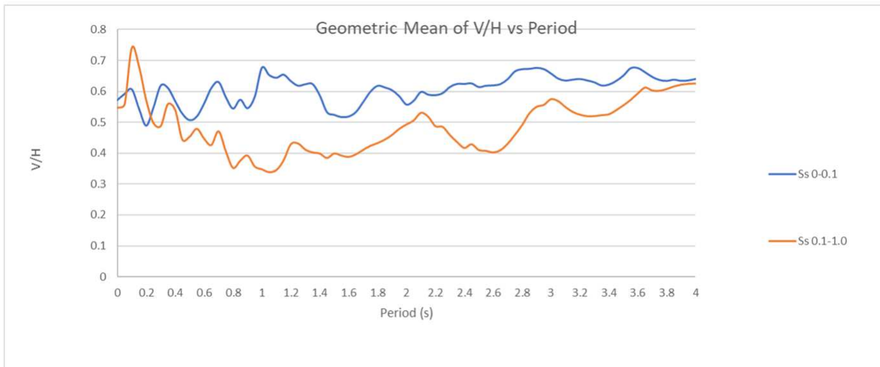

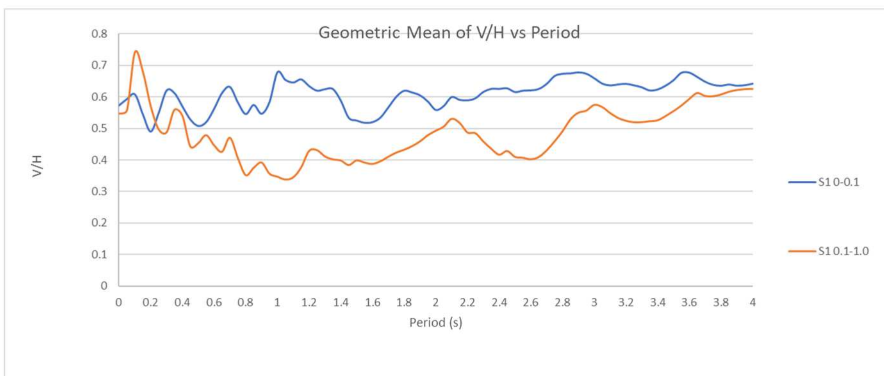

Figure 20: Geometric Mean of V/H vs. Period for Recorded Time History Data of The Great Tohoku Earthquake in the Kanto and Nigata Basins.
Binned by: PGA (top), Ss (middle), S1 (bottom).

The Geometric mean of V/H vs Period plots for the basin sites are graphed into longer periods than the non-basin sites. This means that at the Kanto and Nigata basin sites, the accelerations remained at or above 0.5*PGA for longer periods. This indicates that basin site accelerations did not decay as quickly at longer periods like they did at non-basin sites.

12 Data Analysis: CSZ M9 Tool, Basin Sites

The maximum predicted vertical spectral acceleration at the reviewed CSZ basin stations ranged from 0.34g to 0.60g. See Example CSZ Tool Spectra in Figure 21.

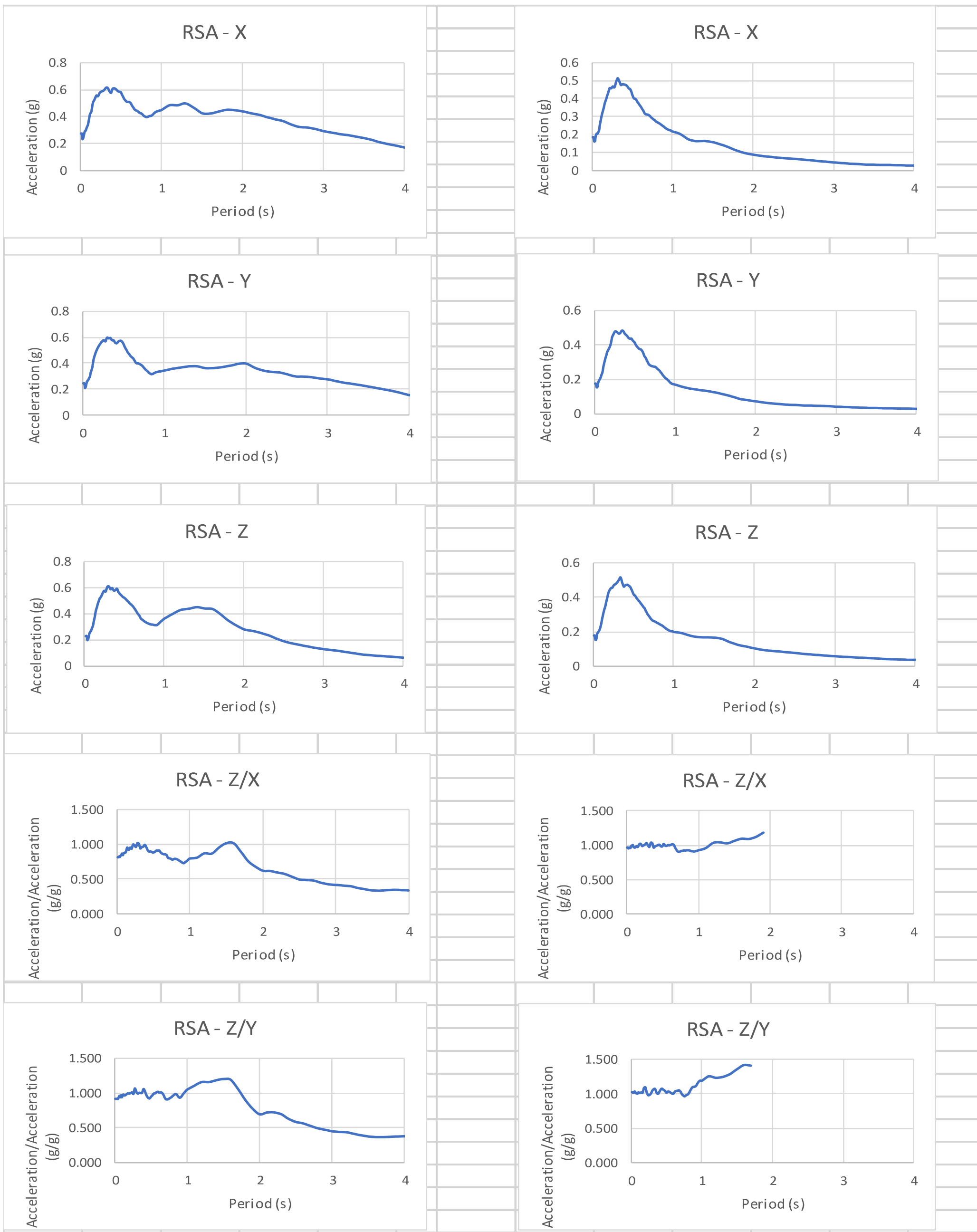

Figure 21: Examples of RSA and V/H Ratio Curves Developed. M9 CSZ Tool Basin Sites Stations Puget Sound Region (Seattle 3)(left) and Northern Oregon (Portland 1) (right). In order from top to bottom: X-direction RSA, Y-direction RSA, Z-direction RSA, X/Z RSA ratio, Y/Z RSA ratio. See Appendix D for RSA curves for all reviewed sites.

For the M9 CSZ predicted ground motions at basin sites, again the results reviewed and reported here were for the geometric mean of the 30 different M9 CSZ rupture scenarios.

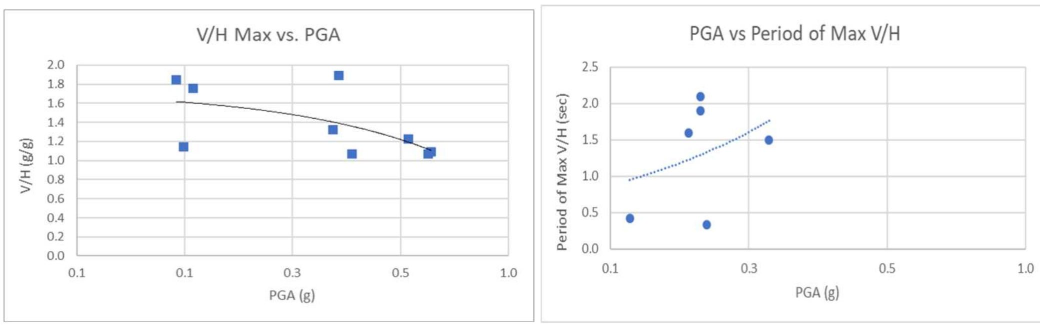

Figure 22: Portland and Puget Sound Basin Sites, V/H Max vs PGA (left), PGA vs Period of Max V/H (right)

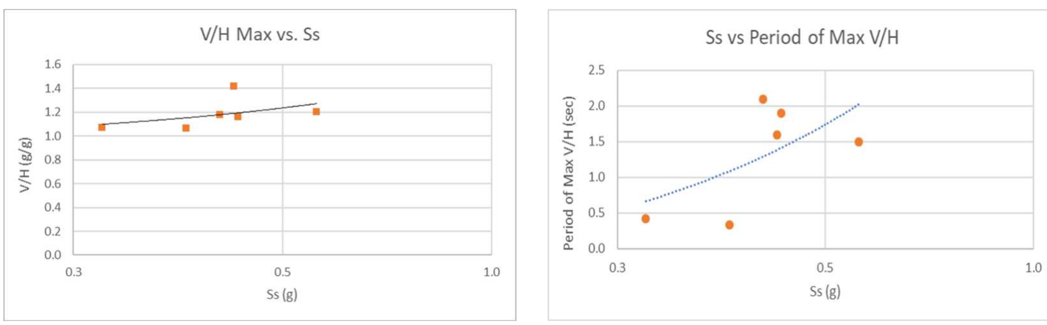

Figure 23: Portland and Puget Sound Basin Sites, V/H Max vs S_S (left), PGA vs Period of Max V/H (right)

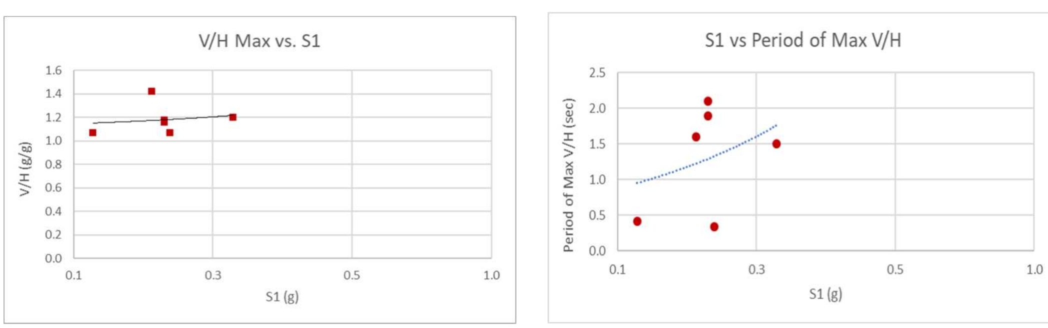

Figure 24: Portland and Puget Sound Basin Sites, V/H Max vs S_1 (left), PGA vs Period of Max V/H (right)

Figure 22, Figure 23 and Figure 24 (left) show the PGA, S_s, and S_1 respectively for each M9 CSZ basin site investigated versus the maximum spectral V/H ratio at that site. This figure indicates that all investigated M9 CSZ basin sites had max V/H ratios greater than 1.0.

Figure 22, Figure 23 and Figure 24 (right) show the PGA, S_s, and S_1 respectively for each basin site investigated versus the spectral period that the maximum spectral V/H ratio occurred. This figure indicates that the max V/H ratios occurred at periods of 0-1.6 seconds across sites. This figure also indicated that there is not a strong correlation between the magnitude of PGA, S_S or S_1 and the period where the max V/H ratio occurs.

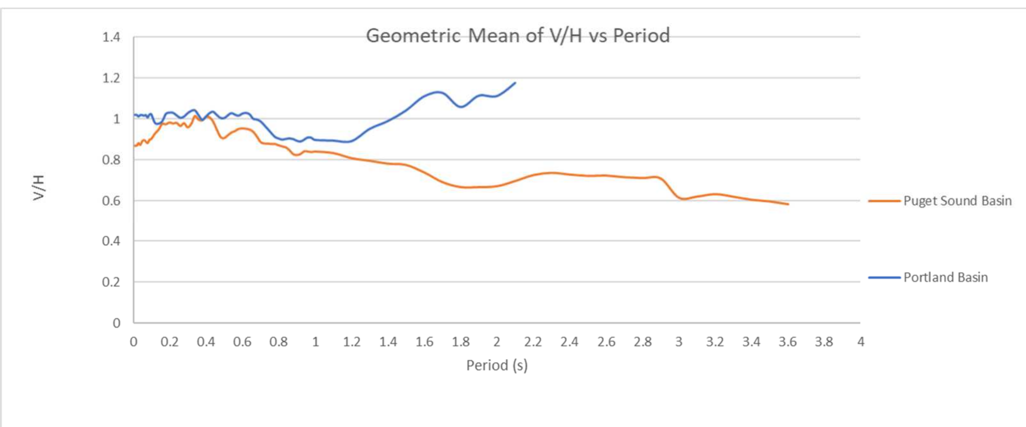

Figure 25: Geometric Mean of V/H vs. Period for CSZ M9 Tool Data, Basin Sites

Results in Figure 25 show that overall Portland V/H ratios are higher than Puget Sound Basin V/H ratios. Between periods 0-1.0 seconds both Puget Sound and Portland basin V/H ratios are near 1.0. At periods greater than 1.0 seconds Portland Basin V/H ratios increase, while Puget Sound Basin V/H ratios decrease.

CSZ Basin site V/H ratios are similar to non-basin CSZ V/H ratios for periods between 0-1.0 seconds. CSZ Basin site V/H ratios are smaller than non-basin site V/H ratios for periods greater than 1.0 seconds.

The Geometric mean of V/H vs Period plots for the M9 CSZ basin sites are graphed for periods ranging from 0-2.0 seconds for the Portland Basin and 0-3.6 seconds for the Puget Sound Basin. These ranges are slightly shorter than the Nigata and Kanto basin sites, but still much longer than the non-basin site ranges. This indicates that M9 CSZ basin site accelerations decayed slightly faster than the Nigata and Kanto basins, but still did not decay as quickly at longer periods as the non-basin sites did.

13 Basin Discussion: Japan Basin Time History Data vs. CSZ M9 Tool Basin Data

On average the CSZ M9 Tool predicts that the Portland and Puget Sound Basins will have higher V/H ratios than the recorded Kanto and Nigata Basin V/H ratios. Portland Basin V/H ratios are larger than the Kanto and Nigata Basin V/H ratios at all periods. Puget Sound Basin V/H ratios are on average larger than the Kanto and Nigata Basin V/H ratios for periods between 0-3.2 seconds. These findings suggest that basin amplification effects during a CSZ earthquake could have more significant impact on vertical ground accelerations and therefore a more significant impact on structures in the Pacific Northwest Basins than what was observed during the Great Tohoku Earthquake. CSZ Basin sites are predicted to experience V/H ratios 30-60% higher for periods between 0-1.0 seconds than recorded basin site data. The maximum predicted magnitude of vertical accelerations at reviewed CSZ sites was approximately 50% larger than the maximum magnitude of vertical accelerations recorded in the Kanto and Nigata basins. This maximum magnitude of predicted vertical spectral accelerations was approximately 0.6g, which is still below 1.0g acceleration.

The predicted CSZ basin data also anticipates a decay in vertical spectral accelerations, but at some sites reviewed, not as quickly. At some CSZ basin sites it is predicted that vertical spectral accelerations will begin to decay as periods increase, but then increase again between periods of 1.0-2.0 seconds. This trend is not seen at the recorded data basin sites where vertical accelerations steadily decay at longer periods.

The geometric mean of V/H ratios show similar trends between both recorded data basin sites and the predicted data sites; V/H ratios remain mostly a consistent value between period ranges of 0.0-1.4 seconds. At periods greater than 1.4 seconds, the predicted CSZ basin sites in the Puget Sound Region decrease, while those in Portland increase. These longer periods will likely not impact most structures significantly though.

The M9 CSZ synthetic seismograms were created using stochastic synthetic seismograms for periods less than 1.0 seconds and an assumed V/H ratio of 1.0. For periods greater than 1.0 seconds, deterministic synthetic seismograms were used from 3D physics based simulations. These assumptions explain why the CSZ predicted V/H ratios are consistently near 1.0 for periods less than 1.0 seconds. The initial 3D model that was used to develop the predicted M9 CSZ seismograms was limited by the grid size that could be used given the computational resources that were available, which limited the period range that deterministic results could be determined for. A refined 3D model using a smaller grid size is currently being developed and will allow for deterministic results for periods between 0.0 seconds and 1.0 second. This study recommends re-evaluating and comparing trends between the recorded data and predicted data when refined predicted CSZ data becomes available. If the current approach of using stochastic results for periods below 1.0 and using a set V/H ratios remains, further consideration could be given to the assumed V/H ratio value; this study has shown that the CSZ assumed V/H ratio may be conservative in magnitude at basin sites in comparison to V/H ratios observed at basin sites during other subduction zone earthquakes, but the CSZ basin sites' vertical accelerations decay faster than recorded basin sites.

14 Conclusions

Review of subduction zone ground motion records has highlighted differences in response spectra trends between recorded data from Japan and Chile and the M9 CSZ predicted ground motions.

Magnitudes of maximum vertical acceleration response across the individual sites were comparable between the M9 CSZ non-basin sites and the recorded data non-basin sites. Recorded data from non-basin sites mostly had maximum vertical acceleration peaks at short periods and then rapid decay of vertical acceleration as periods increased. Conversely, the M9 CSZ non-basin sites are predicted to have higher vertical accelerations for a longer range of periods and then decay less quickly.

All of the predicted M9 CSZ acceleration responses that were reviewed and discussed for this study were the geometric mean of the 30 different predicted M9 CSZ rupture scenarios. This means that there is likely singular rupture scenarios and sites that could have larger or smaller responses than what has been discussed in this study.

Maximum magnitudes of predicted and recorded vertical acceleration response for non-basin sites exceeds 1.0g and could have significant impact on structural response during an M9 CSZ earthquake. Based on this prediction vertical acceleration effects of a Cascadia Subduction Zone earthquake should likely be accounted for in design of earthquake resistant structures in the Pacific Northwest.

The V/H ratios for the M9 CSZ are predicted to be about 30-60% higher than the Nigata and Kanto basin data reviewed. Basin sites in the PNW are predicted to experience maximum vertical spectral accelerations up to 50% greater than the Nigata and Kanto basin site data reviewed. The maximum magnitude of vertical spectral acceleration predicted in the PNW was approximately 2.1g at M9 CSZ sites reviewed. This is a significant response, indicating that vertical acceleration effects should likely be considered for design of earthquake resistant structures in the Pacific Northwest.

The M9 CSZ synthetic seismograms were created using stochastic synthetic seismograms for periods less than 1.0 seconds and an assumed V/H ratio of 1.0.

For periods greater than 1.0 seconds, deterministic synthetic seismograms were used from 3D physics based simulations. These assumptions explain why the CSZ predicted V/H ratios are consistently near 1.0 for periods less than 1.0 seconds. This study has shown that the CSZ assumed V/H ratio may be conservative in comparison to V/H ratios observed during other subduction zone earthquakes, but at non-basin sites the maximum magnitudes of the vertical accelerations for the M9 CSZ are comparable to the maximum magnitudes of reviewed vertical accelerations from recorded subduction events. This study also found that CSZ basin sites' vertical accelerations decay more quickly than reviewed recorded data at Japanese basin sites. If the current approach of using stochastically determined M9 CSZ ground motions for periods less than 1.0 seconds remains, this study would suggest considering a different set V/H ratio equal to 1.0 for periods less than 0.2 seconds and a V/H ratio equal to 0.6 for periods greater than 0.2 seconds.

15 Suggestions for Future Study

Suggested further study for this topic includes re-assessing trends of the M9 CSZ predicted ground motions when the refined 3D geophysics model is available and re-comparing trends with the recorded ground motions trends from Japan and Chile. Additional suggestions include: further investigating subduction zone earthquake vertical accelerations' relation to site variables including rupture distance and site soil classifications and review of case studies of bridges subjected to significant subduction zone vertical seismic accelerations with consideration of the impact of combined vertical and horizontal ground motions.

16 References

AASHTO. (2015). Guide specifications for LRFD seismic bridge design, Washington, DC.

Button, M. R., Cronin, C. J., & Mayes, R. L. (2002). Effect of vertical motions on seismic response of highway bridges. Journal of structural engineering, 128(12), 1551-1564.

Bozorgnia, Y., & Campbell, K. W. (2004). The vertical-to-horizontal response spectral ratio and tentative procedures for developing simplified V/H and vertical design spectra. Journal of Earthquake Engineering, 8(02), 175-207.

Bozorgnia, Y., & Stewart, J. P. (2019, April). PEER 2020/02 - Data Resources for NGA- Subduction Project Electronic Supplement. Retrieved August 1, 2020, from ttps://apps.peer.berkeley.edu/publications/peer_reports/reports_2020/NGA-Sub_flatfile_PSA5perc_2019-Apr.xlsx

Castro, S., Benavente, R., Crempien, J., Candia, G., de la Llera, J.C. (2021). A Consistently Processed Strong Motion Database for Chilean Earthquakes. Submitted.

Dusicka, P. (in progress: 2022), Portland State University, M9 CSZ Online Tool, https://m9csz.cee.pdx.edu/

Elgamal, A., & He, L. (2004). Vertical earthquake ground motion records: an overview. Journal of Earthquake Engineering, 8(05), 663-697.

Frankel, A., & Grant, A. (2021). Site Response, Basin Amplification, and Earthquake Stress Drops in the Portland, Oregon Area. Bulletin of the Seismological Society of America, 111(2), 671-685.

Frankel, A., Wirth, E., Marafi, N., Vidale, J., & Stephenson, W. (2018). Broadband Synthetic Seismograms for Magnitude 9 Earthquakes on the Cascadia Megathrust Based on 3D Simulations and Stochastic Synthetics, Part 1: Methodology and Overall Results. Bulletin of the Seismological Society of America, 108(5A), 2347-2369.

Kim, S. J., Holub, C. J., & Elnashai, A. S. (2011). Analytical assessment of the effect of vertical earthquake motion on RC bridge piers. Journal of Structural Engineering, 137(2), 252-260.

Kim, S. J., Holub, C. J., & Elnashai, A. S. (2011). Experimental investigation of the behavior of RC bridge piers subjected to horizontal and vertical earthquake motion. Engineering Structures, 33(7), 2221-2235.

Kunnath S.K., Erduran E, Chai YH, Yashinsky M. Effect of near–fault vertical ground motions on seismic response of highway overcrossings. J Bridge Eng, ASCE 2008;13(3):282–90.

Kunnath, S. K., Abrahamson, N., Chai, Y.H. (2008). Development of guidelines for incorporation of vertical ground motion effects in seismic design of highway bridges. California Department of Transportation, Sacramento, California.

Marafi, N. A., Eberhard, M. O., Berman, J. W., Wirth, E. A., & Frankel, A. D. (2017). Effects of deep basins on structural collapse during large subduction earthquakes. Earthquake Spectra, 33(3), 963-997.

Midorikawa, S., Miura, H., & Si, H. (2012). Preliminary analysis for characteristics of strong ground motion from gigantic earthquakes. In Proceedings of the 15th World Conference on Earthquake Engineering. Tokyo, Japan: International Association for Earthquake Engineering.

National Research Institute for Earth Science and Disaster Resilience (2019), NIED K-NET, KiK-net, National Research Institute for Earth Science and Disaster Resilience, doi:10.17598/NIED.0004

Oregon Department of Transportation. (2020). Bridge Design Manual, Salem, Oregon.

Papazoglou, A. J., & Elnashai, A. S. (1996). Analytical and field evidence of the damaging effect of vertical earthquake ground motion. Earthquake Engineering & Structural Dynamics, 25(10), 1109-1137.

SeismoSignal (2021). Strong Motion Data Signal Processor [Computer software]. https://seismosoft.com/

State of California Department of Transportation, Caltrans Seismic Design Criteria Version 2.0, April 2019

Washington Department of Transportation. (2019). Bridge Design Manual (LRFD), Olympia, Washington.

APPENDIX A:

NON-BASIN RECORDED RSA DATA
JAPAN & CHILE

EQ	Station
Illapel 8.4	2051

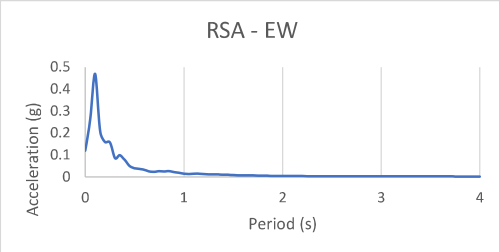

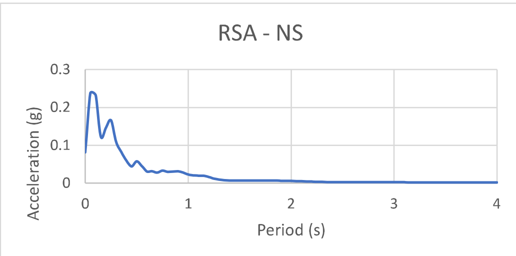

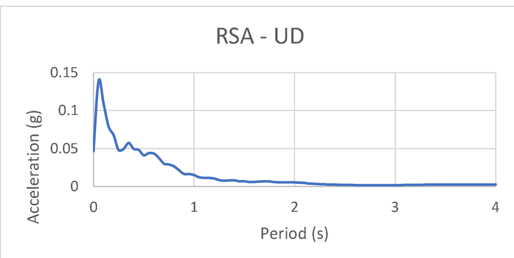

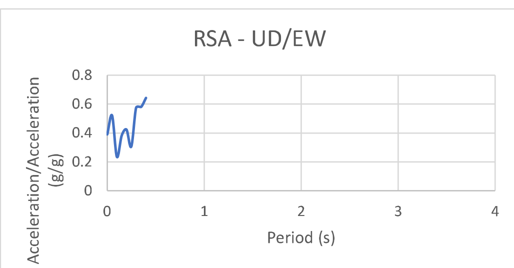

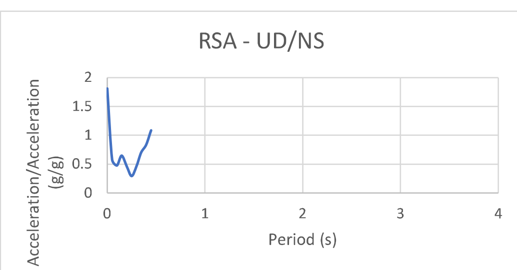

Max UD (g)	0.139
Per Max UD (s)	0.05

Max UD/EW (g)	0.643
Per Max UD/EW (s)	0.40

Max UD/NS (g)	1.807
Per Max UD/NS (s)	0.00

RSA - EW		RSA - NS		MAX(EW, NS)	
PGA =	0.119	PGA =	0.082	PGA =	0.119
Ss =	0.159	Ss =	0.147	Ss =	0.159
S1 =	0.015	S1 =	0.023	S1 =	0.023

EQ	Station
Iquique 7.6	480

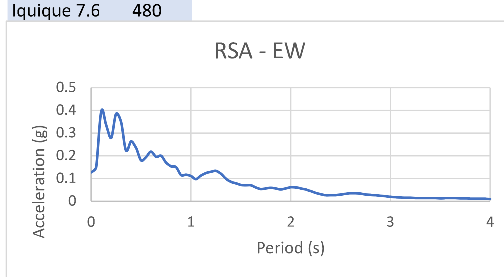

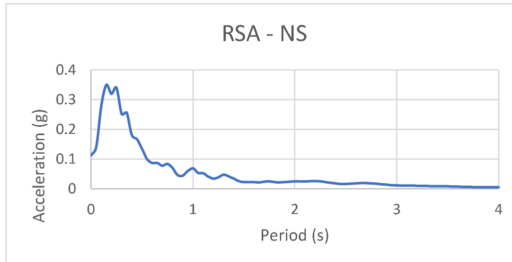

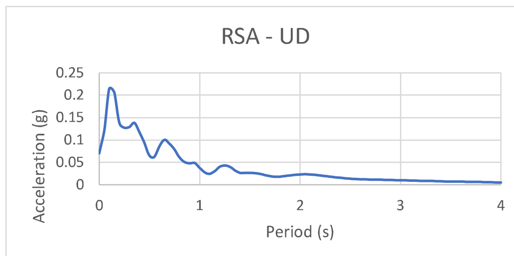

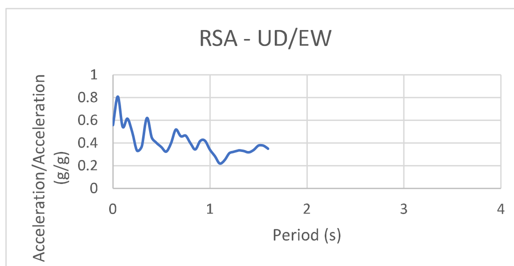

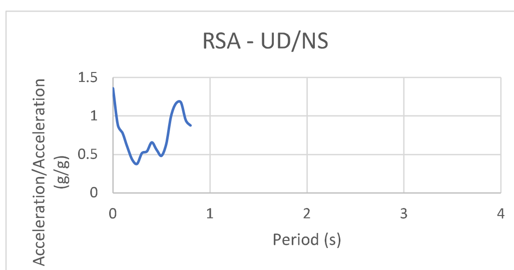

Max UD (g)	0.214
Per Max UD (s)	0.10

Max UD/EW (g)	0.808
Per Max UD/EW (s)	0.05

Max UD/NS (g)	1.358
Per Max UD/NS (s)	0.00

RSA - EW		RSA - NS		MAX(EW, NS)	
PGA =	0.126	PGA =	0.112	PGA =	0.126
Ss =	0.279	Ss =	0.320	Ss =	0.320
S1 =	0.111	S1 =	0.069	S1 =	0.111

EQ	Station
Iquique 7.6	494

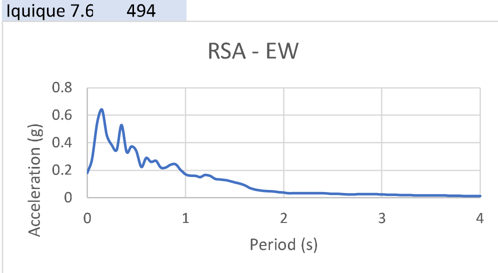

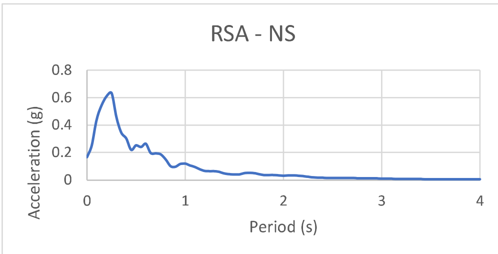

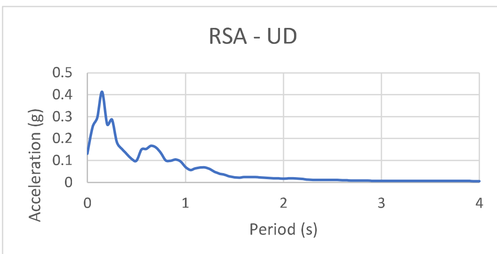

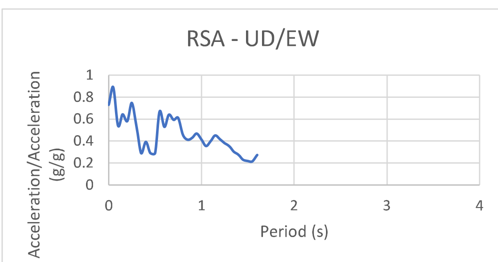

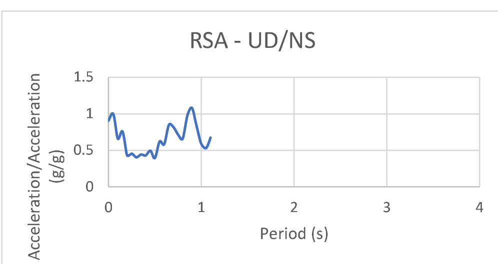

Max UD (g)	0.413
Per Max UD (s)	0.15
Max UD/EW (g)	0.890
Per Max UD/EW (s)	0.05
Max UD/NS (g)	0.996
Per Max UD/NS (s)	0.05

RSA - EW		RSA - NS		MAX(EW, NS)	
PGA =	0.180	PGA =	0.167	PGA =	0.180
Ss =	0.455	Ss =	0.609	Ss =	0.609
S1 =	0.171	S1 =	0.120	S1 =	0.171

EQ	Station
Iquique 8.2	337

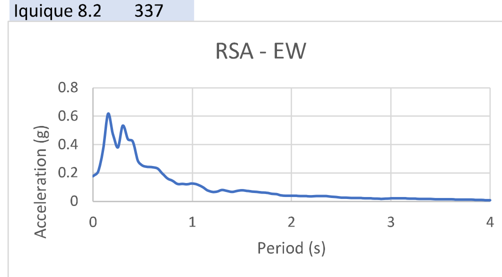

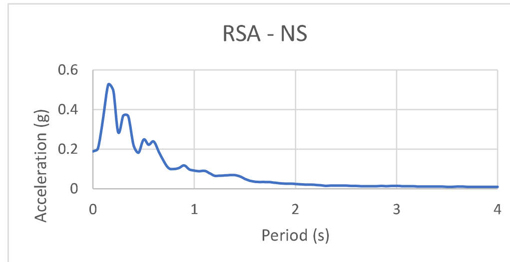

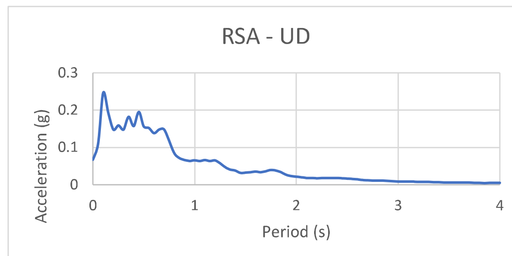

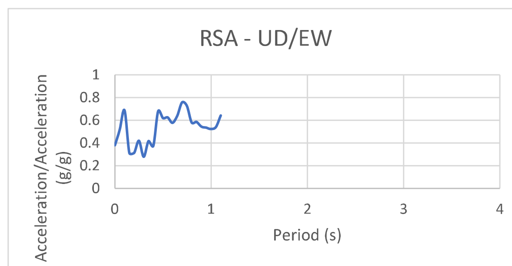

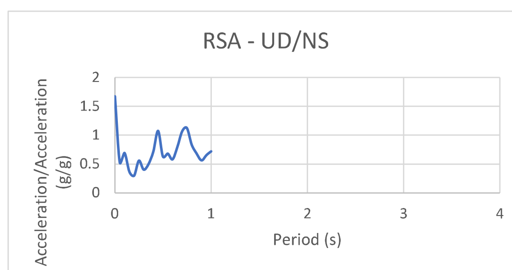

Max UD (g)	0.246
Per Max UD (s)	0.10
Max UD/EW (g)	0.758
Per Max UD/EW (s)	0.70
Max UD/NS (g)	1.673
Per Max UD/NS (s)	0.00

RSA - EW		RSA - NS		MAX(EW, NS)	
PGA =	0.177	PGA =	0.189	PGA =	0.189
Ss =	0.475	Ss =	0.495	Ss =	0.495
S1 =	0.126	S1 =	0.092	S1 =	0.126

EQ	Station
Iquique 7.6	481

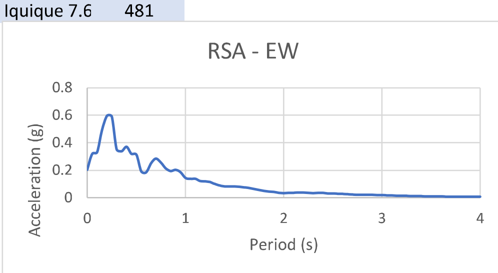

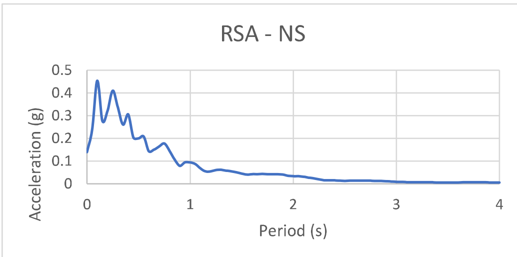

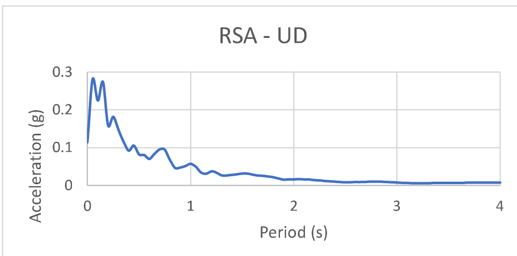

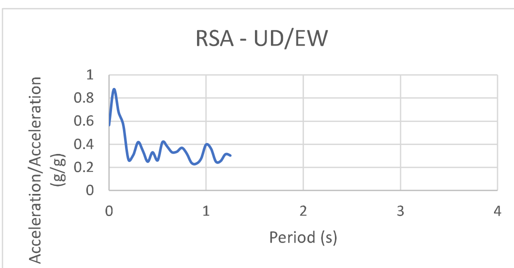

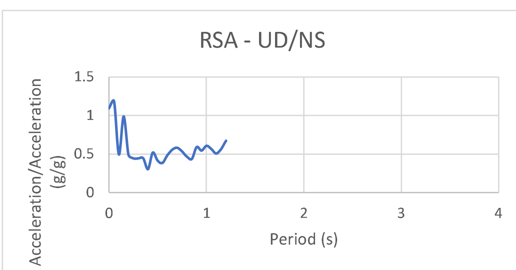

Max UD (g)	0.281
Per Max UD (s)	0.05
Max UD/EW (g)	0.877
Per Max UD/EW (s)	0.05
Max UD/NS (g)	1.183
Per Max UD/NS (s)	0.05

RSA - EW		RSA - NS		MAX(EW, NS)	
PGA =	0.202	PGA =	0.139	PGA =	0.202
Ss =	0.597	Ss =	0.325	Ss =	0.597
S1 =	0.144	S1 =	0.094	S1 =	0.144

EQ	Station
Iquique 7.6	472

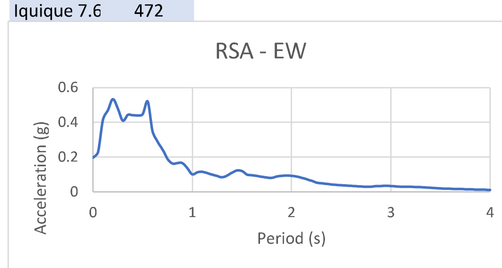

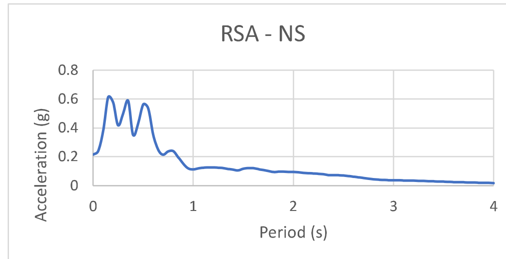

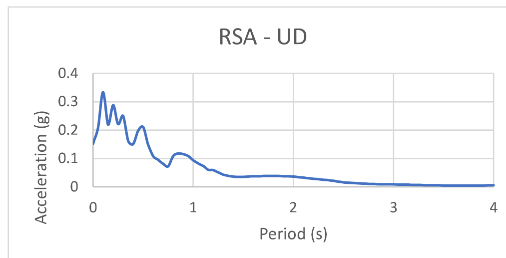

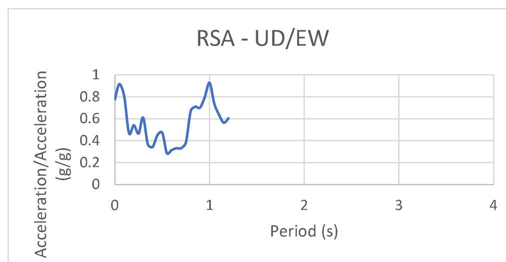

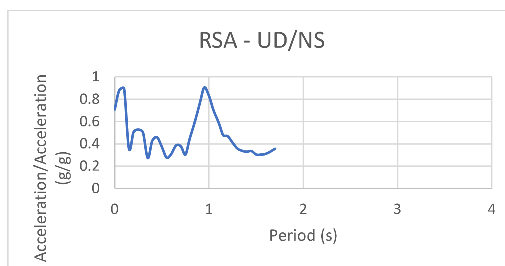

Max UD (g)	0.333
Per Max UD (s)	0.10
Max UD/EW (g)	0.927
Per Max UD/EW (s)	1.00
Max UD/NS (g)	0.904
Per Max UD/NS (s)	0.95

RSA - EW		RSA - NS		MAX(EW, NS)	
PGA =	0.196	PGA =	0.214	PGA =	0.214
Ss =	0.534	Ss =	0.576	Ss =	0.576
S1 =	0.101	S1 =	0.113	S1 =	0.113

EQ	Station
Tohoku 9.0	FKS014

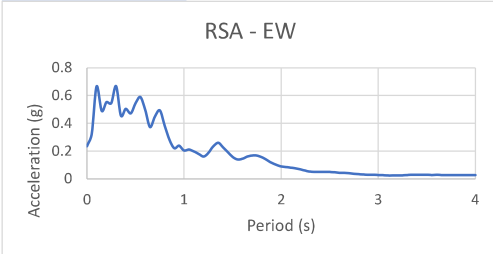

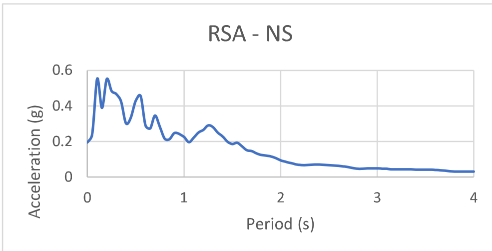

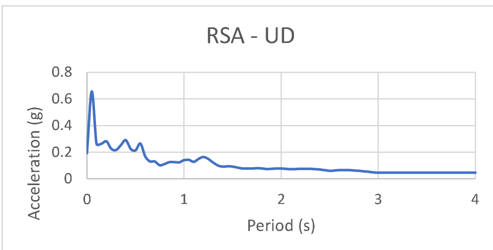

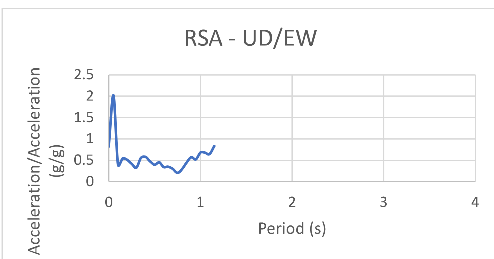

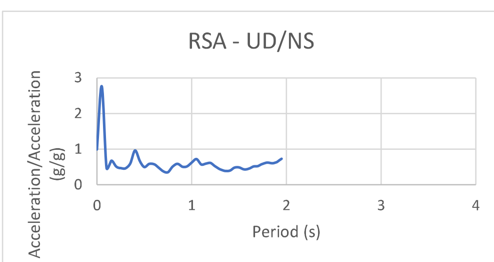

Max UD (g)	0.656
Per Max UD (s)	0.05
Max UD/EW (g)	2.020
Per Max UD/EW (s)	0.05
Max UD/NS (g)	2.765
Per Max UD/NS (s)	0.05

RSA - EW		RSA - NS		MAX(EW, NS)	
PGA =	0.235	PGA =	0.194	PGA =	0.235
Ss =	0.552	Ss =	0.550	Ss =	0.552
S1 =	0.205	S1 =	0.225	S1 =	0.225

EQ	Station
Iquique 7.6	478

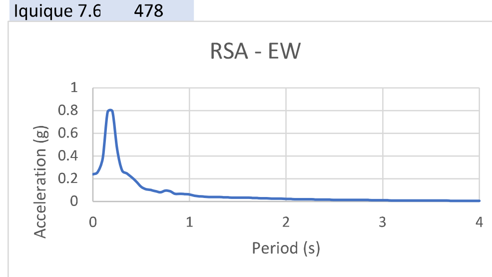

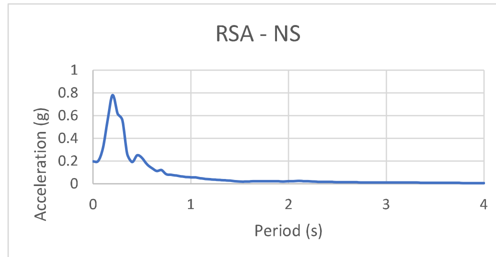

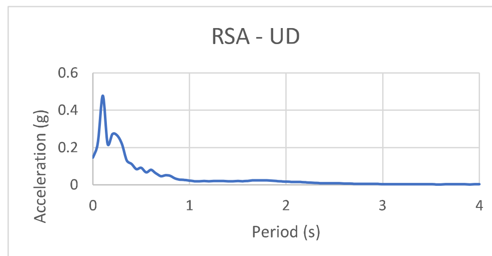

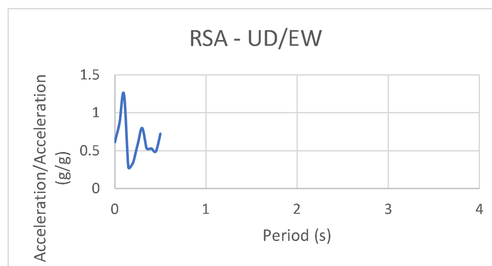

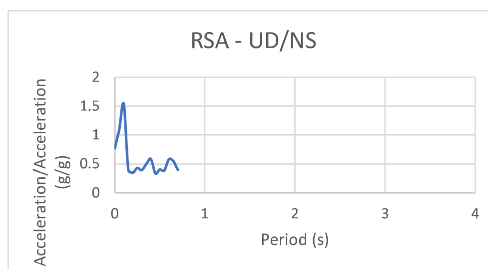

Max UD (g)	0.479
Per Max UD (s)	0.10
Max UD/EW (g)	1.251
Per Max UD/EW (s)	0.10
Max UD/NS (g)	1.534
Per Max UD/NS (s)	0.10

RSA - EW		RSA - NS		MAX(EW, NS)	
PGA =	0.239	PGA =	0.197	PGA =	0.239
Ss =	0.794	Ss =	0.780	Ss =	0.794
S1 =	0.060	S1 =	0.058	S1 =	0.060

EQ	Station
Iquique 8.2	352

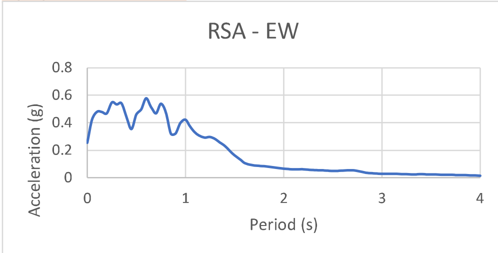

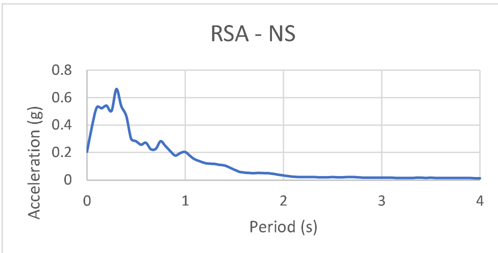

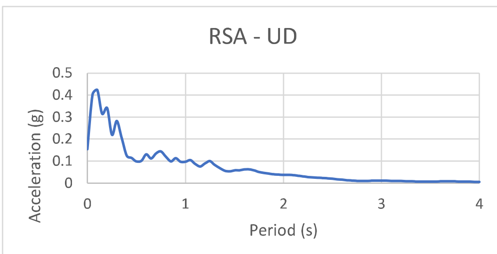

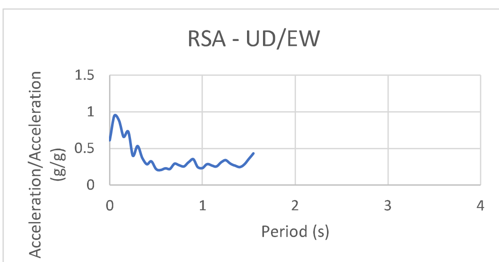

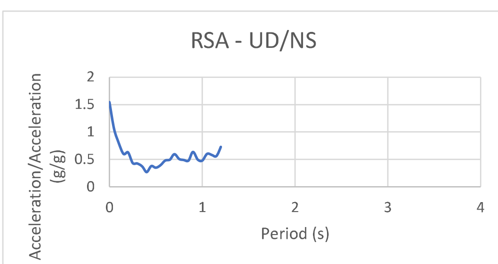

Max UD (g)	0.424
Per Max UD (s)	0.10
Max UD/EW (g)	0.944
Per Max UD/EW (s)	0.05
Max UD/NS (g)	1.542
Per Max UD/NS (s)	0.00

RSA - EW		RSA - NS		MAX(EW, NS)	
PGA =	0.253	PGA =	0.205	PGA =	0.253
Ss =	0.468	Ss =	0.541	Ss =	0.541
S1 =	0.422	S1 =	0.204	S1 =	0.422

EQ	Station
Iquique 8.2	351

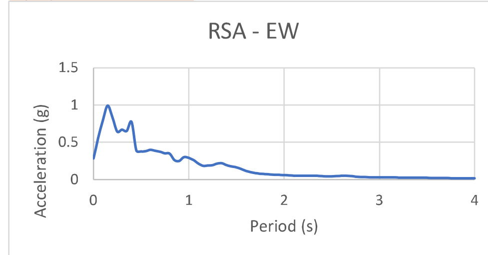

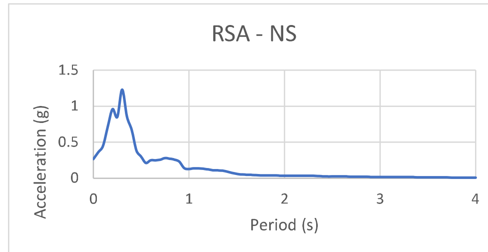

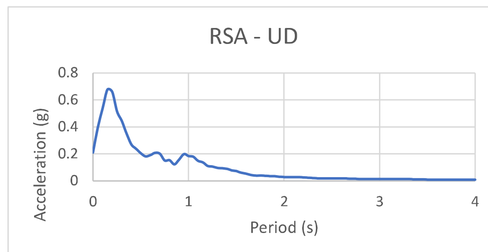

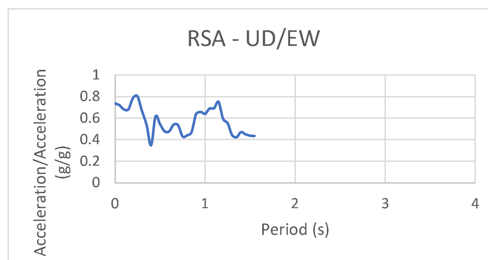

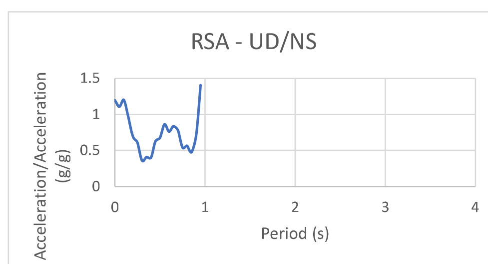

Max UD (g)	0.675
Per Max UD (s)	0.15
Max UD/EW (g)	0.800
Per Max UD/EW (s)	0.25
Max UD/NS (g)	1.406
Per Max UD/NS (s)	0.95

RSA - EW		RSA - NS		MAX(EW, NS)	
PGA =	0.284	PGA =	0.265	PGA =	0.284
Ss =	0.838	Ss =	0.959	Ss =	0.959
S1 =	0.289	S1 =	0.127	S1 =	0.289

EQ	Station
Illapel 8.4	2023

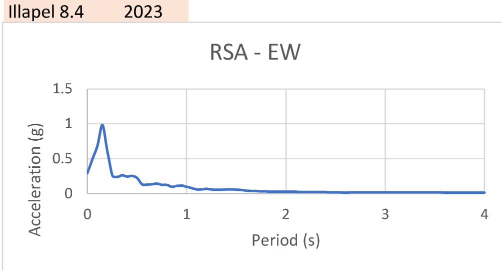

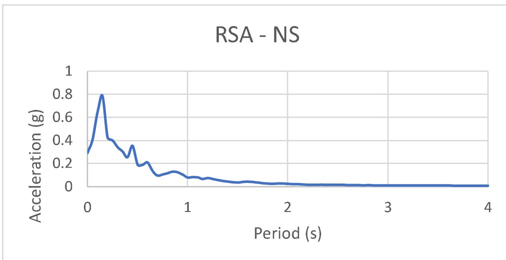

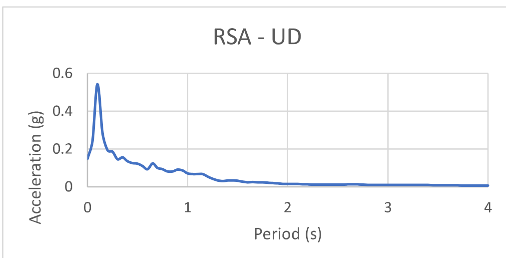

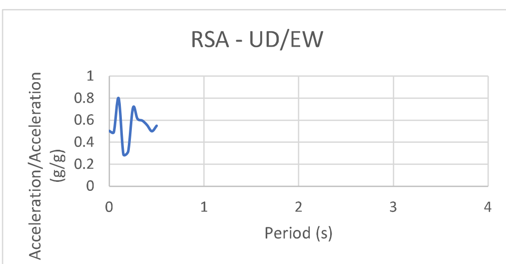

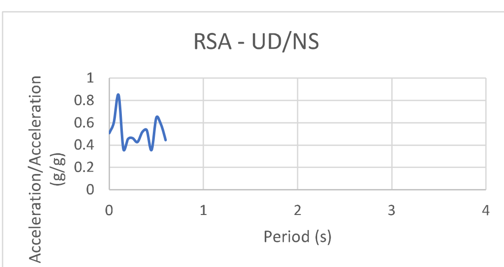

Max UD (g)	0.542
Per Max UD (s)	0.10
Max UD/EW (g)	0.798
Per Max UD/EW (s)	0.10
0	0
Max UD/NS (g)	0.848
Per Max UD/NS (s)	0.10

RSA - EW		RSA - NS		MAX(EW, NS)	
PGA =	0.295	PGA =	0.292	PGA =	0.295
Ss =	0.616	Ss =	0.428	Ss =	0.616
S1 =	0.096	S1 =	0.079	S1 =	0.096

EQ	Station
Tohoku 9.0	IWTH22

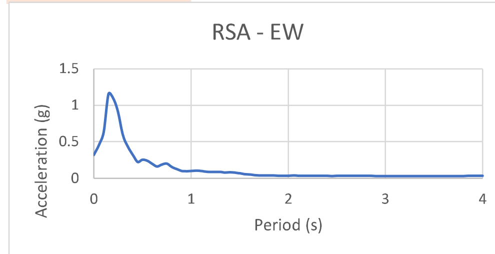

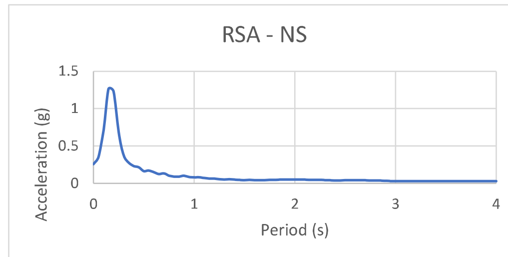

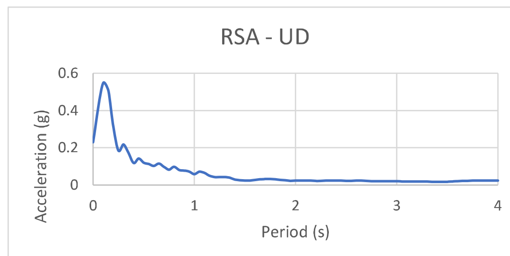

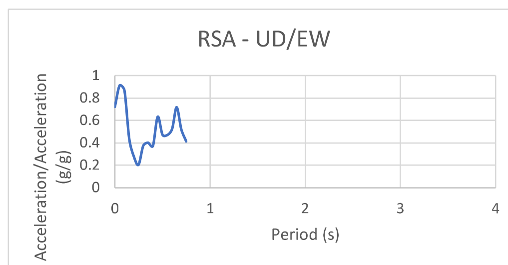

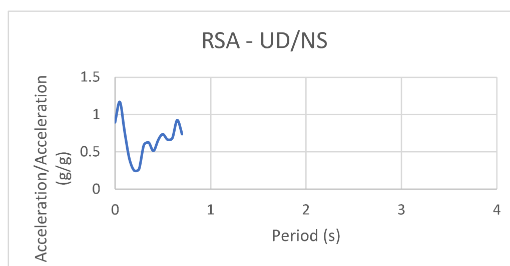

Max UD (g)	0.550
Per Max UD (s)	0.10
Max UD/EW (g)	0.914
Per Max UD/EW (s)	0.05
Max UD/NS (g)	1.170
Per Max UD/NS (s)	0.05

RSA - EW		RSA - NS		MAX(EW, NS)	
PGA =	0.320	PGA =	0.257	PGA =	0.320
Ss =	1.092	Ss =	1.228	Ss =	1.228
S1 =	0.101	S1 =	0.079	S1 =	0.101

EQ	Station
Illapel 8.4	2031

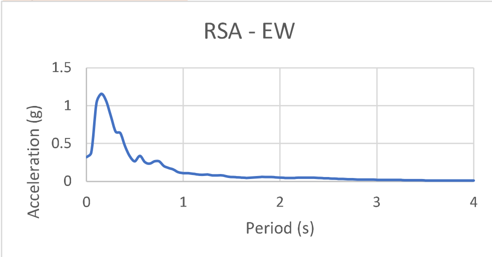

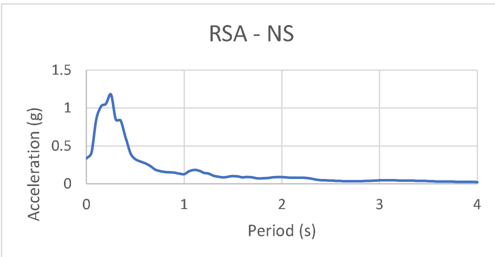

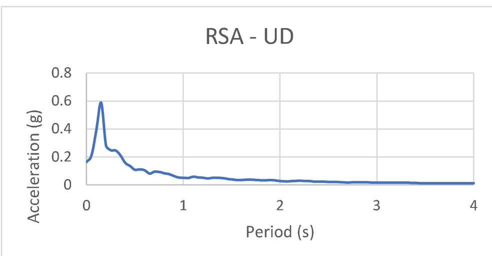

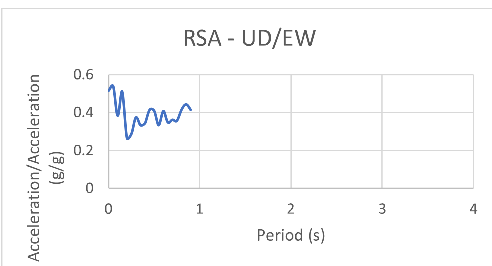

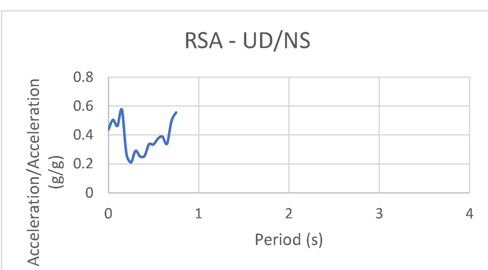

Max UD (g)	0.588
Per Max UD (s)	0.15
Max UD/EW (g)	0.539
Per Max UD/EW (s)	0.05
Max UD/NS (g)	0.574
Per Max UD/NS (s)	0.15

RSA - EW		RSA - NS		MAX(EW, NS)	
PGA =	0.317	PGA =	0.336	PGA =	0.336
Ss =	1.068	Ss =	1.056	Ss =	1.068
S1 =	0.109	S1 =	0.128	S1 =	0.128

EQ	Station
Tohoku 9.0	IWT008

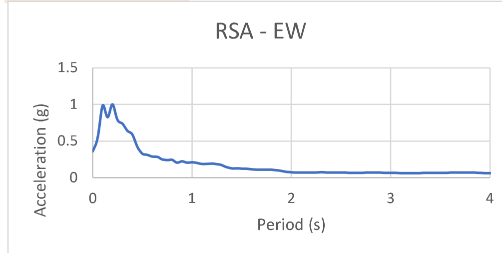

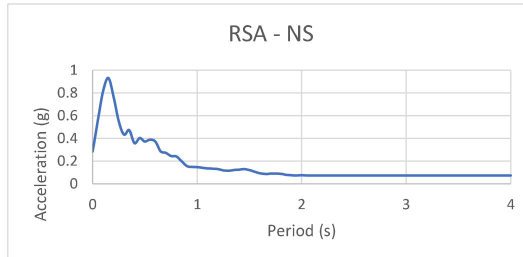

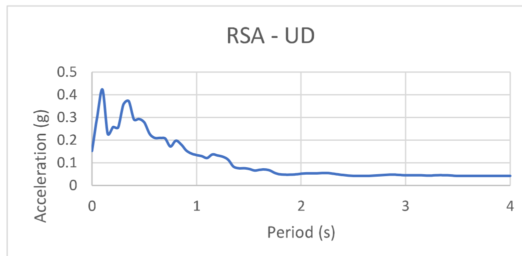

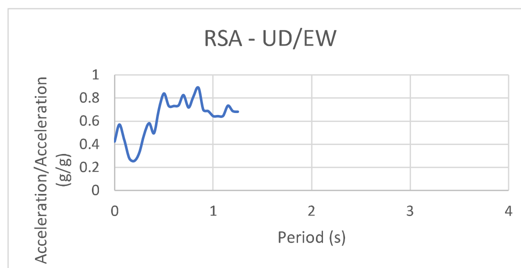

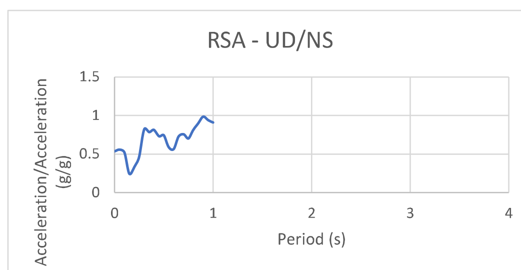

Max UD (g)	0.423
Per Max UD (s)	0.10
Max UD/EW (g)	0.890
Per Max UD/EW (s)	0.85
Max UD/NS (g)	0.984
Per Max UD/NS (s)	0.90

RSA - EW		RSA - NS		MAX(EW, NS)	
PGA =	0.359	PGA =	0.286	PGA =	0.359
Ss =	1.002	Ss =	0.774	Ss =	1.002
S1 =	0.209	S1 =	0.148	S1 =	0.209

EQ	Station
Tohoku 9.0	IWTH18

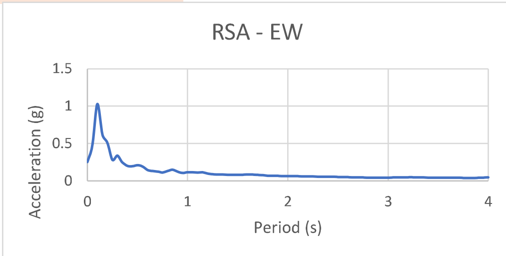

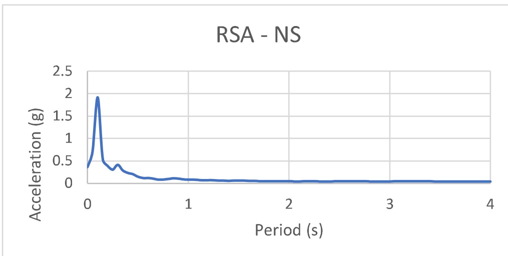

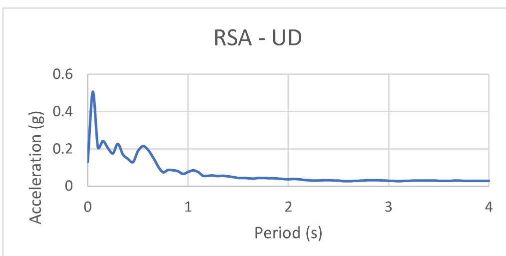

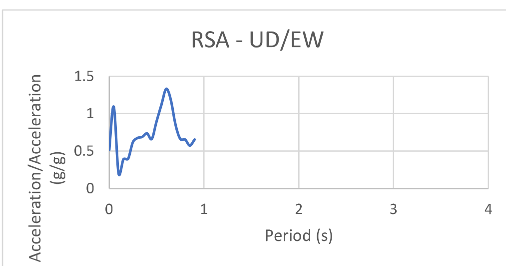

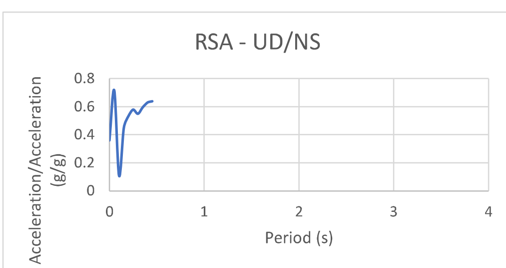

Max UD (g)	0.507
Per Max UD (s)	0.05
Max UD/EW (g)	1.332
Per Max UD/EW (s)	0.60
Max UD/NS (g)	0.716
Per Max UD/NS (s)	0.05

RSA - EW		RSA - NS		MAX(EW, NS)	
PGA =	0.252	PGA =	0.361	PGA =	0.361
Ss =	0.514	Ss =	0.388	Ss =	0.514
S1 =	0.115	S1 =	0.085	S1 =	0.115

EQ	Station
Iquique 8.2	335

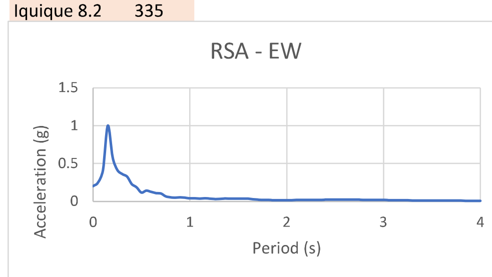

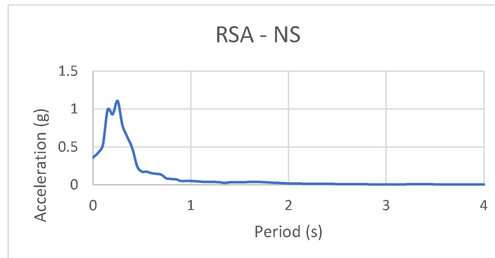

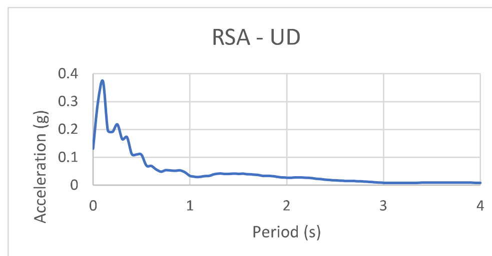

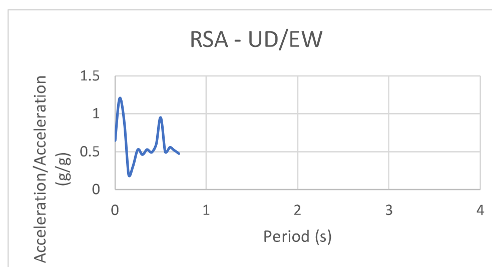

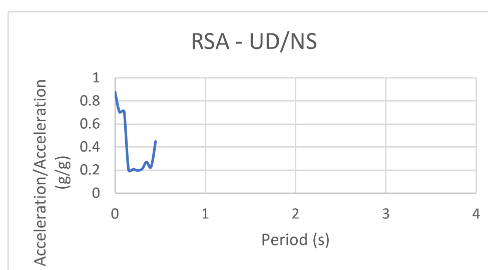

Max UD (g)	0.372
Per Max UD (s)	0.10
Max UD/EW (g)	1.204
Per Max UD/EW (s)	0.05
Max UD/NS (g)	0.877
Per Max UD/NS (s)	0.00

RSA - EW		RSA - NS		MAX(EW, NS)	
PGA =	0.202	PGA =	0.361	PGA =	0.361
Ss =	0.587	Ss =	0.928	Ss =	0.928
S1 =	0.041	S1 =	0.050	S1 =	0.050

EQ	Station
Iquique 7.6	492

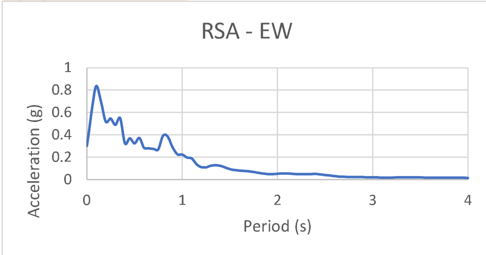

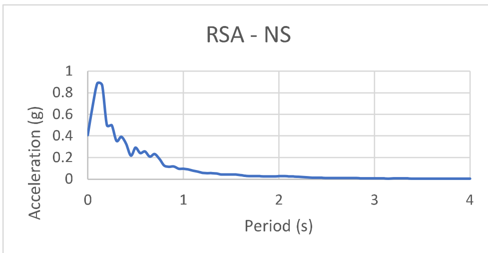

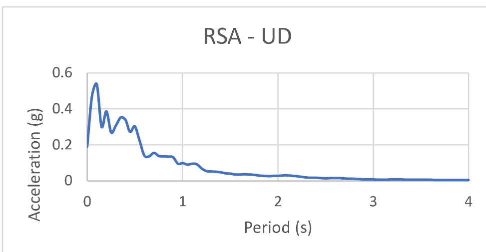

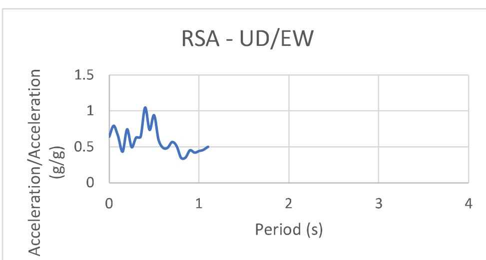

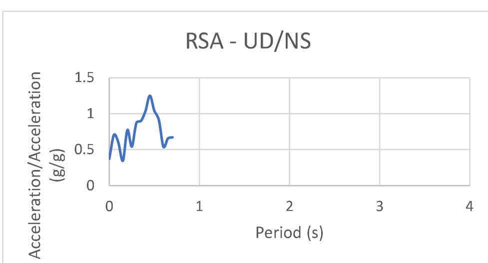

Max UD (g)	0.537
Per Max UD (s)	0.10
Max UD/EW (g)	1.044
Per Max UD/EW (s)	0.40
Max UD/NS (g)	1.250
Per Max UD/NS (s)	0.45

RSA - EW		RSA - NS		MAX(EW, NS)	
PGA =	0.299	PGA =	0.408	PGA =	0.408
Ss =	0.518	Ss =	0.498	Ss =	0.518
S1 =	0.223	S1 =	0.096	S1 =	0.223

EQ	Station
Miyagi 7.1	IWTH21

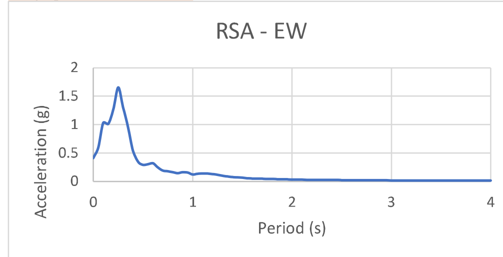

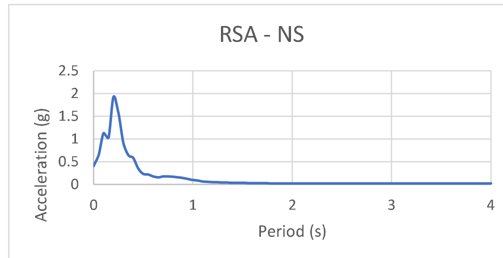

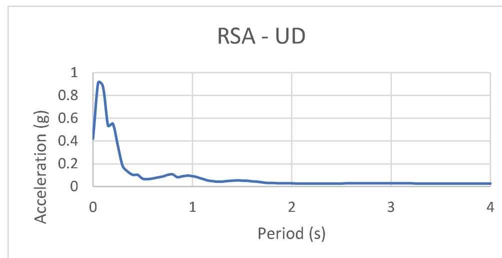

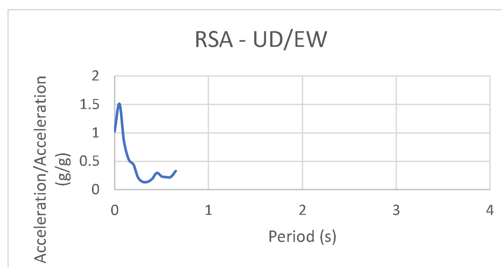

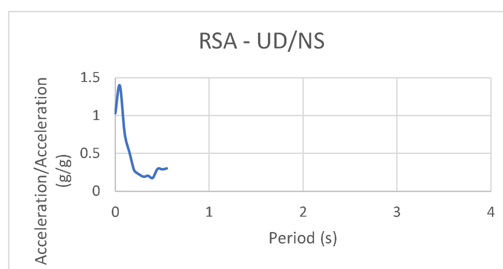

Max UD (g)	0.911
Per Max UD (s)	0.05
Max UD/EW (g)	1.512
Per Max UD/EW (s)	0.05
Max UD/NS (g)	1.397
Per Max UD/NS (s)	0.05

RSA - EW		RSA - NS		MAX(EW, NS)	
PGA =	0.409	PGA =	0.408	PGA =	0.409
Ss =	1.256	Ss =	1.925	Ss =	1.925
S1 =	0.120	S1 =	0.099	S1 =	0.120

EQ	Station
Tohoku 9.0	IBRH14

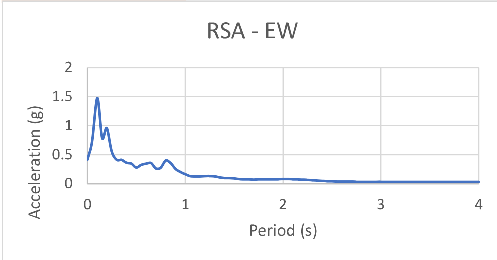

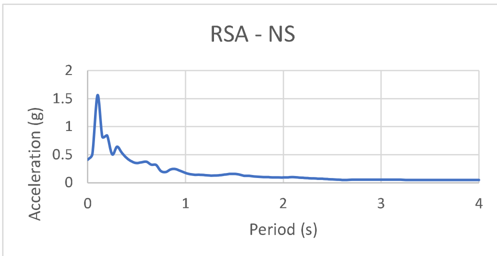

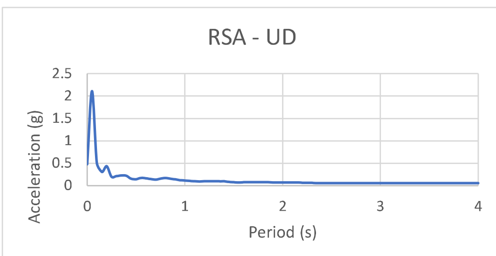

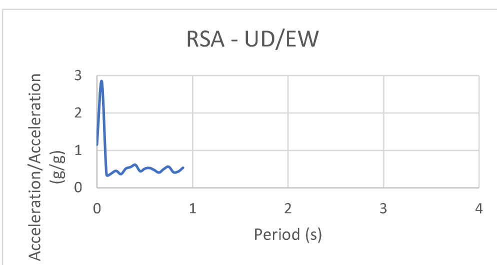

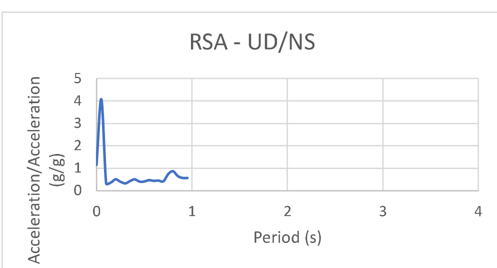

Max UD (g)	2.113
Per Max UD (s)	0.05
Max UD/EW (g)	2.845
Per Max UD/EW (s)	0.05
Max UD/NS (g)	4.077
Per Max UD/NS (s)	0.05

RSA - EW		RSA - NS		MAX(EW, NS)	
PGA =	0.413	PGA =	0.412	PGA =	0.413
Ss =	0.954	Ss =	0.843	Ss =	0.954
S1 =	0.162	S1 =	0.174	S1 =	0.174

EQ	Station
Iquique 8.2	348

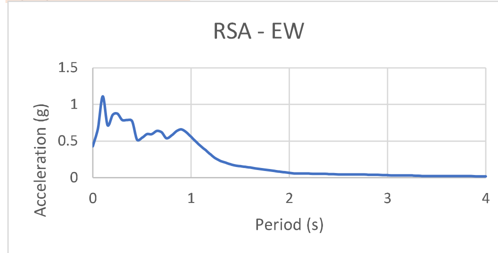

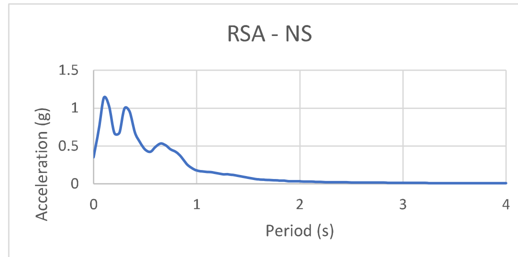

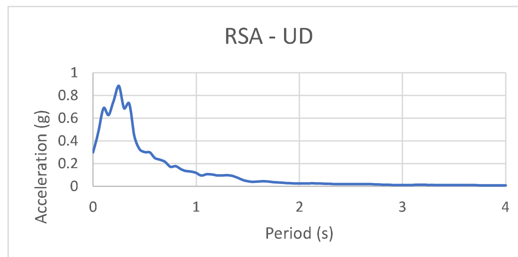

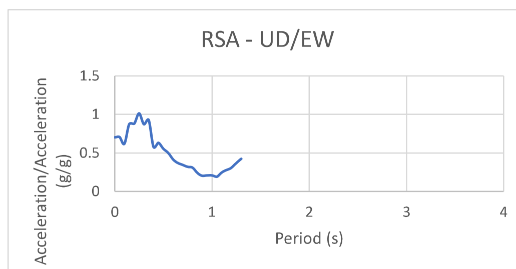

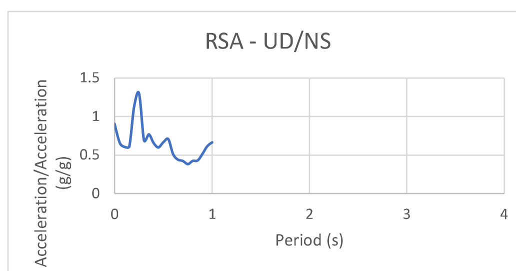

Max UD (g)	0.884
Per Max UD (s)	0.25
Max UD/EW (g)	1.014
Per Max UD/EW (s)	0.25
Max UD/NS (g)	1.303
Per Max UD/NS (s)	0.25

RSA - EW		RSA - NS		MAX(EW, NS)	
PGA =	0.427	PGA =	0.350	PGA =	0.427
Ss =	0.857	Ss =	0.673	Ss =	0.857
S1 =	0.557	S1 =	0.177	S1 =	0.557

EQ	Station
Tohoku 9.0	IWTH21

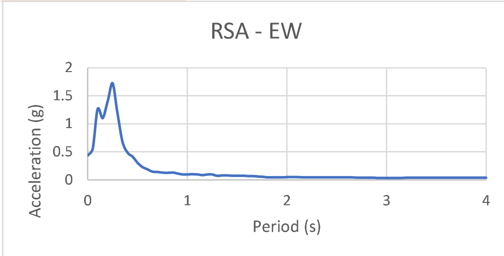

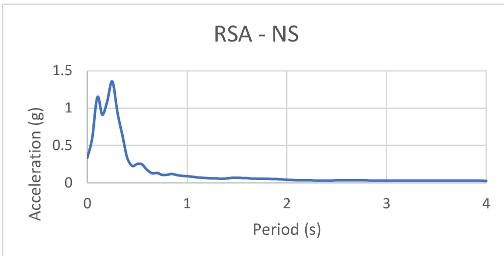

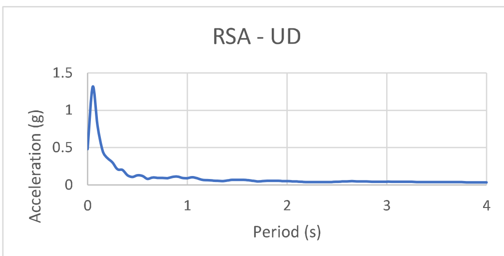

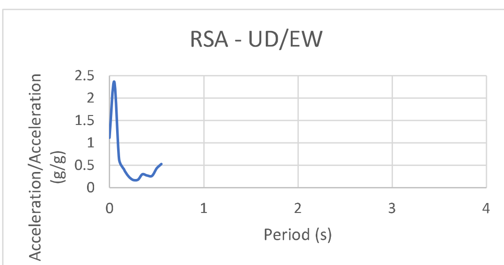

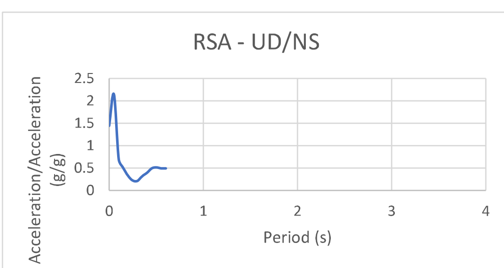

Max UD (g)	1.315
Per Max UD (s)	0.05
Max UD/EW (g)	2.362
Per Max UD/EW (s)	0.05
Max UD/NS (g)	2.143
Per Max UD/NS (s)	0.05

RSA - EW		RSA - NS		MAX(EW, NS)	
PGA =	0.431	PGA =	0.334	PGA =	0.431
Ss =	1.394	Ss =	1.099	Ss =	1.394
S1 =	0.099	S1 =	0.088	S1 =	0.099

EQ	Station
Miyagi 7.1	IWTH28

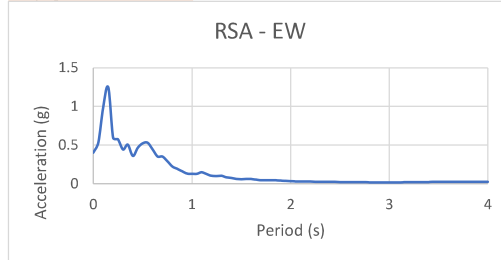

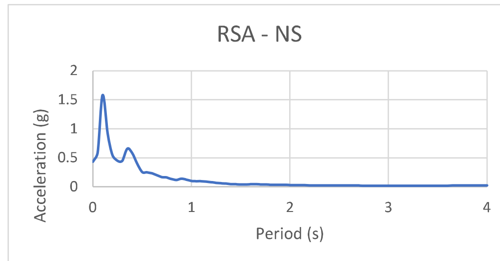

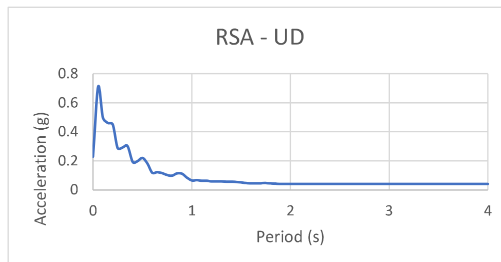

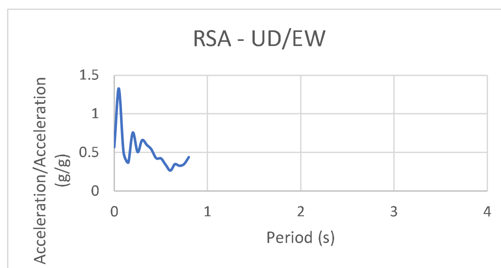

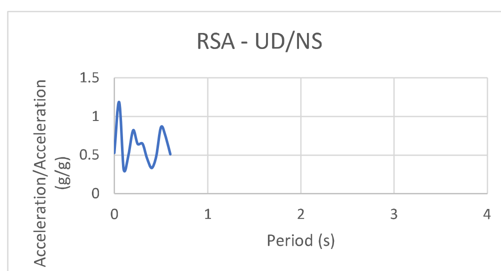

Max UD (g)	0.710
Per Max UD (s)	0.05
Max UD/EW (g)	1.328
Max UD/NS (g)	1.188
Per Max UD/NS (s)	0.05

RSA - EW		RSA - NS		MAX(EW, NS)	
PGA =	0.403	PGA =	0.432	PGA =	0.432
Ss =	0.595	Ss =	0.548	Ss =	0.595
S1 =	0.127	S1 =	0.102	S1 =	0.127

EQ	Station
Tohoku 9.0	FKSH09

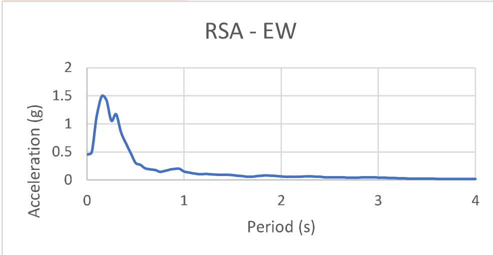

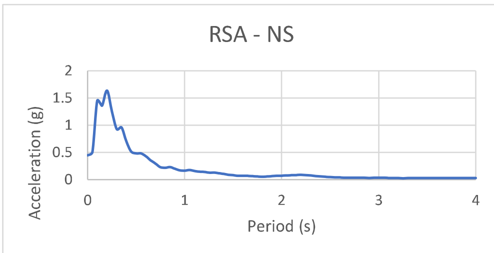

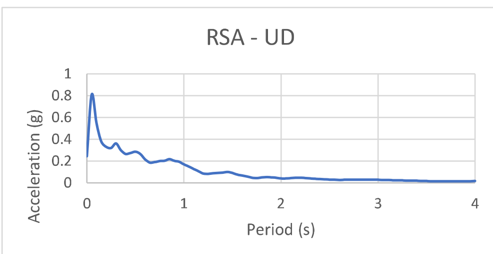

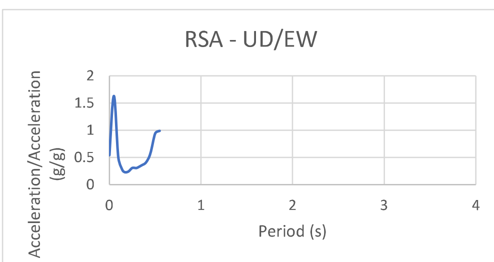

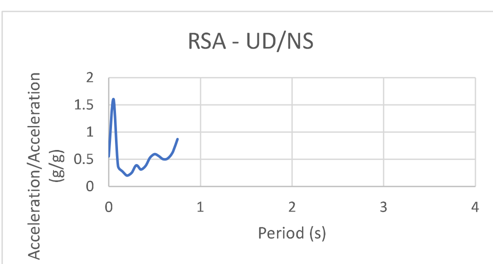

Max UD (g)	0.810
Per Max UD (s)	0.05
Max UD/EW (g)	1.630
Per Max UD/EW (s)	0.05
Max UD/NS (g)	1.604
Per Max UD/NS (s)	0.05

RSA - EW		RSA - NS		MAX(EW, NS)	
PGA =	0.453	PGA =	0.444	PGA =	0.453
Ss =	1.419	Ss =	1.636	Ss =	1.636
S1 =	0.152	S1 =	0.162	S1 =	0.162

EQ	Station
Tohoku 9.0	MYGH03

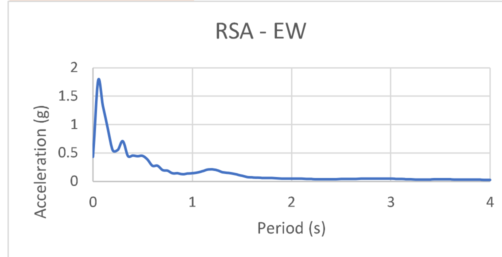

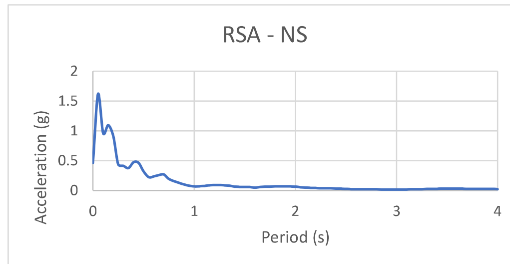

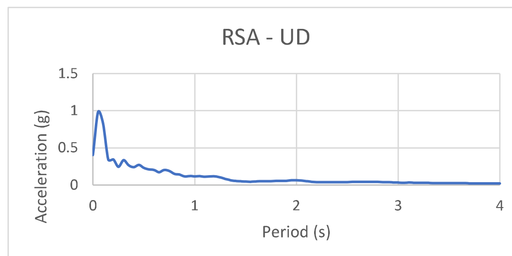

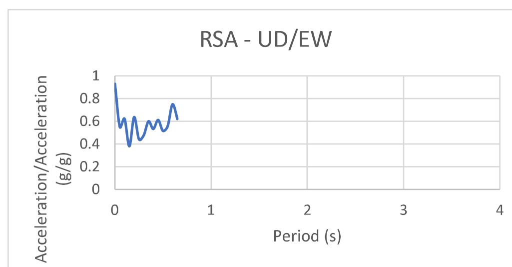

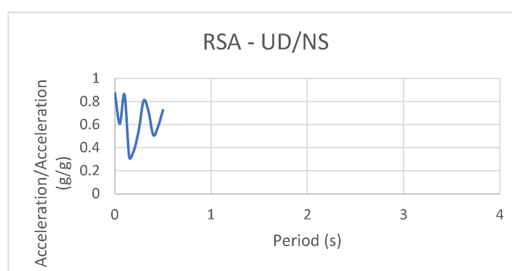

Max UD (g)	0.980
Per Max UD (s)	0.05
Max UD/EW (g)	0.930
Per Max UD/EW (s)	0.00
Max UD/NS (g)	0.872
Per Max UD/NS (s)	0.00

RSA - EW		RSA - NS		MAX(EW, NS)	
PGA =	0.433	PGA =	0.462	PGA =	0.462
Ss =	0.542	Ss =	0.910	Ss =	0.910
S1 =	0.141	S1 =	0.069	S1 =	0.141

EQ	Station
Iquique 8.2	329

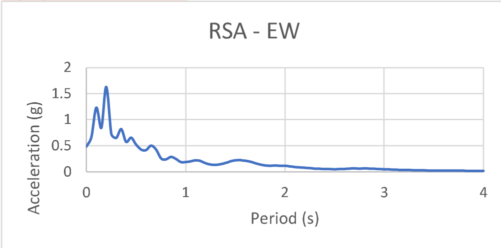

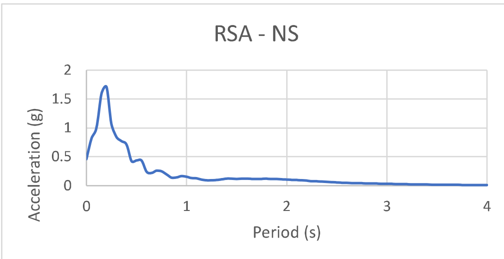

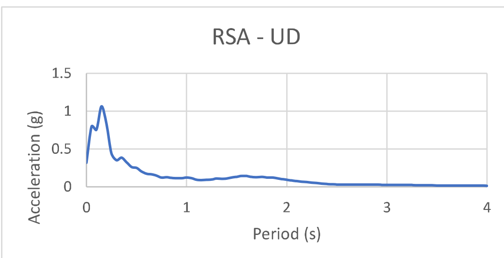

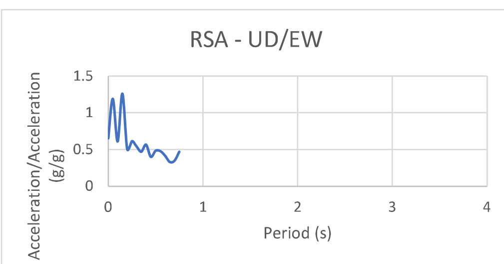

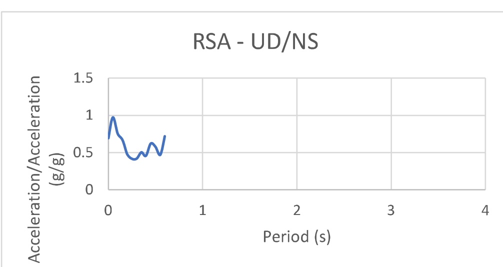

Max UD (g)	1.064
Per Max UD (s)	0.15
Max UD/EW (g)	1.259
Per Max UD/EW (s)	0.15
Max UD/NS (g)	0.972
Per Max UD/NS (s)	0.05

RSA - EW		RSA - NS		MAX(EW, NS)	
PGA =	0.485	PGA =	0.458	PGA =	0.485
Ss =	1.631	Ss =	1.709	Ss =	1.709
S1 =	0.187	S1 =	0.154	S1 =	0.187

EQ	Station
Tohoku 9.0	IWTH23

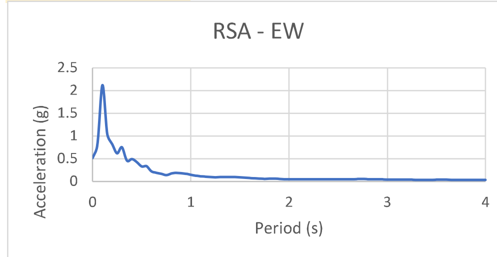

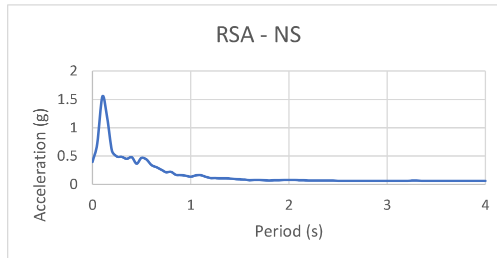

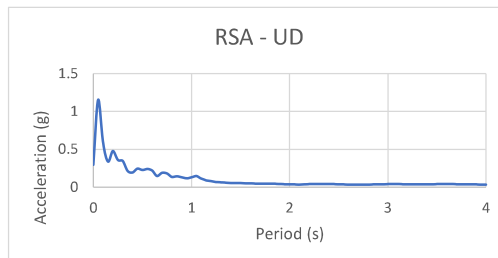

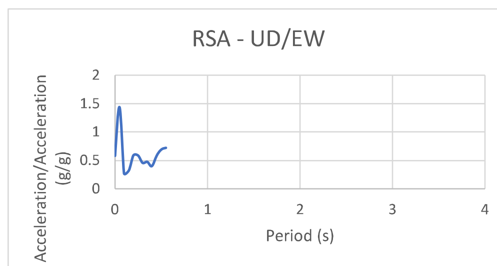

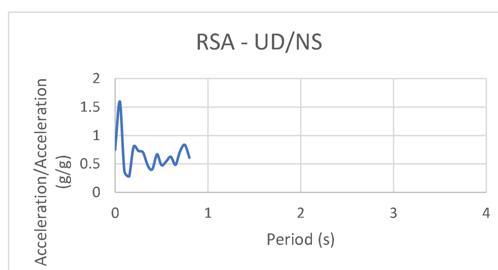

Max UD (g)	1.153
Per Max UD (s)	0.05
Max UD/EW (g)	1.437
Per Max UD/EW (s)	0.05
Max UD/NS (g)	1.596
Per Max UD/NS (s)	0.05

RSA - EW		RSA - NS		MAX(EW, NS)	
PGA =	0.511	PGA =	0.397	PGA =	0.511
Ss =	0.812	Ss =	0.593	Ss =	0.812
S1 =	0.146	S1 =	0.136	S1 =	0.146

EQ	Station
Tohoku 9.0	MYGH12

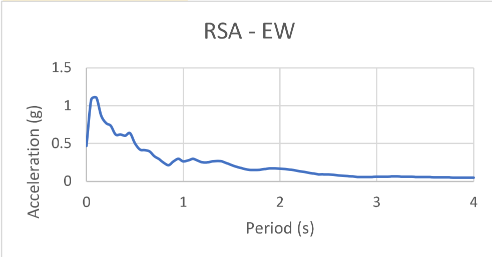

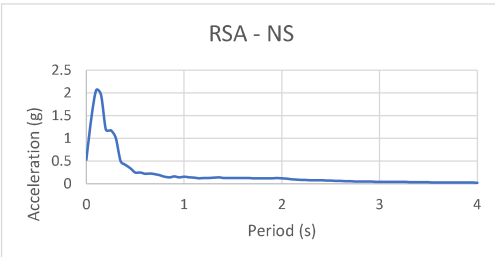

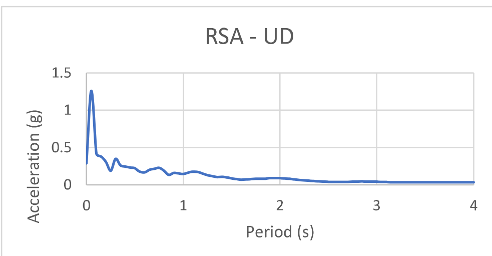

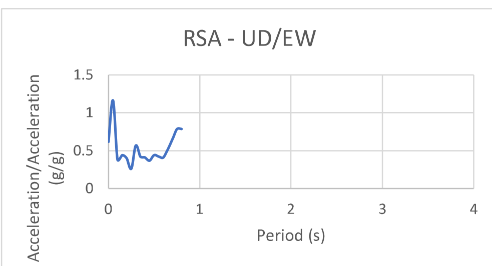

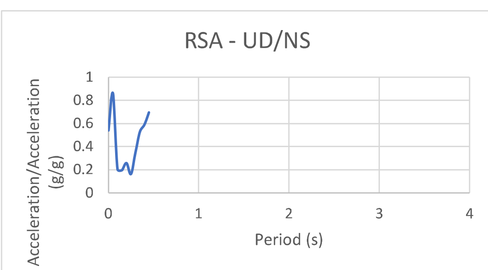

Max UD (g)	1.258
Per Max UD (s)	0.05
Max UD/EW (g)	1.164
Per Max UD/EW (s)	0.05
Max UD/NS (g)	0.858
Per Max UD/NS (s)	0.05

RSA - EW		RSA - NS		MAX(EW, NS)	
PGA =	0.467	PGA =	0.531	PGA =	0.531
Ss =	0.770	Ss =	1.193	Ss =	1.193
S1 =	0.263	S1 =	0.157	S1 =	0.263

EQ	Station
Miyagi 7.1	IWTH23

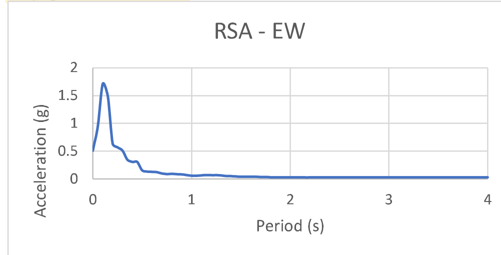

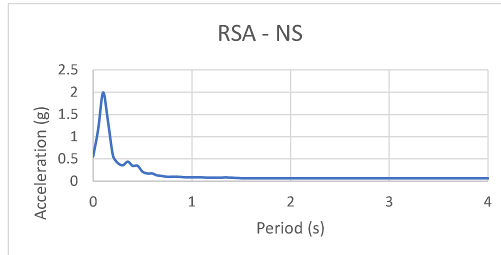

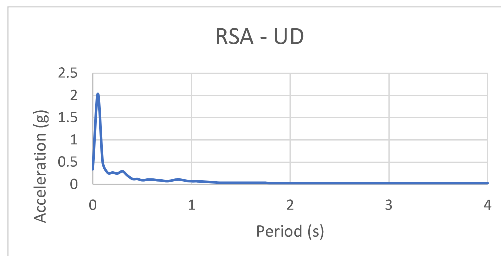

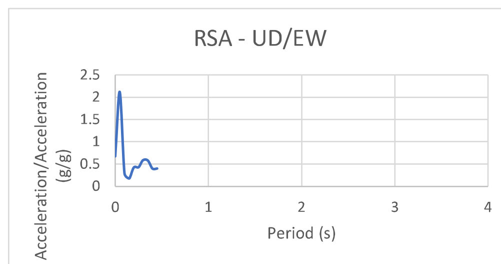

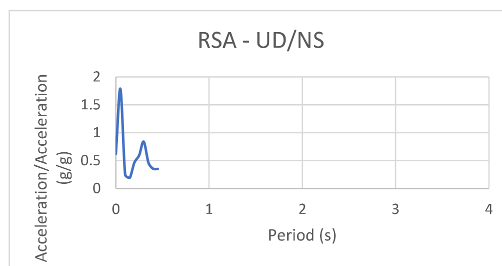

Max UD (g)	2.038
Per Max UD (s)	0.05
Max UD/EW (g)	2.115
Per Max UD/EW (s)	0.05
Max UD/NS (g)	1.791
Per Max UD/NS (s)	0.05

RSA - EW		RSA - NS		MAX(EW, NS)	
PGA =	0.508	PGA =	0.553	PGA =	0.553
Ss =	0.634	Ss =	0.579	Ss =	0.634
S1 =	0.062	S1 =	0.087	S1 =	0.087

EQ	Station
Tohoku 9.0	MYGH04

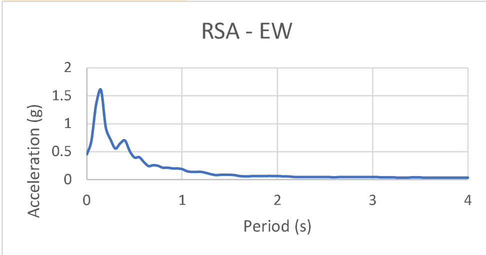

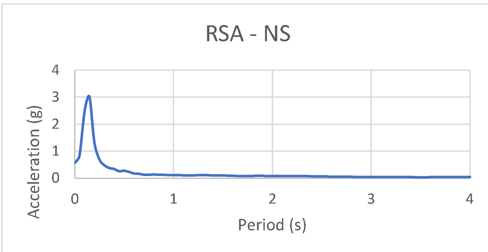

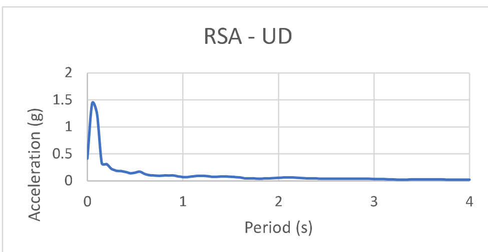

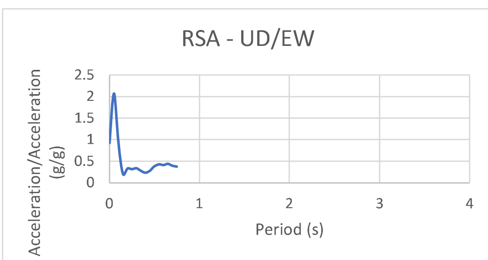

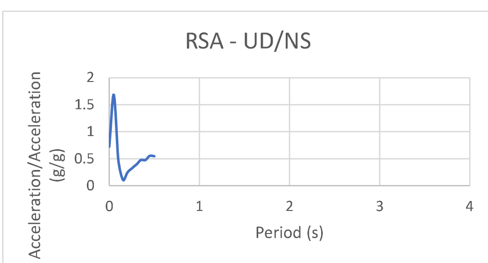

Max UD (g)	1.437
Per Max UD (s)	0.05
Max UD/EW (g)	2.071
Per Max UD/EW (s)	0.05
Max UD/NS (g)	1.686
Per Max UD/NS (s)	0.05

RSA - EW		RSA - NS		MAX(EW, NS)	
PGA =	0.449	PGA =	0.569	PGA =	0.569
Ss =	0.930	Ss =	1.273	Ss =	1.273
S1 =	0.185	S1 =	0.113	S1 =	0.185

EQ	Station
Tohoku 9.0	IWT009

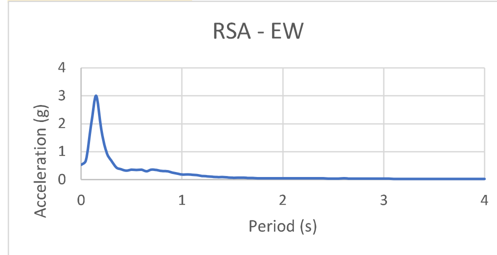

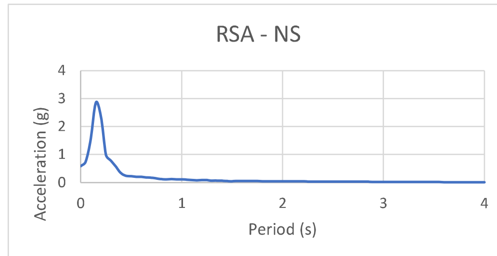

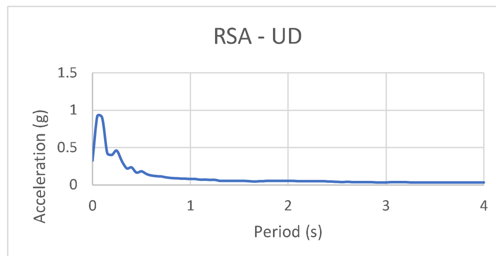

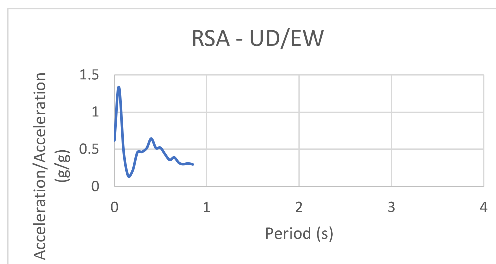

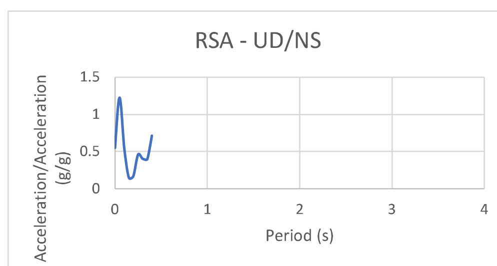

Max UD (g)	0.920
Per Max UD (s)	0.05
Max UD/EW (g)	1.338
Per Max UD/EW (s)	0.05
Max UD/NS (g)	1.225
Per Max UD/NS (s)	0.05

RSA - EW		RSA - NS		MAX(EW, NS)	
PGA =	0.521	PGA =	0.587	PGA =	0.587
Ss =	1.806	Ss =	2.385	Ss =	2.385
S1 =	0.180	S1 =	0.113	S1 =	0.180

EQ	Station
Tohoku 9.0	IBRH16

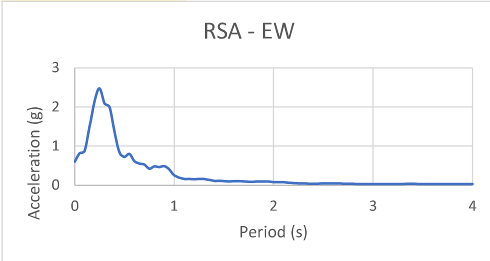

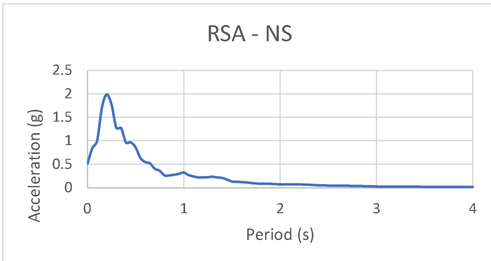

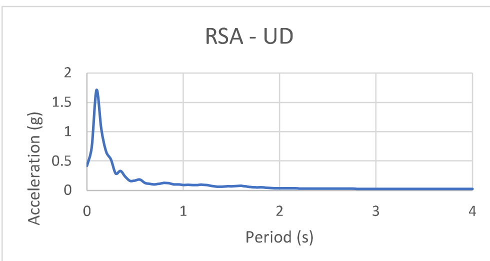

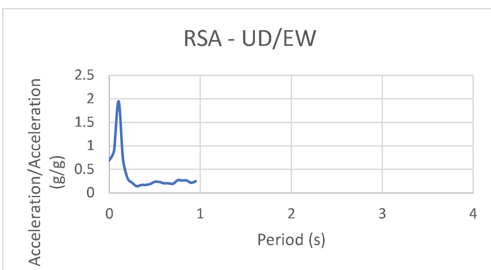

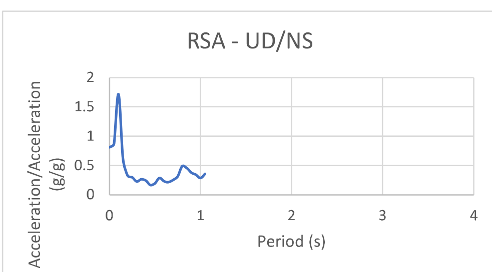

Max UD (g)	1.709
Per Max UD (s)	0.10
Max UD/EW (g)	1.944
Per Max UD/EW (s)	0.10
Max UD/NS (g)	1.713
Per Max UD/NS (s)	0.10

RSA - EW		RSA - NS		MAX(EW, NS)	
PGA =	0.602	PGA =	0.514	PGA =	0.602
Ss =	2.150	Ss =	1.985	Ss =	2.150
S1 =	0.258	S1 =	0.324	S1 =	0.324

EQ	Station
Tohoku 9.0	IWTH02

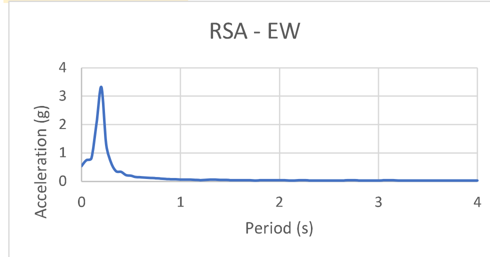

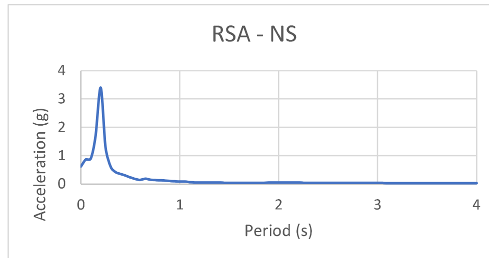

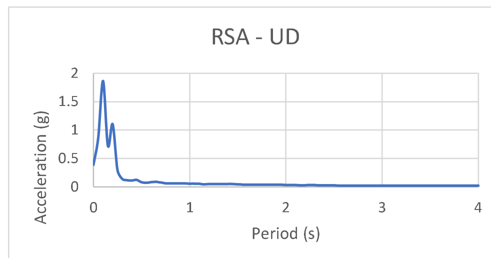

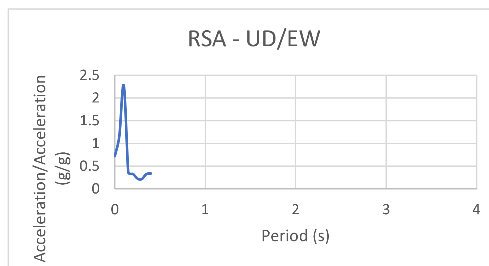

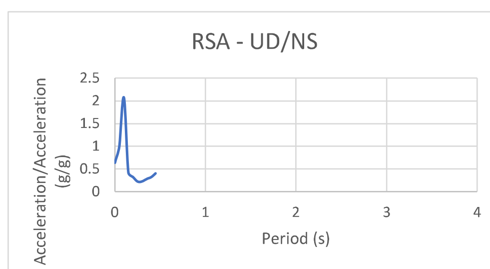

Max UD (g)	1.862
Per Max UD (s)	0.10
Max UD/EW (g)	2.277
Per Max UD/EW (s)	0.10
Max UD/NS (g)	2.071
Per Max UD/NS (s)	0.10

RSA - EW		RSA - NS		MAX(EW, NS)	
PGA =	0.540	PGA =	0.613	PGA =	0.613
Ss =	3.318	Ss =	3.396	Ss =	3.396
S1 =	0.061	S1 =	0.086	S1 =	0.086

EQ	Station
Miyagi 7.1	MYGH04

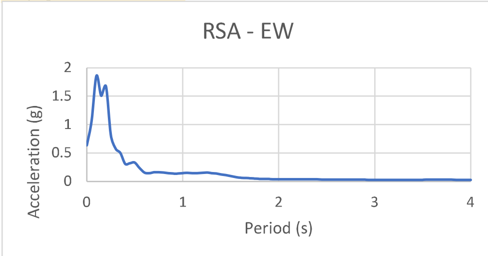

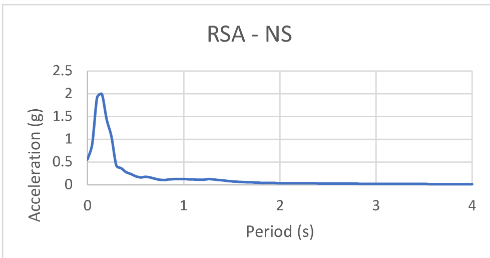

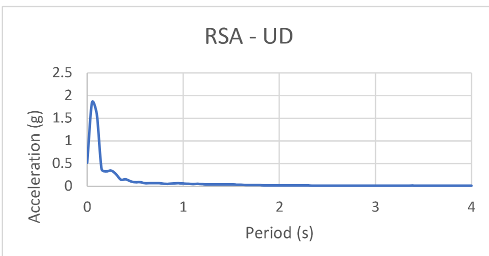

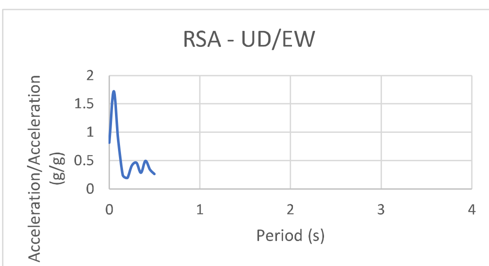

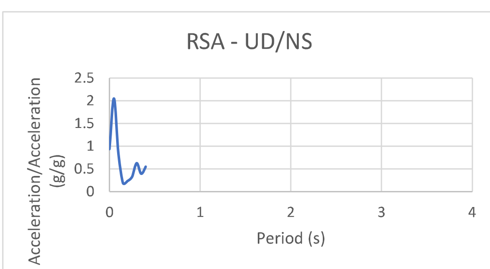

Max UD (g)	1.843
Per Max UD (s)	0.05
Max UD/EW (g)	1.725
Per Max UD/EW (s)	0.05
Max UD/NS (g)	2.051
Per Max UD/NS (s)	0.05

RSA - EW		RSA - NS		MAX(EW, NS)	
PGA =	0.631	PGA =	0.552	PGA =	0.631
Ss =	1.668	Ss =	1.437	Ss =	1.668
S1 =	0.145	S1 =	0.125	S1 =	0.145

EQ	Station
Miyagi 7.1	IWTH02

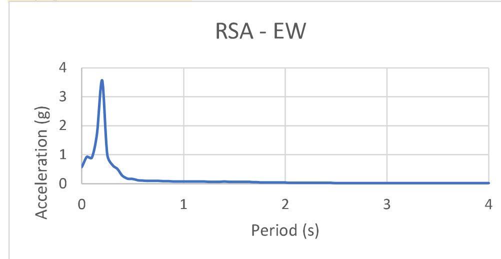

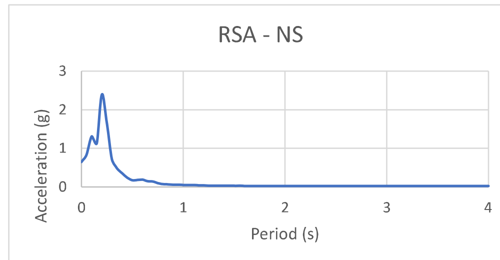

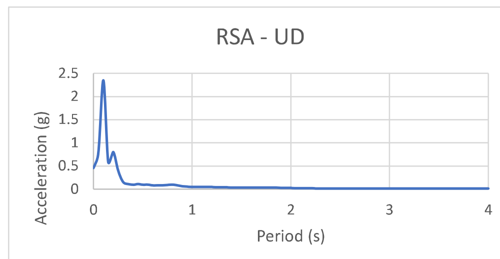

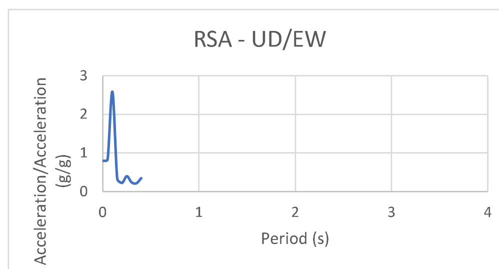

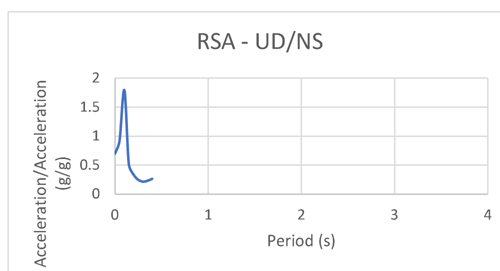

Max UD (g)	2.346
Per Max UD (s)	0.10
Max UD/EW (g)	2.589
Per Max UD/EW (s)	0.10
Max UD/NS (g)	1.793
Per Max UD/NS (s)	0.10

RSA - EW		RSA - NS		MAX(EW, NS)	
PGA =	0.569	PGA =	0.649	PGA =	0.649
Ss =	3.559	Ss =	2.399	Ss =	3.559
S1 =	0.080	S1 =	0.056	S1 =	0.080

EQ	Station
Tohoku 9.0	MYG002

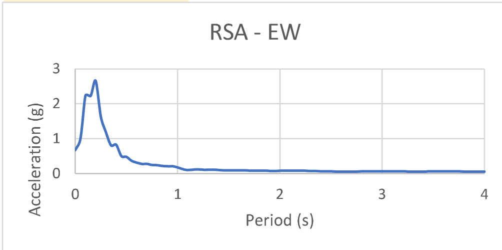

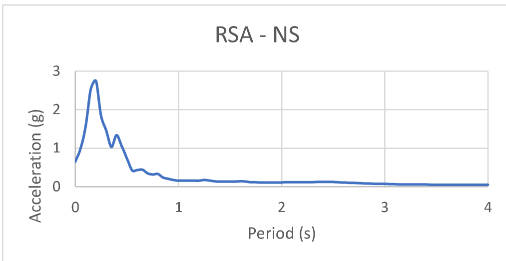

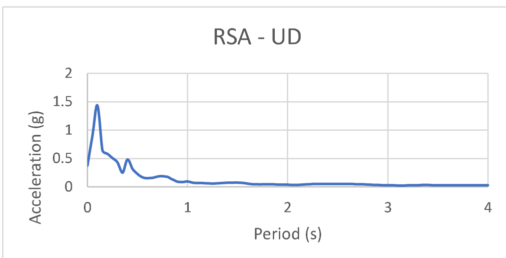

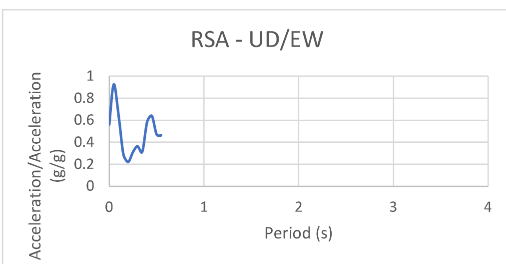

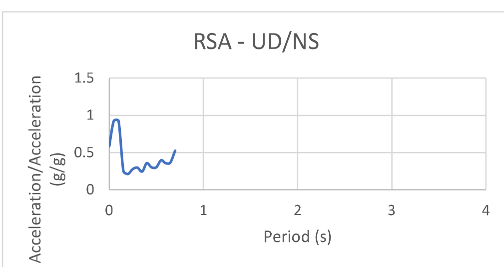

Max UD (g)	1.435
Per Max UD (s)	0.10
Max UD/EW (g)	0.924
Per Max UD/EW (s)	0.05
Max UD/NS (g)	0.926
Per Max UD/NS (s)	0.05

RSA - EW		RSA - NS		MAX(EW, NS)	
PGA =	0.671	PGA =	0.645	PGA =	0.671
Ss =	2.657	Ss =	2.744	Ss =	2.744
S1 =	0.176	S1 =	0.157	S1 =	0.176

EQ	Station
Miyagi 7.1	IWT009

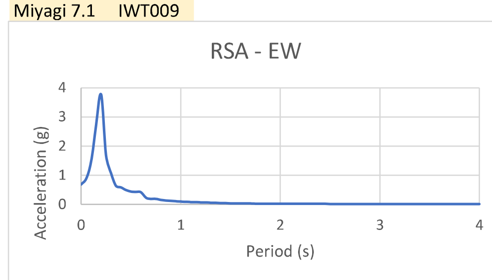

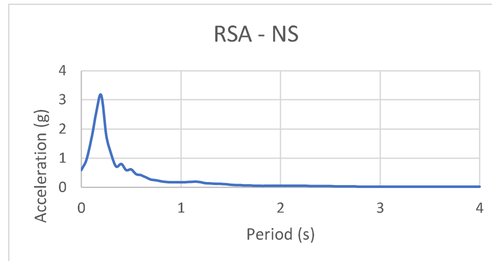

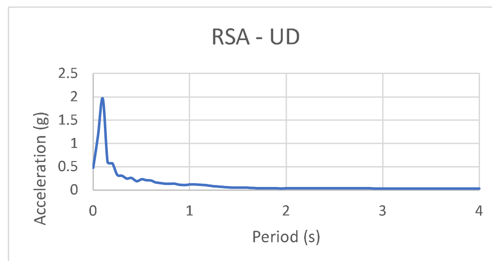

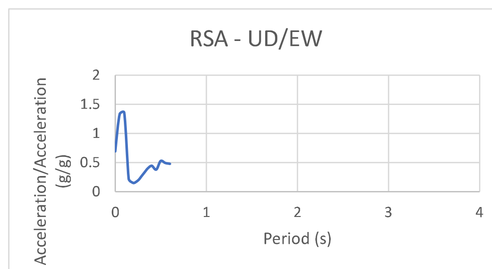

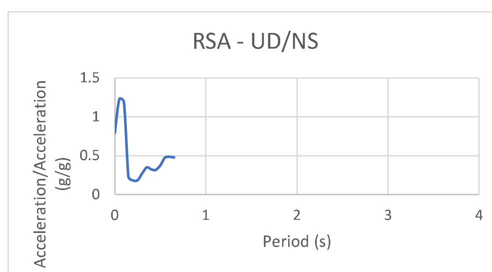

Max UD (g)	1.960
Per Max UD (s)	0.10
Max UD/EW (g)	1.355
Per Max UD/EW (s)	0.10
Max UD/NS (g)	1.232
Per Max UD/NS (s)	0.05

RSA - EW		RSA - NS		MAX(EW, NS)	
PGA =	0.685	PGA =	0.598	PGA =	0.685
Ss =	3.761	Ss =	3.158	Ss =	3.761
S1 =	0.096	S1 =	0.179	S1 =	0.179

EQ	Station
Miyagi 7.1	MYGH03

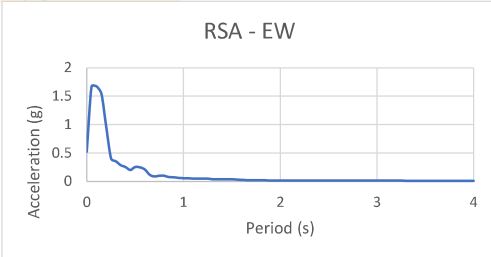

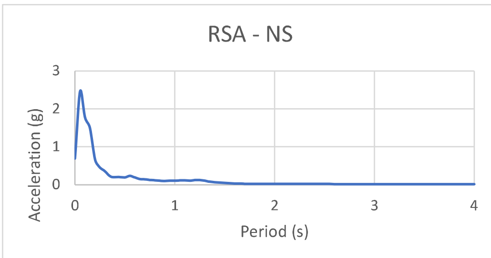

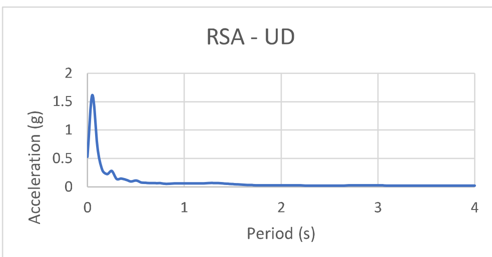

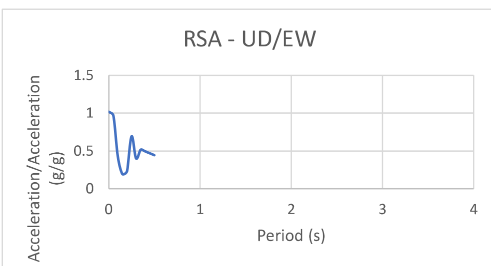

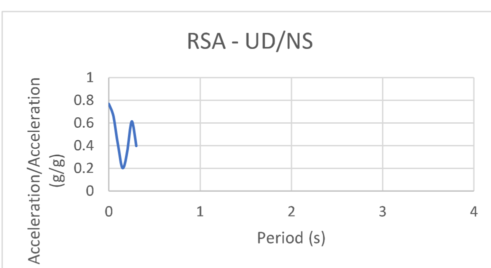

Max UD (g)	1.616
Per Max UD (s)	0.05
Max UD/EW (g)	1.018
Per Max UD/EW (s)	0.00
Max UD/NS (g)	0.771
Per Max UD/NS (s)	0.00

RSA - EW		RSA - NS		MAX(EW, NS)	
PGA =	0.521	PGA =	0.688	PGA =	0.688
Ss =	0.955	Ss =	0.666	Ss =	0.955
S1 =	0.057	S1 =	0.109	S1 =	0.109

EQ	Station
Tohoku 9.0	IWTH27

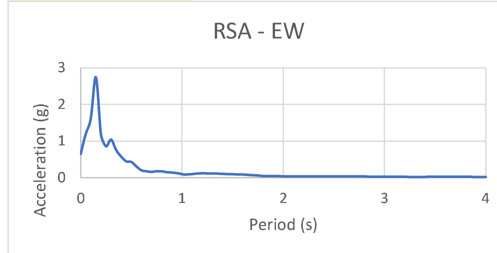

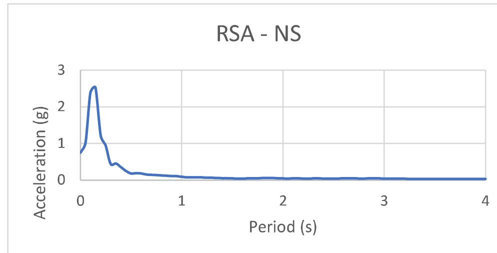

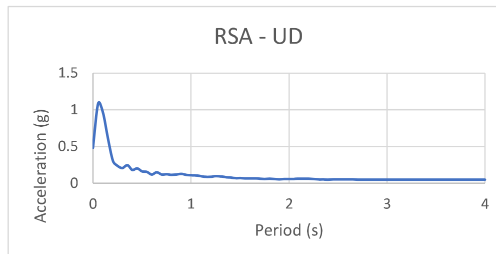

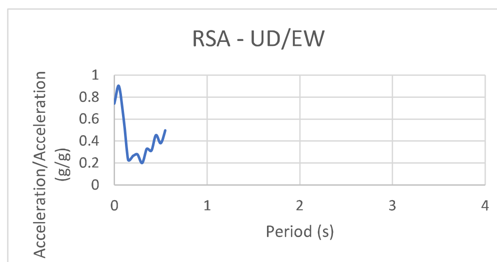

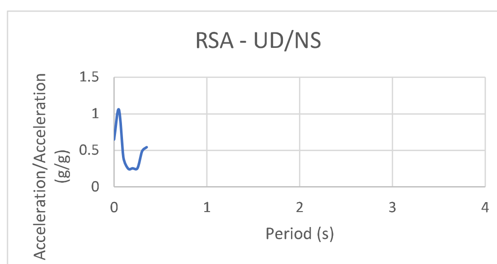

Max UD (g)	1.084
Per Max UD (s)	0.05
Max UD/EW (g)	0.902
Per Max UD/EW (s)	0.05
Max UD/NS (g)	1.056
Per Max UD/NS (s)	0.05

RSA - EW		RSA - NS		MAX(EW, NS)	
PGA =	0.647	PGA =	0.744	PGA =	0.744
Ss =	1.185	Ss =	1.224	Ss =	1.224
S1 =	0.096	S1 =	0.089	S1 =	0.096

EQ	Station
Tohoku 9.0	IBRH15

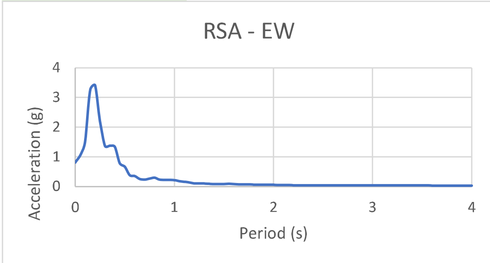

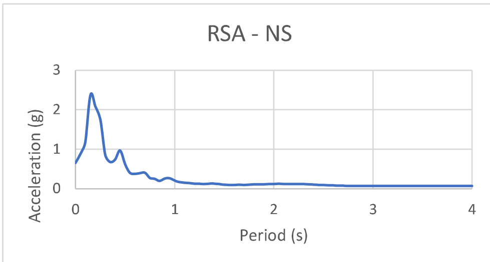

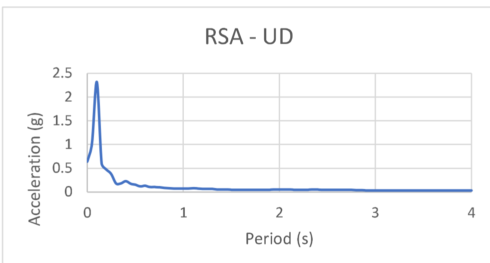

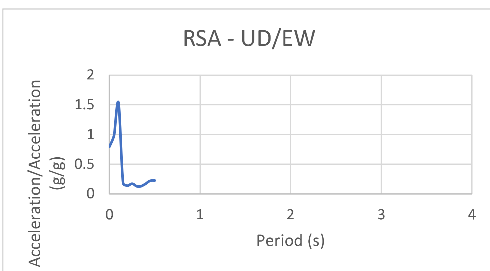

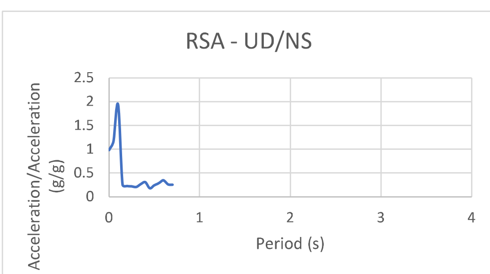

Max UD (g)	2.316
Per Max UD (s)	0.10
Max UD/EW (g)	1.528
Per Max UD/EW (s)	0.10
Max UD/NS (g)	1.939
Per Max UD/NS (s)	0.10

RSA - EW		RSA - NS		MAX(EW, NS)	
PGA =	0.808	PGA =	0.649	PGA =	0.808
Ss =	3.410	Ss =	2.086	Ss =	3.410
S1 =	0.215	S1 =	0.203	S1 =	0.215

EQ	Station
Tohoku 9.0	TCGH13

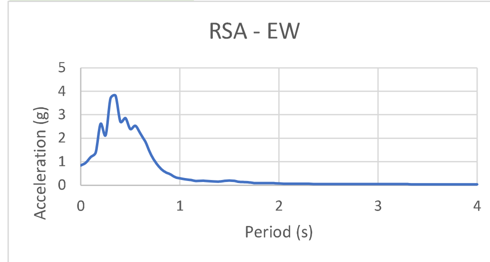

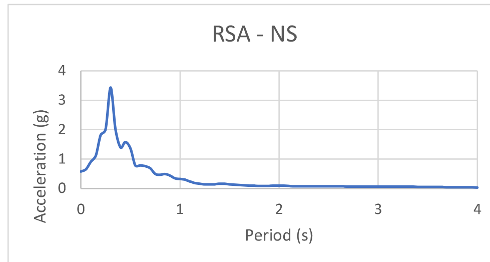

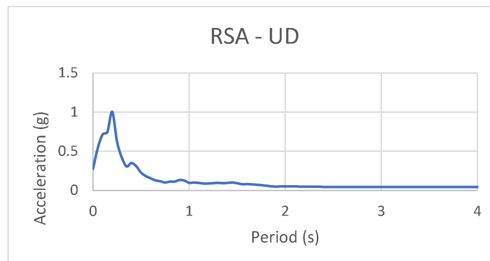

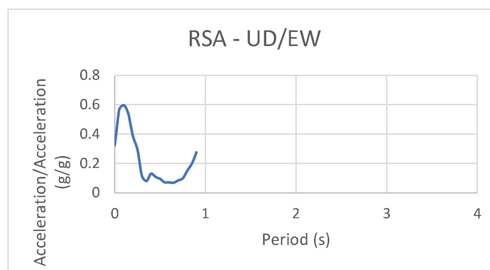

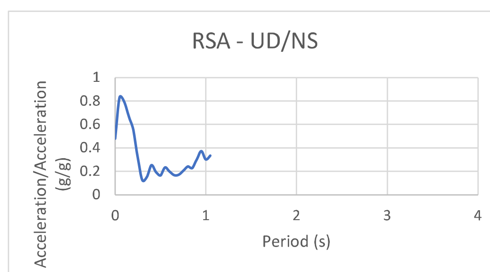

Max UD (g)	1.004
Per Max UD (s)	0.20
Max UD/EW (g)	0.597
Per Max UD/EW (s)	0.10
Max UD/NS (g)	0.833
Per Max UD/NS (s)	0.05

RSA - EW		RSA - NS		MAX(EW, NS)	
PGA =	0.844	PGA =	0.572	PGA =	0.844
Ss =	2.606	Ss =	1.820	Ss =	2.606
S1 =	0.296	S1 =	0.319	S1 =	0.319

EQ	Station
Miyagi 7.1	MYG012

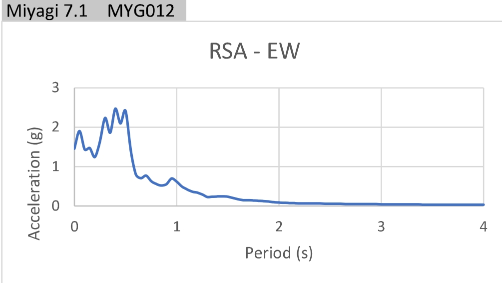

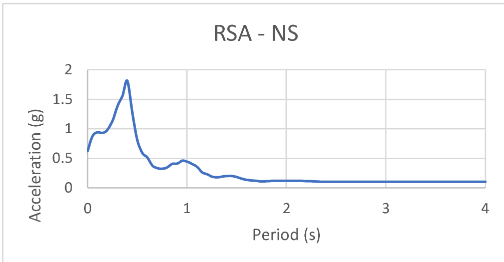

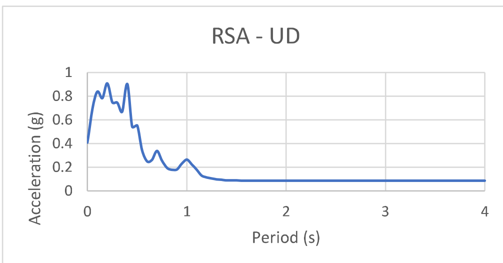

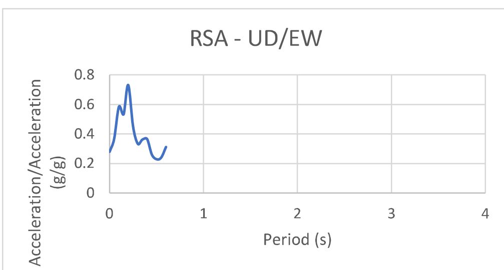

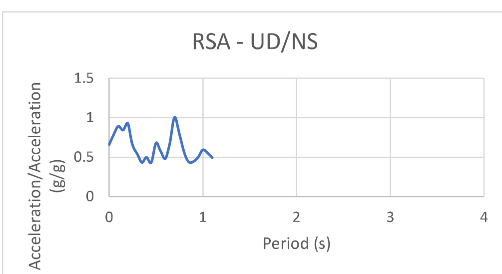

Max UD (g)	0.910
Per Max UD (s)	0.20
Max UD/EW (g)	0.731
Per Max UD/EW (s)	0.20
Max UD/NS (g)	1.004
Per Max UD/NS (s)	0.70

RSA - EW		RSA - NS		MAX(EW, NS)	
PGA =	1.457	PGA =	0.622	PGA =	1.457
Ss =	1.244	Ss =	0.983	Ss =	1.244
S1 =	0.620	S1 =	0.445	S1 =	0.620

EQ	Station
Tohoku 9.0	MYG012

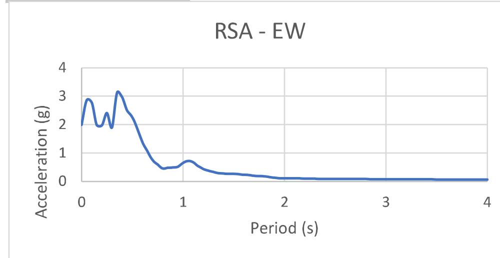

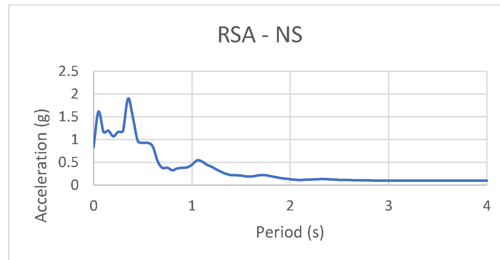

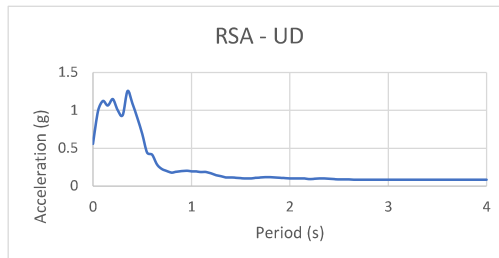

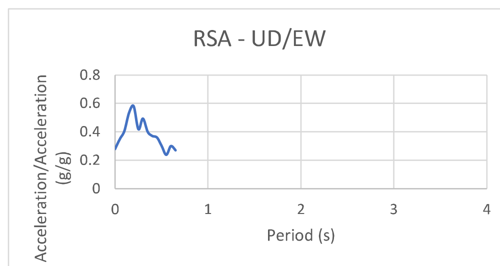

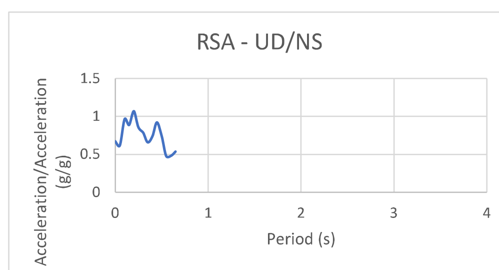

Max UD (g)	1.255
Per Max UD (s)	0.35
Max UD/EW (g)	0.582
Per Max UD/EW (s)	0.20
Max UD/NS (g)	1.068
Per Max UD/NS (s)	0.20

RSA - EW		RSA - NS		MAX(EW, NS)	
PGA =	1.986	PGA =	0.830	PGA =	1.986
Ss =	1.970	Ss =	1.074	Ss =	1.970
S1 =	0.649	S1 =	0.448	S1 =	0.649

APPENDIX B:

NON-BASIN M9 CSZ RSA DATA

Site: Seattle 1

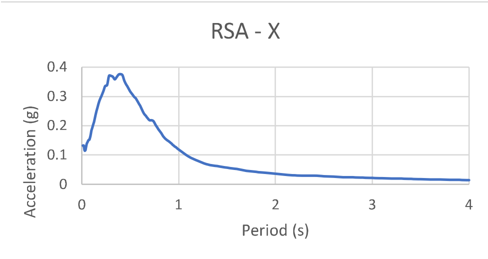

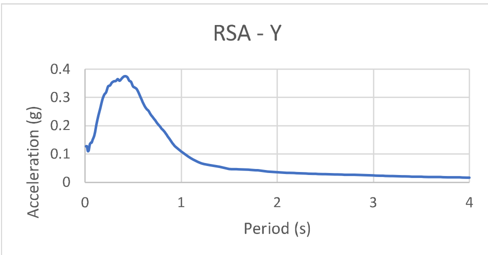

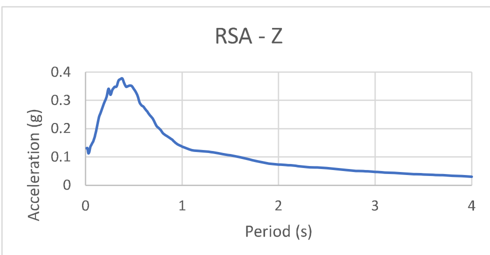

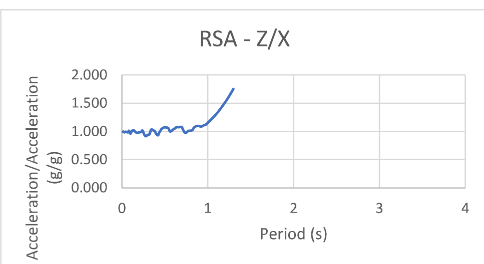

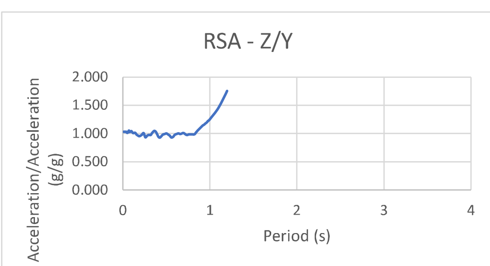

Max UD (g)	0.37778
Per Max UD (s)	0.38
Max UD/EW (g)	1.750
Per Max UD/EW (s)	1.30
Max UD/NS (g)	1.755
Per Max UD/NS (s)	1.20

RSA - X		RSA - Y		MAX(X, Y)	
PGA =	0.132	PGA =	0.127	PGA =	0.132
Ss =	0.301	Ss =	0.310	Ss =	0.310
S1 =	0.119	S1 =	0.110	S1 =	0.119

Site: Portland 1

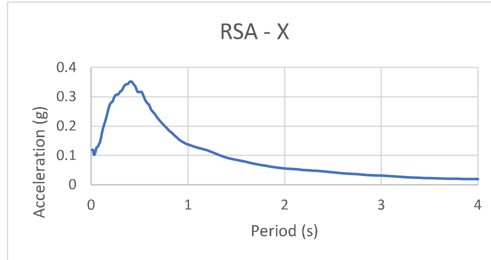

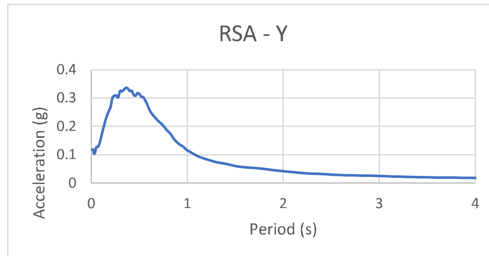

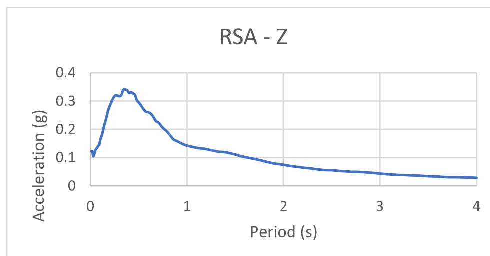

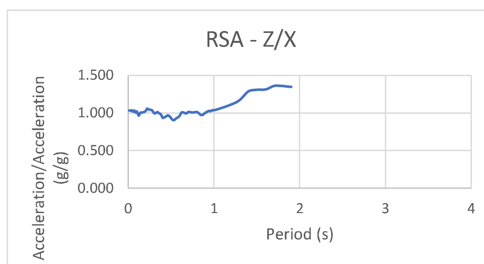

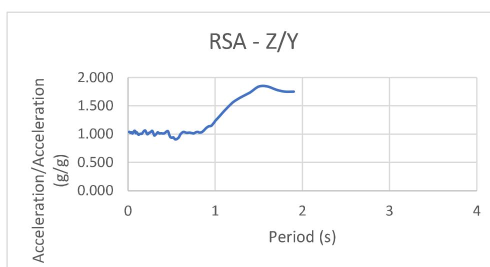

Max UD (g)	0.340197
Per Max UD (s)	0.36
Max UD/EW (g)	1.358
Per Max UD/EW (s)	1.70
Max UD/NS (g)	1.843
Per Max UD/NS (s)	1.60

RSA - X		RSA - Y		MAX(X, Y)	
PGA =	0.119	PGA =	0.118	PGA =	0.119
Ss =	0.278	Ss =	0.268	Ss =	0.278
S1 =	0.137	S1 =	0.116	S1 =	0.137

Station: Medford 1

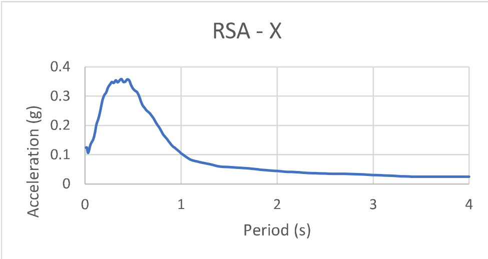

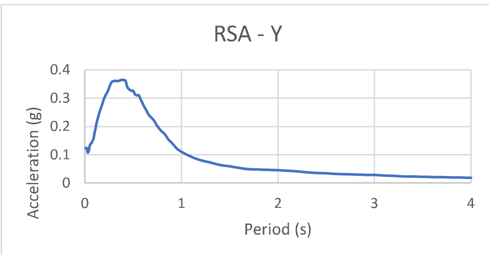

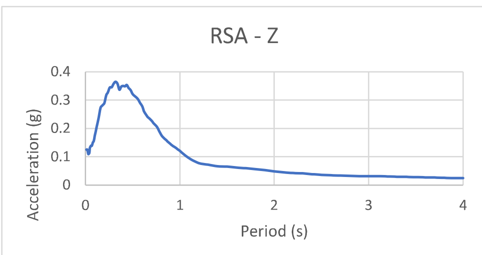

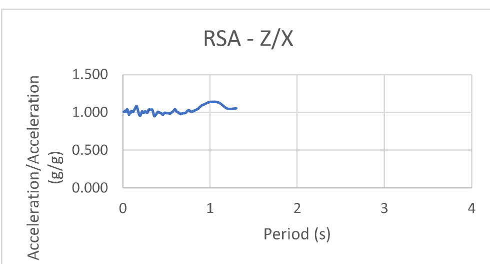

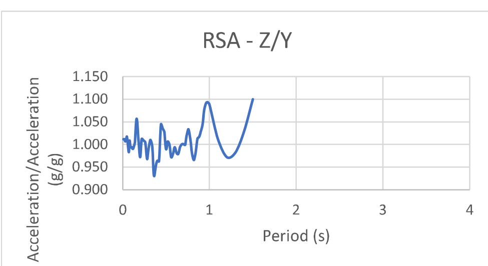

Max UD (g)	0.365323
Per Max UD (s)	0.32
Max UD/EW (g)	1.140
Per Max UD/EW (s)	1.00
Max UD/NS (g)	1.100
Per Max UD/NS (s)	1.50

RSA - X		RSA - Y		MAX(X, Y)	
PGA =	0.124	PGA =	0.123	PGA =	0.124
Ss =	0.303	Ss =	0.298	Ss =	0.303
S1 =	0.105	S1 =	0.110	S1 =	0.110

Station: Seattle 2

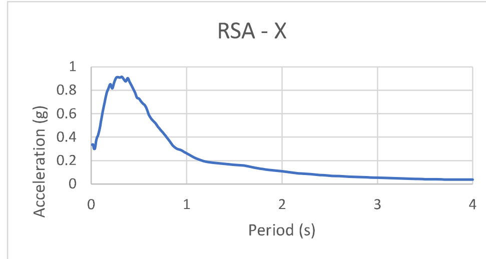

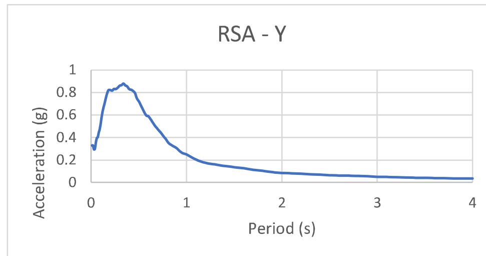

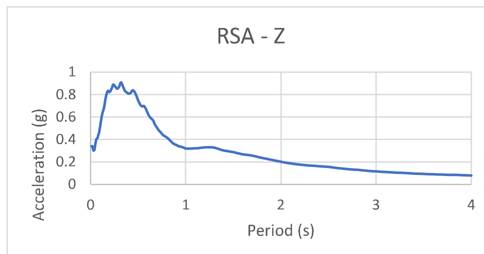

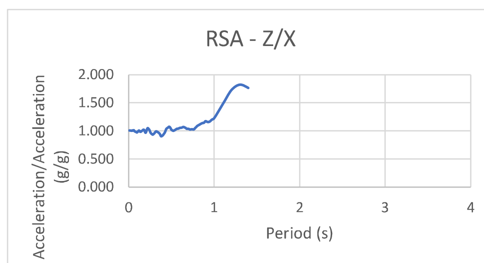

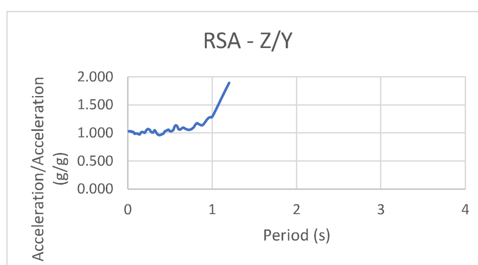

Max UD (g)	0.908856
Per Max UD (s)	0.32
Max UD/EW (g)	1.824
Per Max UD/EW (s)	1.30
Max UD/NS (g)	1.893
Per Max UD/NS (s)	1.20

RSA - X		RSA - Y		MAX(X, Y)	
PGA =	0.337	PGA =	0.329	PGA =	0.337
Ss =	0.851	Ss =	0.821	Ss =	0.851
S1 =	0.262	S1 =	0.249	S1 =	0.262

Station: Portland 2

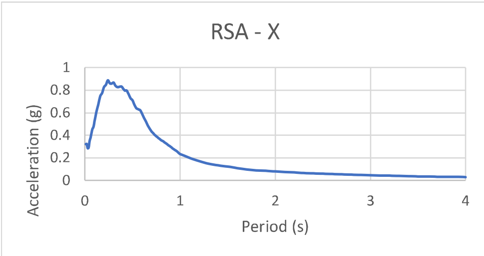

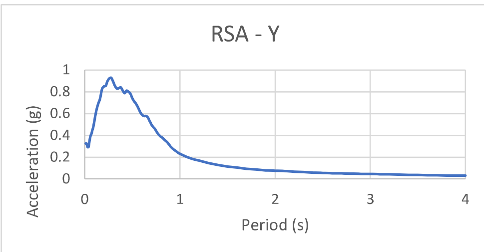

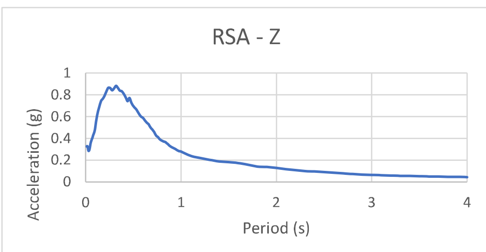

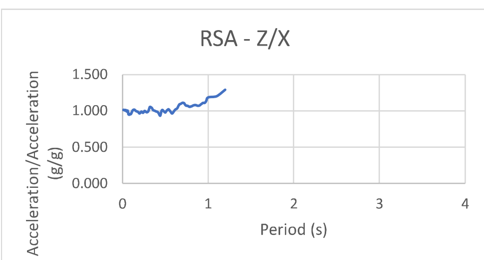

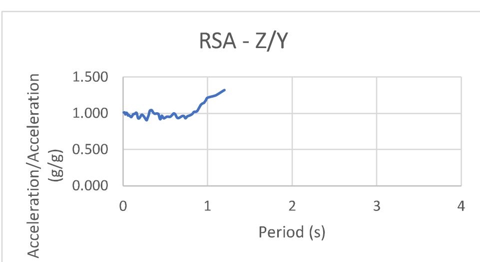

Max UD (g)	0.881793
Per Max UD (s)	0.32
Max UD/EW (g)	1.292
Per Max UD/EW (s)	1.20
Max UD/NS (g)	1.321
Per Max UD/NS (s)	1.20

RSA - X		RSA - Y		MAX(X, Y)	
PGA =	0.322	PGA =	0.324	PGA =	0.324
Ss =	0.828	Ss =	0.848	Ss =	0.848
S1 =	0.235	S1 =	0.230	S1 =	0.235

Station: Medford 2

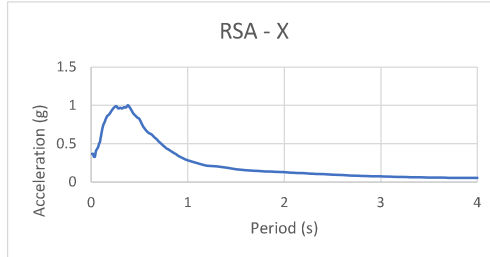

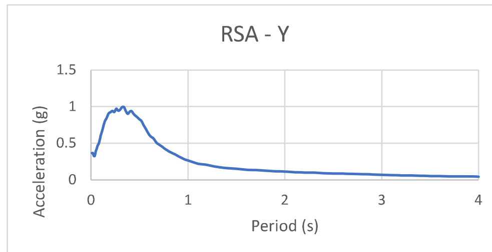

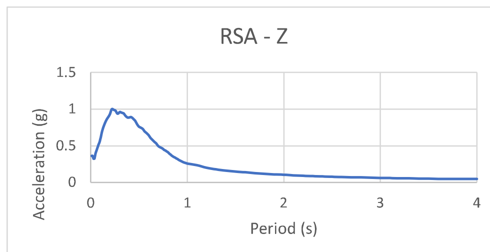

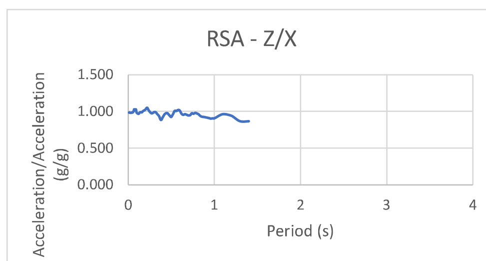

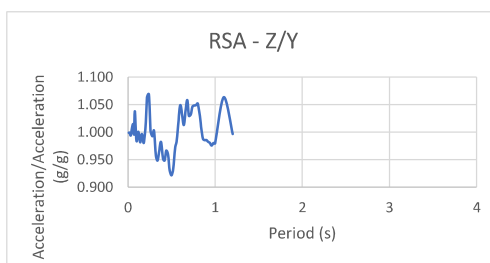

Max UD (g)	0.998091
Per Max UD (s)	0.22
Max UD/EW (g)	1.052
Per Max UD/EW (s)	0.22
Max UD/NS (g)	1.069
Per Max UD/NS (s)	0.24

RSA - X		RSA - Y		MAX(X, Y)	
PGA =	0.367	PGA =	0.363	PGA =	0.367
Ss =	0.910	Ss =	0.925	Ss =	0.925
S1 =	0.285	S1 =	0.264	S1 =	0.285

Station: Seattle 3

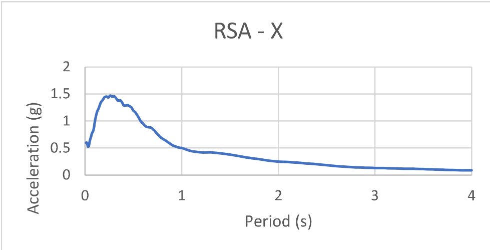

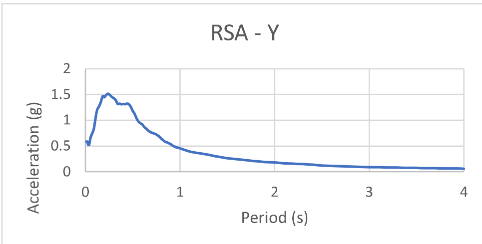

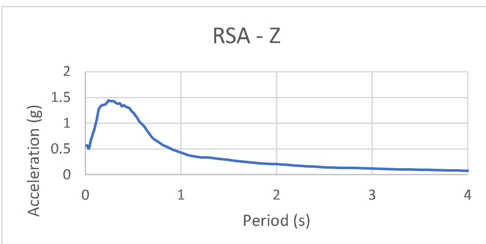

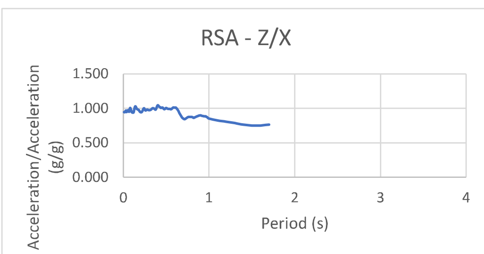

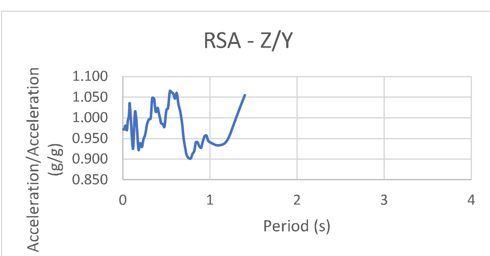

Max UD (g)	1.438564
Per Max UD (s)	0.24

Max UD/EW (g)	1.045
Per Max UD/EW (s)	0.40

Max UD/NS (g)	1.065
Per Max UD/NS (s)	0.54

RSA - X		RSA - Y		MAX(X, Y)	
PGA =	0.598	PGA =	0.582	PGA =	0.598
Ss =	1.438	Ss =	1.447	Ss =	1.447
S1 =	0.501	S1 =	0.454	S1 =	0.501

Station: Portland 3

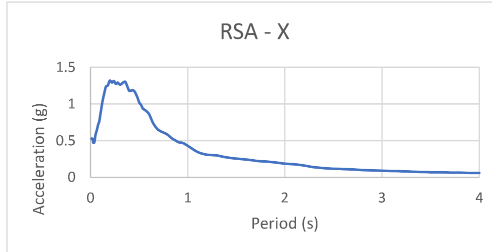

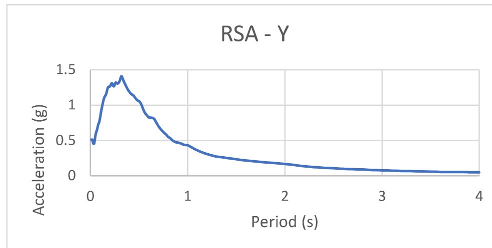

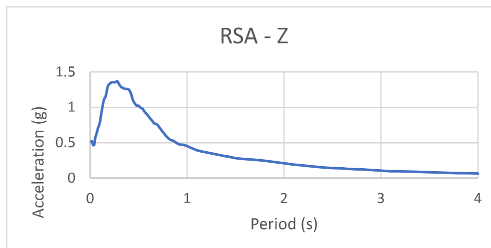

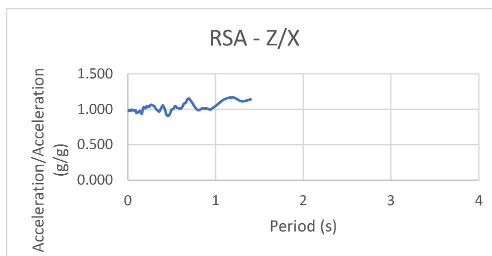

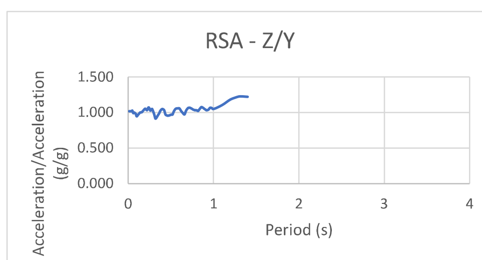

Max UD (g)	1.369607
Per Max UD (s)	0.28

Max UD/EW (g)	1.170
Per Max UD/EW (s)	1.20

Max UD/NS (g)	1.225
Per Max UD/NS (s)	1.30

RSA - X		RSA - Y		MAX(X, Y)	
PGA =	0.528	PGA =	0.508	PGA =	0.528
Ss =	1.318	Ss =	1.264	Ss =	1.318
S1 =	0.433	S1 =	0.432	S1 =	0.433

Station: Medford 3

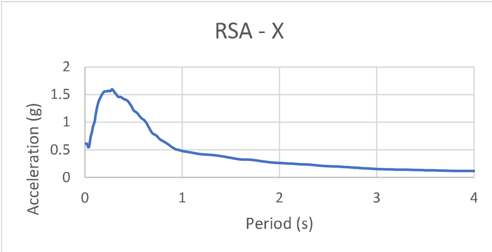

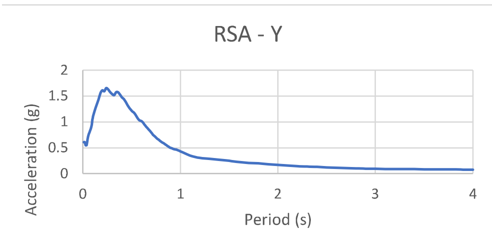

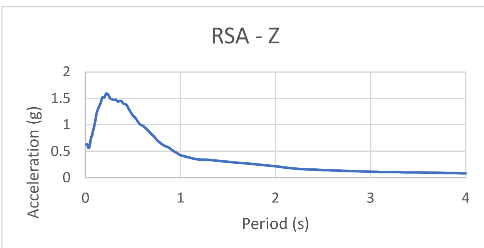

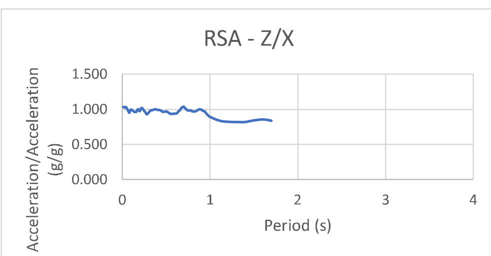

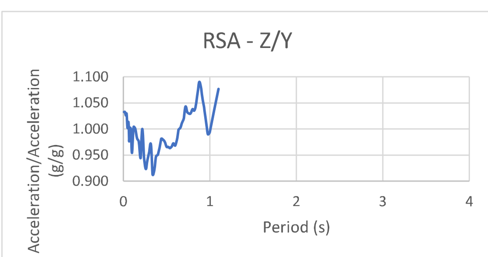

Max UD (g)	1.591482
Per Max UD (s)	0.22

Max UD/EW (g)	1.037
Per Max UD/EW (s)	0.70

Max UD/NS (g)	1.090
Per Max UD/NS (s)	0.88

RSA - X		RSA - Y		MAX(X, Y)	
PGA =	0.609	PGA =	0.609	PGA =	0.609
Ss =	1.558	Ss =	1.610	Ss =	1.610
S1 =	0.480	S1 =	0.432	S1 =	0.480

APPENDIX C:

BASIN SITES RECORDED RSA DATA
JAPAN & CHILE

Station: NIG024

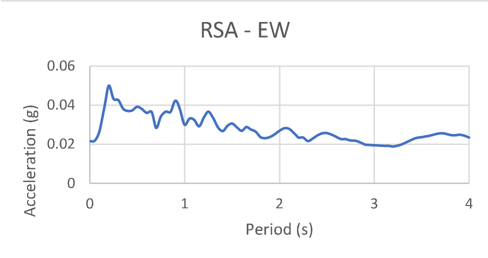

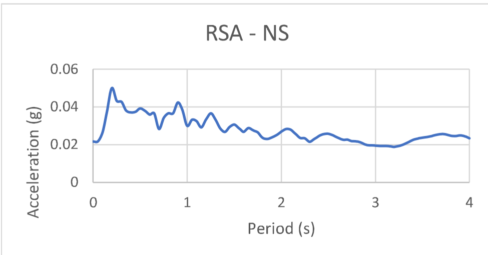

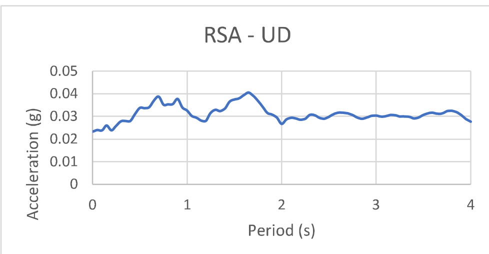

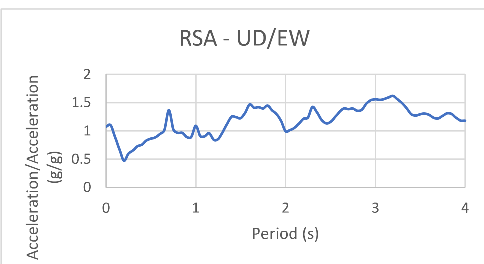

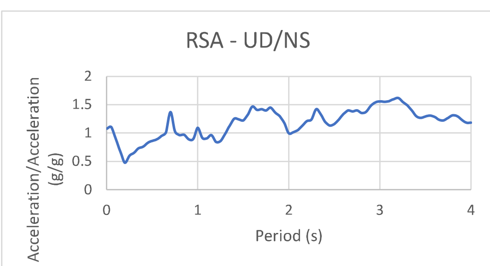

Max UD (g)	0.04055
Per Max UD (s)	1.65
Max UD/EW (g)	1.619
Per Max UD/EW (s)	3.20
Max UD/NS (g)	1.619
Per Max UD/NS (s)	3.20

RSA - EW		RSA - NS		MAX(EW, NS)	
PGA =	0.022	PGA =	0.022	PGA =	0.022
Ss =	0.050	Ss =	0.050	Ss =	0.050
S1 =	0.030	S1 =	0.030	S1 =	0.030

Station: NIG026

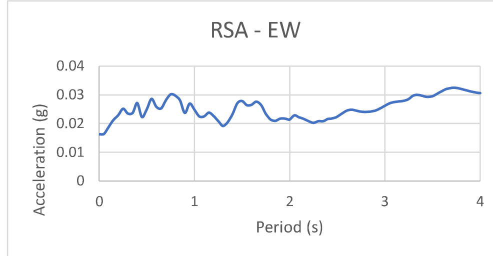

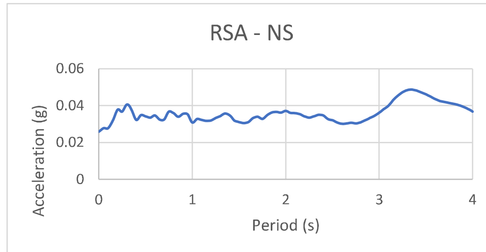

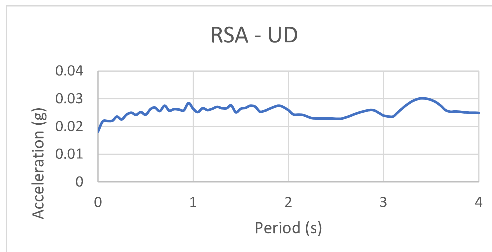

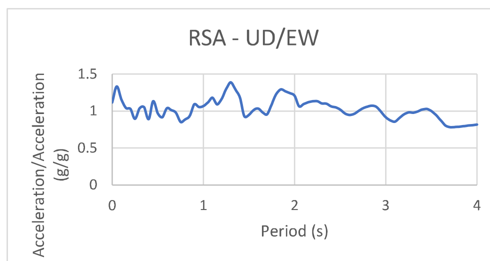

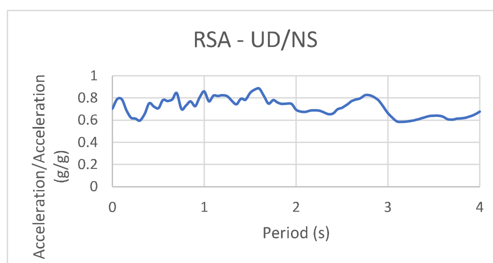

Max UD (g)	0.03016
Per Max UD (s)	3.40
Max UD/EW (g)	1.390
Per Max UD/EW (s)	1.30
Max UD/NS (g)	0.884
Per Max UD/NS (s)	1.60

RSA - EW		RSA - NS		MAX(EW, NS)	
PGA =	0.016	PGA =	0.026	PGA =	0.026
Ss =	0.023	Ss =	0.038	Ss =	0.038
S1 =	0.025	S1 =	0.031	S1 =	0.031

Station: NIG016

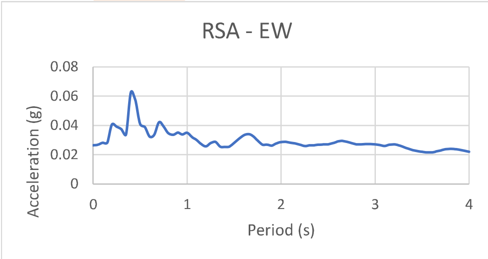

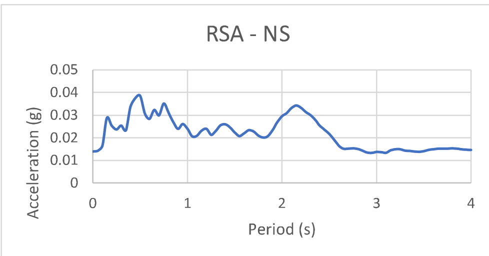

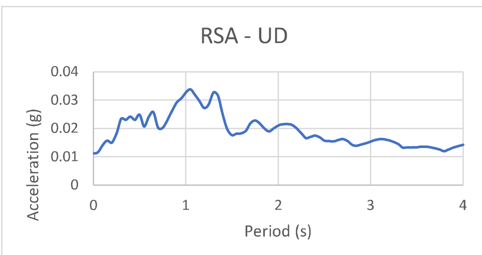

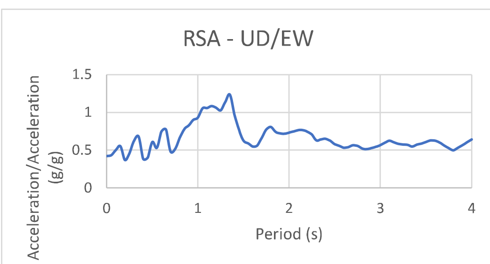

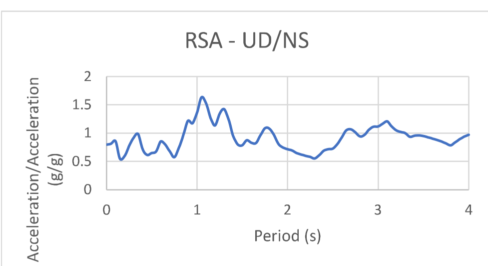

Max UD (g)	0.03382
Per Max UD (s)	1.05
Max UD/EW (g)	1.236
Per Max UD/EW (s)	1.35
Max UD/NS (g)	1.631
Per Max UD/NS (s)	1.05

RSA - EW		RSA - NS		MAX(EW, NS)	
PGA =	0.026	PGA =	0.014	PGA =	0.026
Ss =	0.041	Ss =	0.025	Ss =	0.041
S1 =	0.035	S1 =	0.024	S1 =	0.035

Station: NIG013

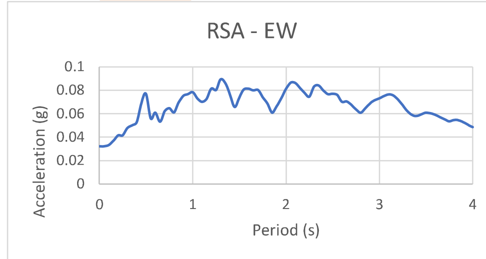

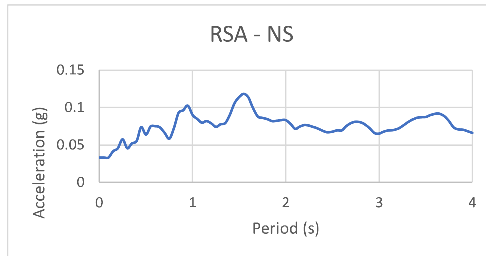

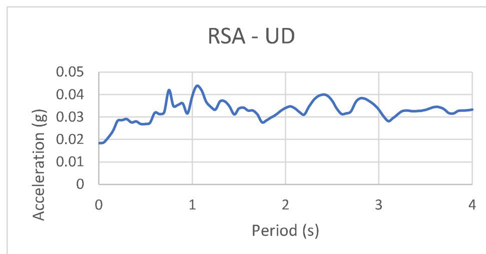

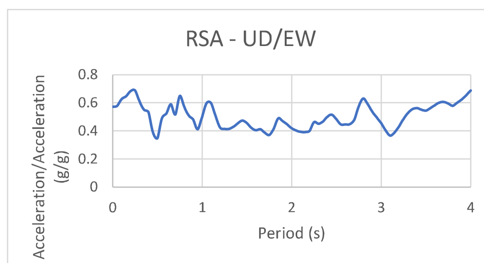

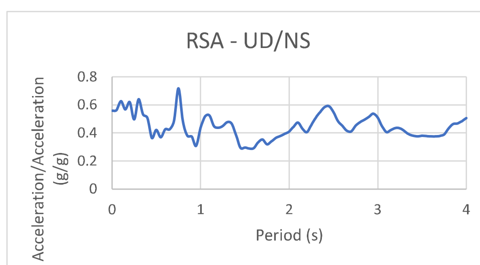

Max UD (g)	0.04381
Per Max UD (s)	1.05
Max UD/EW (g)	0.689
Per Max UD/EW (s)	4.00
Max UD/NS (g)	0.718
Per Max UD/NS (s)	0.75

RSA - EW		RSA - NS		MAX(EW, NS)	
PGA =	0.032	PGA =	0.033	PGA =	0.033
Ss =	0.041	Ss =	0.045	Ss =	0.045
S1 =	0.078	S1 =	0.090	S1 =	0.090

Station: NIG010

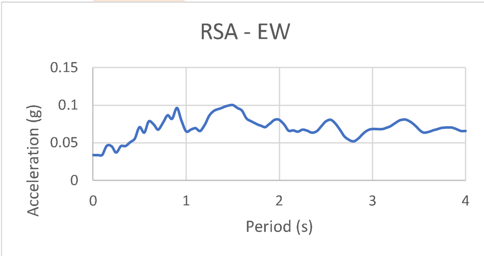

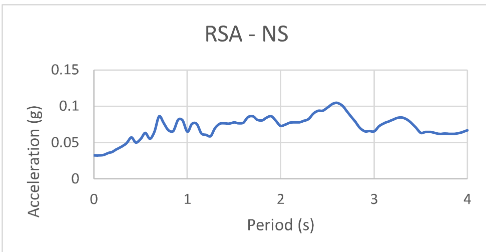

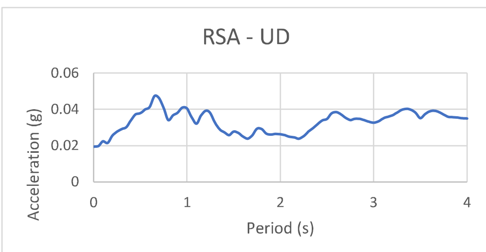

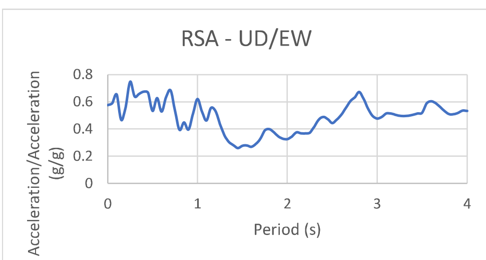

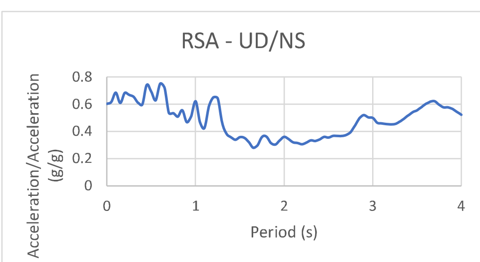

Max UD (g)	0.04732
Per Max UD (s)	0.65
Max UD/EW (g)	0.748
Per Max UD/EW (s)	0.25
Max UD/NS (g)	0.751
Per Max UD/NS (s)	0.60

RSA - EW		RSA - NS		MAX(EW, NS)	
PGA =	0.034	PGA =	0.032	PGA =	0.034
Ss =	0.045	Ss =	0.037	Ss =	0.045
S1 =	0.065	S1 =	0.065	S1 =	0.065

Station: NIG025

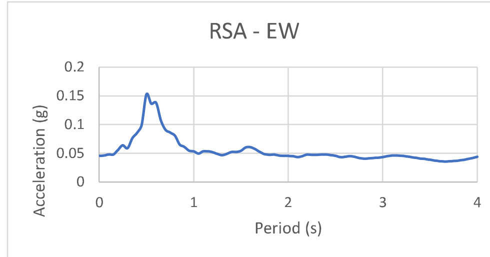

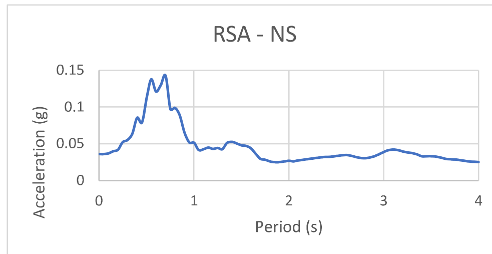

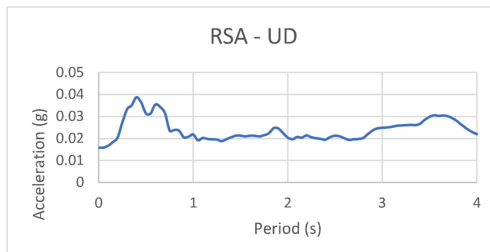

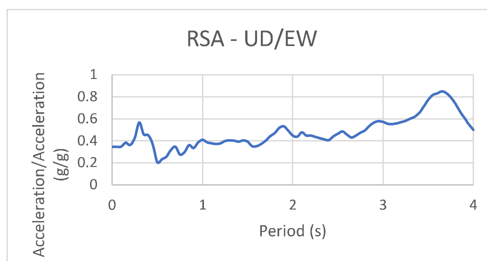

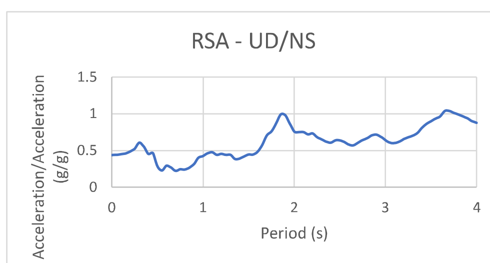

Max UD (g)	0.03871
Per Max UD (s)	0.40
Max UD/EW (g)	0.850
Per Max UD/EW (s)	3.65
Max UD/NS (g)	1.040
Per Max UD/NS (s)	3.70

RSA - EW		RSA - NS		MAX(EW, NS)	
PGA =	0.046	PGA =	0.036	PGA =	0.046
Ss =	0.056	Ss =	0.042	Ss =	0.056
S1 =	0.053	S1 =	0.051	S1 =	0.053

Station: CHB026

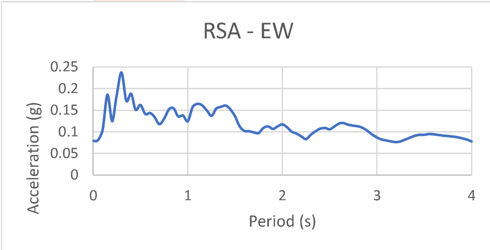

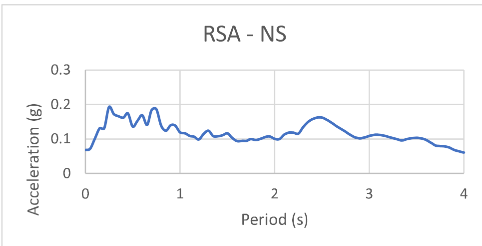

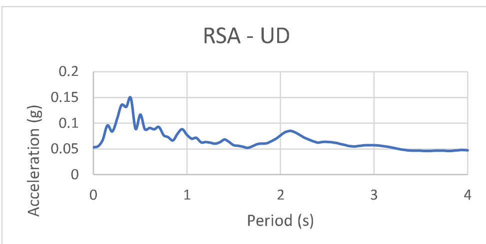

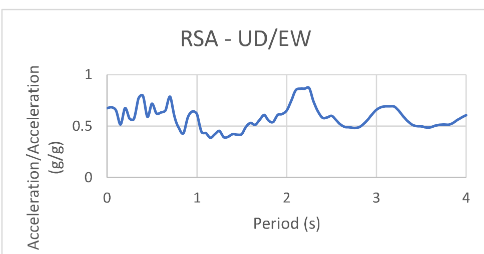

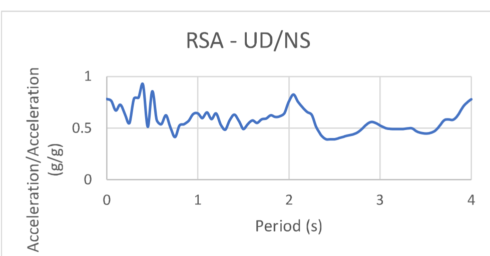

Max UD (g)	0.14914
Per Max UD (s)	0.40
Max UD/EW (g)	0.869
Per Max UD/EW (s)	2.25
Max UD/NS (g)	0.923
Per Max UD/NS (s)	0.40

RSA - EW		RSA - NS		MAX(EW, NS)	
PGA =	0.079	PGA =	0.068	PGA =	0.079
Ss =	0.124	Ss =	0.131	Ss =	0.131
S1 =	0.125	S1 =	0.120	S1 =	0.125

Station: CHB013

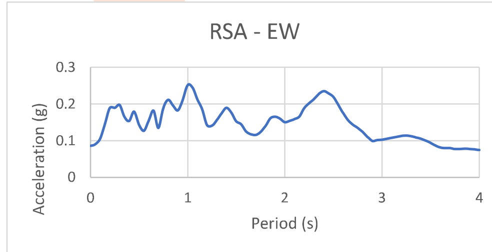

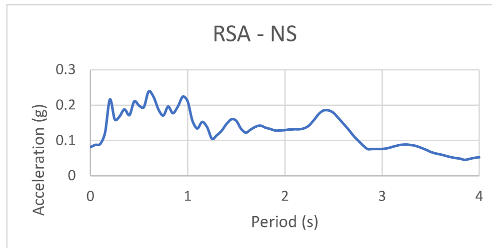

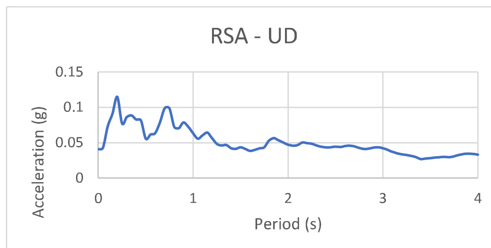

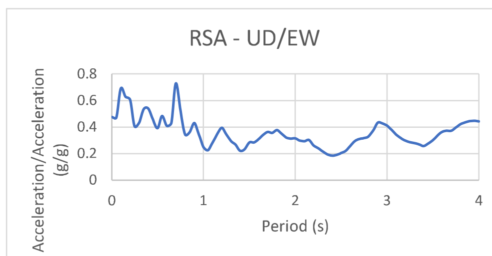

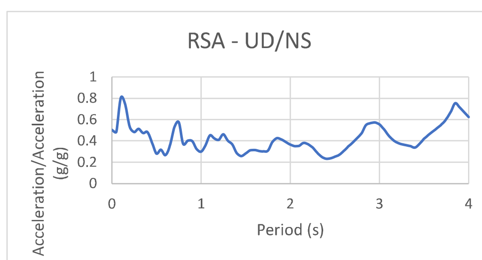

Max UD (g)	0.1149
Per Max UD (s)	0.20
Max UD/EW (g)	0.728
Per Max UD/EW (s)	0.70
Max UD/NS (g)	0.806
Per Max UD/NS (s)	0.10

RSA - EW		RSA - NS		MAX(EW, NS)	
PGA =	0.086	PGA =	0.081	PGA =	0.086
Ss =	0.189	Ss =	0.216	Ss =	0.216
S1 =	0.252	S1 =	0.210	S1 =	0.252

Station: CHB017

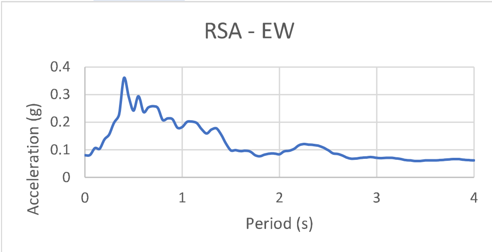

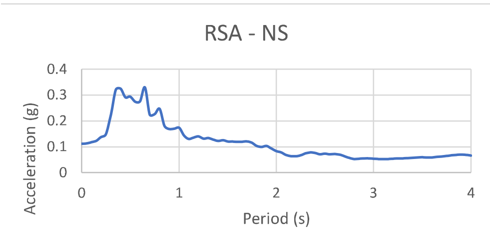

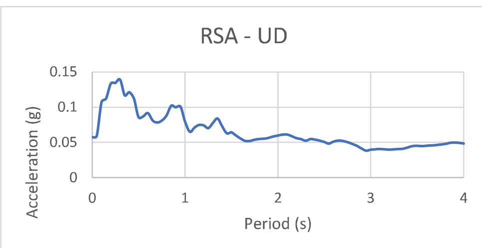

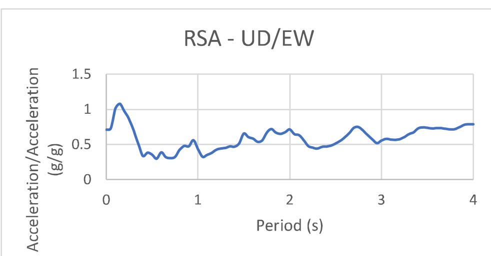

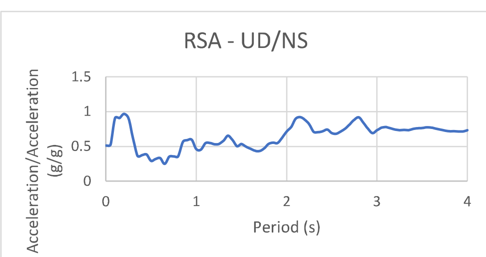

Max UD (g)	0.1391
Per Max UD (s)	0.30
Max UD/EW (g)	1.078
Per Max UD/EW (s)	0.15
Max UD/NS (g)	0.970
Per Max UD/NS (s)	0.20

RSA - EW		RSA - NS		MAX(EW, NS)	
PGA =	0.081	PGA =	0.112	PGA =	0.112
Ss =	0.138	Ss =	0.138	Ss =	0.138
S1 =	0.182	S1 =	0.174	S1 =	0.182

Station: CHBH10

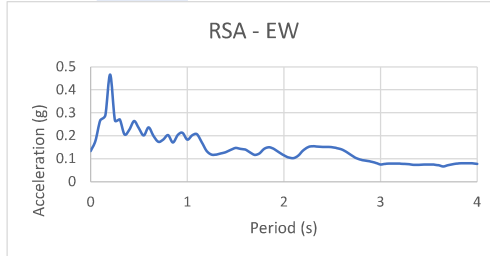

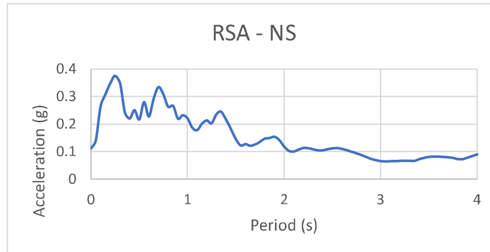

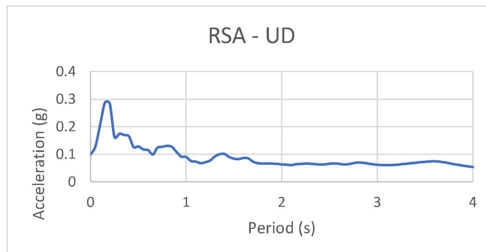

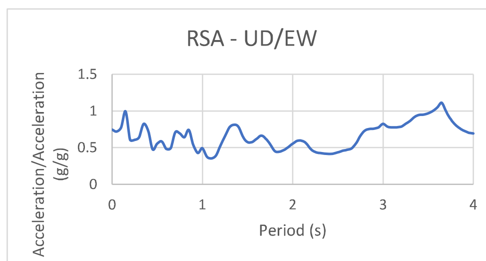

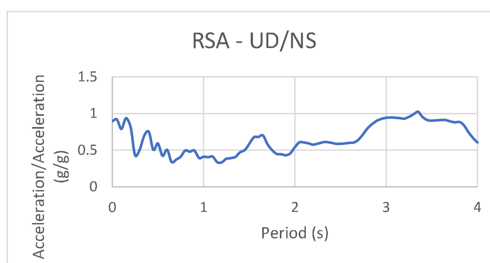

Max UD (g)	0.28829
Per Max UD (s)	0.15
Max UD/EW (g)	0.997
Per Max UD/EW (s)	0.15
Max UD/NS (g)	0.938
Per Max UD/NS (s)	0.15

RSA - EW		RSA - NS		MAX(EW, NS)	
PGA =	0.133	PGA =	0.111	PGA =	0.133
Ss =	0.467	Ss =	0.347	Ss =	0.467
S1 =	0.183	S1 =	0.220	S1 =	0.220

Station: CHB015

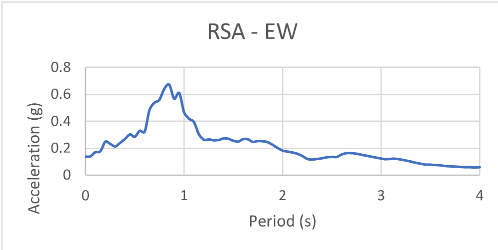

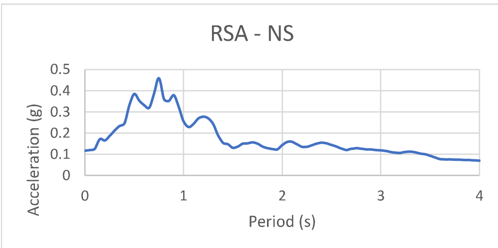

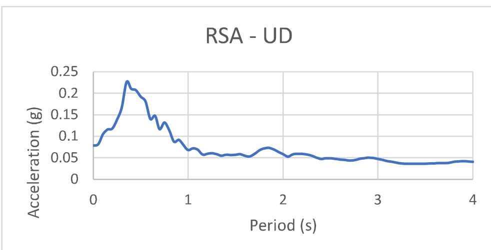

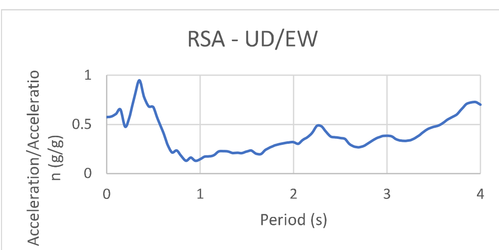

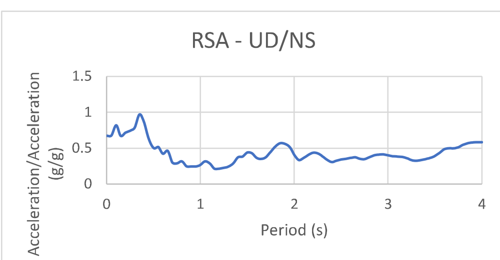

Max UD (g)	0.22631
Per Max UD (s)	0.35
Max UD/EW (g)	0.947
Per Max UD/EW (s)	0.35
Max UD/NS (g)	0.971
Per Max UD/NS (s)	0.35

RSA - EW		RSA - NS		MAX(EW, NS)	
PGA =	0.137	PGA =	0.117	PGA =	0.137
Ss =	0.247	Ss =	0.165	Ss =	0.247
S1 =	0.468	S1 =	0.256	S1 =	0.468

Station: TKY007

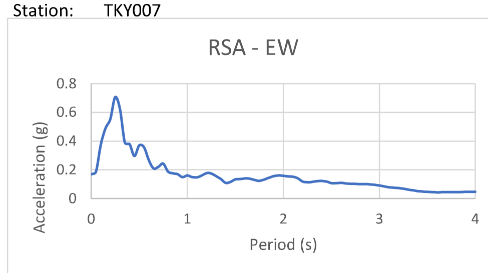

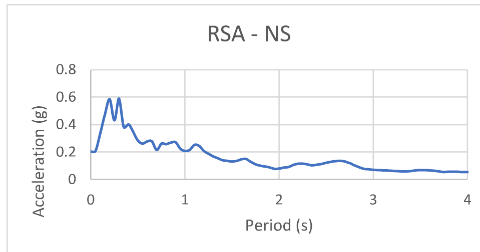

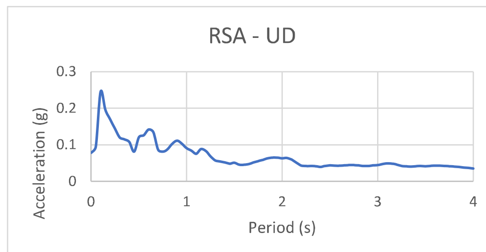

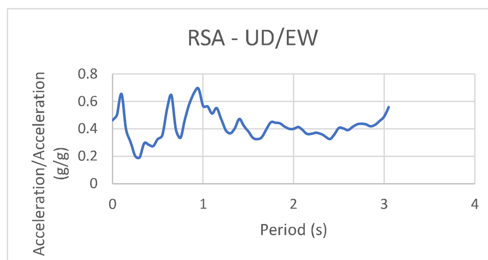

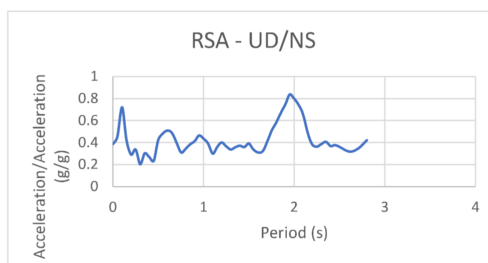

Max UD (g)	0.24445
Per Max UD (s)	0.10
Max UD/EW (g)	0.694
Per Max UD/EW (s)	0.95
Max UD/NS (g)	0.836
Per Max UD/NS (s)	1.95

RSA - EW		RSA - NS		MAX(EW, NS)	
PGA =	0.169	PGA =	0.202	PGA =	####
Ss =	0.556	Ss =	0.584	Ss =	####
S1 =	0.161	S1 =	0.209	S1 =	####

Station: CHB012

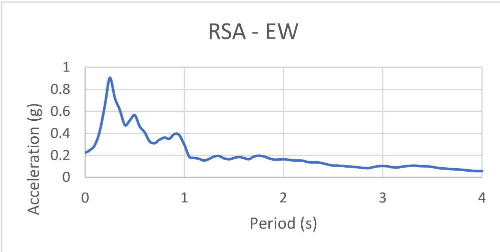

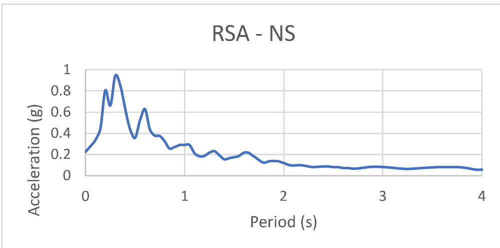

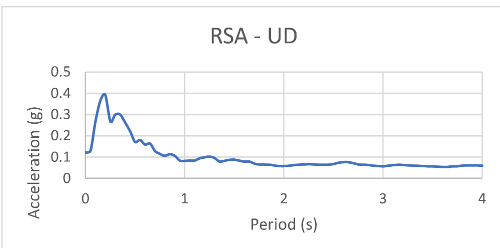

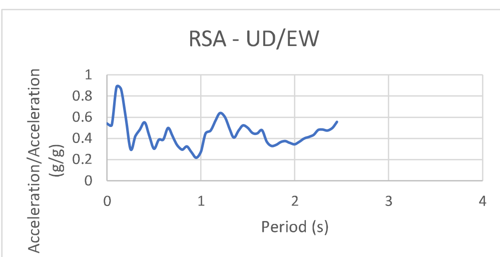

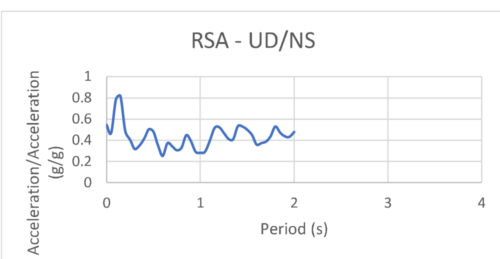

Max UD (g)	0.39229
Per Max UD (s)	0.20

Max UD/EW (g)	0.887
Per Max UD/EW (s)	0.10

Max UD/NS (g)	0.815
Per Max UD/NS (s)	0.15

RSA - EW		RSA - NS		MAX(EW, NS)	
PGA =	0.223	PGA =	0.223	PGA =	0.223
Ss =	0.662	Ss =	0.804	Ss =	0.804
S1 =	0.295	S1 =	0.291	S1 =	0.295

APPENDIX D:

BASIN SITE M9 CSZ RSA DATA

Site: Seattle 1

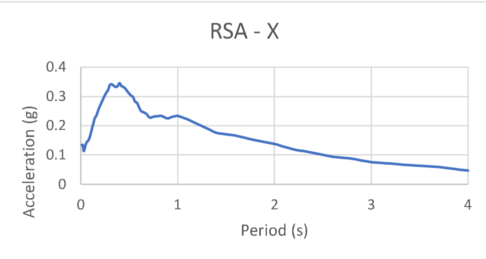

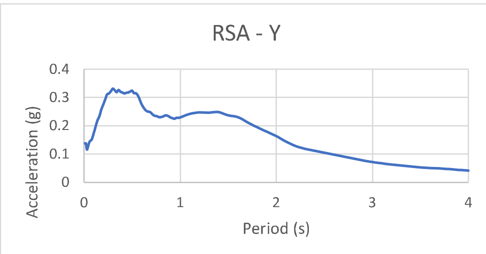

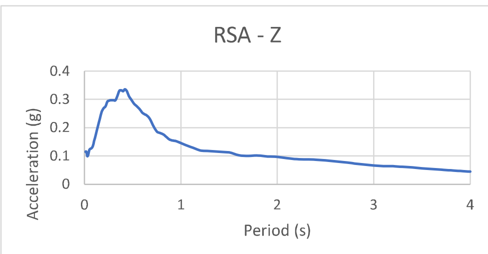

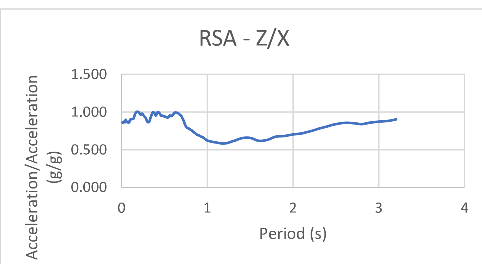

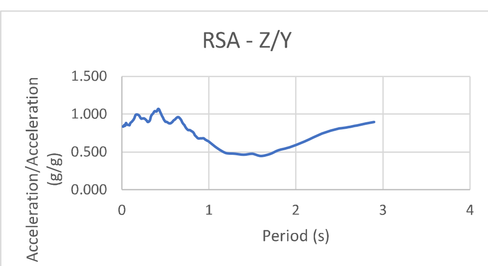

Max UD (g)	0.33612
Per Max UD (s)	0.42
Max UD/EW (g)	1.004
Per Max UD/EW (s)	0.18
Max UD/NS (g)	1.069
Per Max UD/NS (s)	0.42

RSA - X		RSA - Y		MAX(X, Y)	
PGA =	0.134	PGA =	0.138	PGA =	0.138
Ss =	0.270	Ss =	0.275	Ss =	0.275
S1 =	0.234	S1 =	0.229	S1 =	0.234

Site: Seattle 2

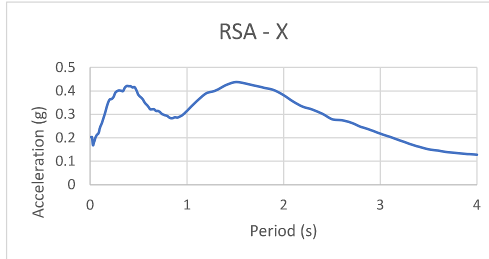

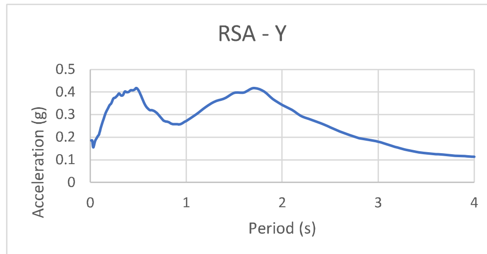

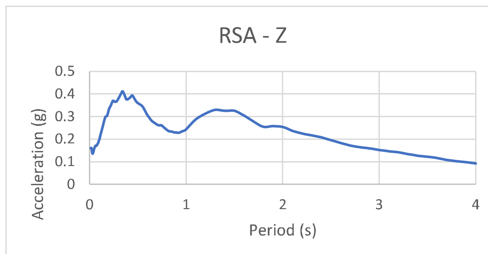

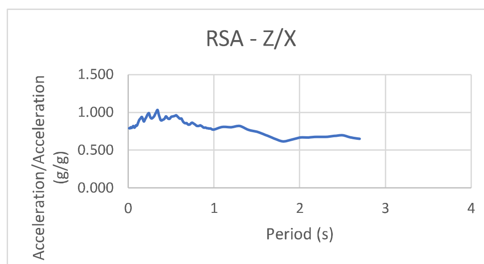

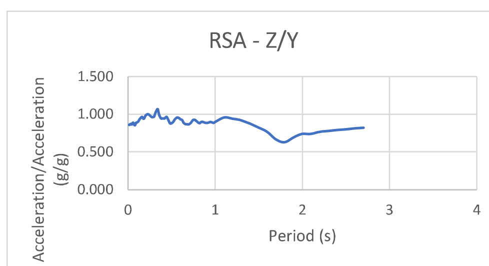

Max UD (g)	0.411615
Per Max UD (s)	0.34
Max UD/EW (g)	1.031
Per Max UD/EW (s)	0.34
Max UD/NS (g)	1.067
Per Max UD/NS (s)	0.34

RSA - X		RSA - Y		MAX(X, Y)	
PGA =	0.202	PGA =	0.185	PGA =	0.202
Ss =	0.363	Ss =	0.340	Ss =	0.363
S1 =	0.315	S1 =	0.272	S1 =	0.315

Station: Seattle 3

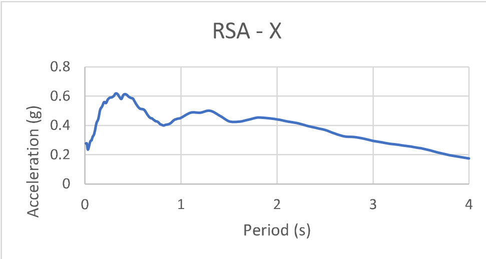

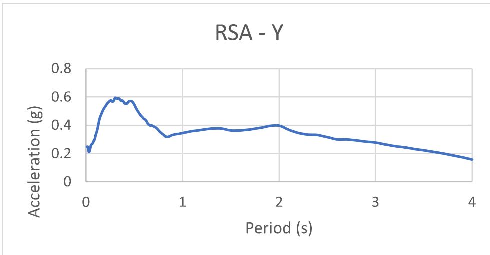

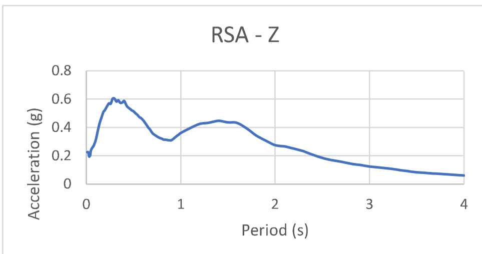

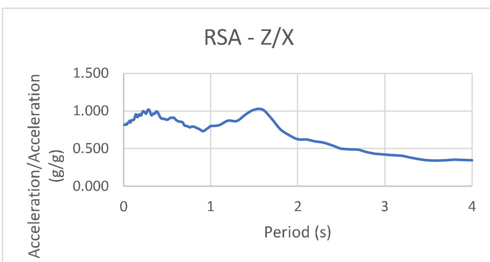

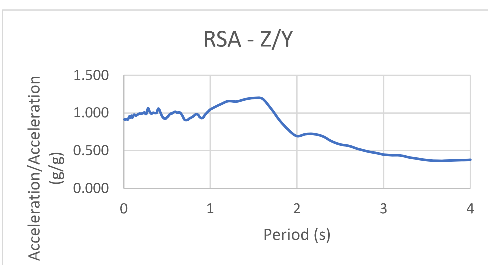

Max UD (g)	0.60377
Per Max UD (s)	0.30
Max UD/EW (g)	1.017
Per Max UD/EW (s)	0.28
Max UD/NS (g)	1.200
Per Max UD/NS (s)	1.50

RSA - X		RSA - Y		MAX(X, Y)	
PGA =	0.276	PGA =	0.247	PGA =	0.276
Ss =	0.560	Ss =	0.530	Ss =	0.560
S1 =	0.451	S1 =	0.344	S1 =	0.451

Station: Portland 1

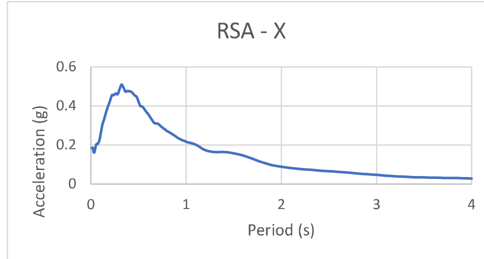

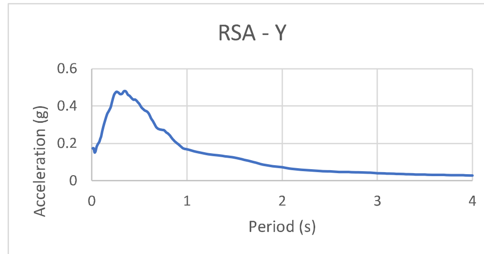

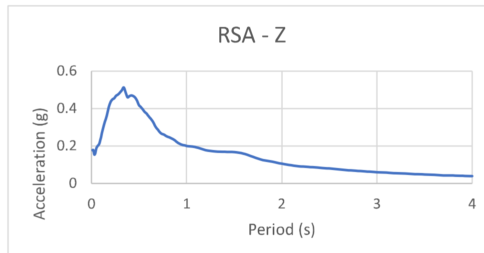

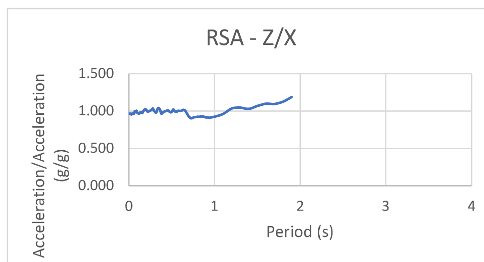

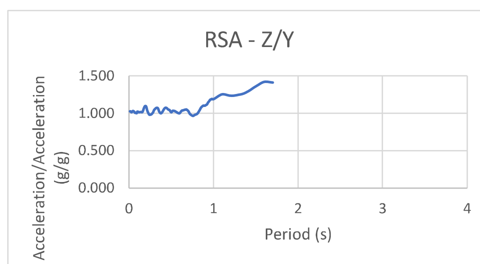

Max UD (g)	0.512885
Per Max UD (s)	0.34
Max UD/EW (g)	1.187
Per Max UD/EW (s)	1.90
Max UD/NS (g)	1.418
Per Max UD/NS (s)	1.60

RSA - X		RSA - Y		MAX(X, Y)	
PGA =	0.185	PGA =	0.174	PGA =	0.185
Ss =	0.426	Ss =	0.398	Ss =	0.426
S1 =	0.217	S1 =	0.169	S1 =	0.217

Station: Portland 2

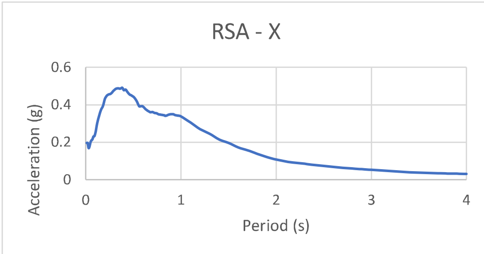

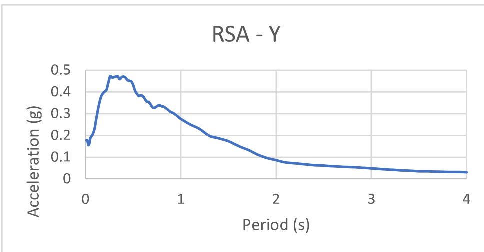

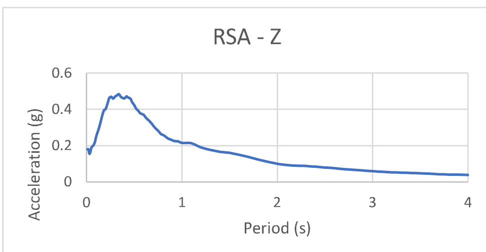

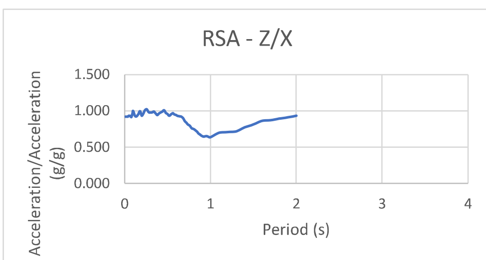

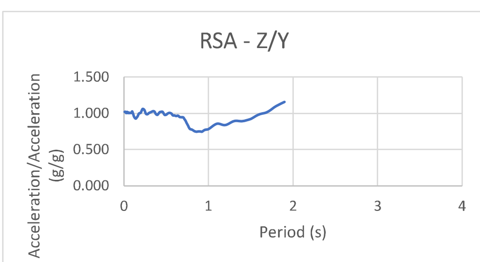

Max UD (g)	0.483944
Per Max UD (s)	0.34
Max UD/EW (g)	1.023
Per Max UD/EW (s)	0.26
Max UD/NS (g)	1.157
Per Max UD/NS (s)	1.90

RSA - X		RSA - Y		MAX(X, Y)	
PGA =	0.196	PGA =	0.177	PGA =	0.196
Ss =	0.431	Ss =	0.401	Ss =	0.431
S1 =	0.338	S1 =	0.275	S1 =	0.338

Station: Portland 3

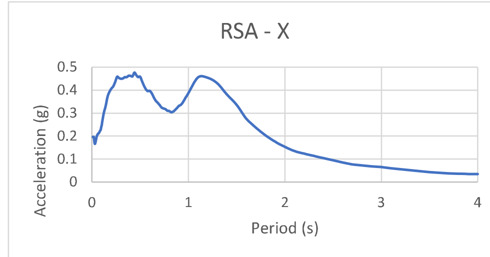

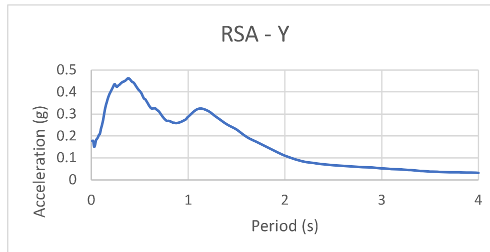

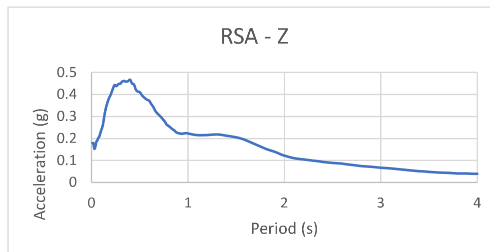

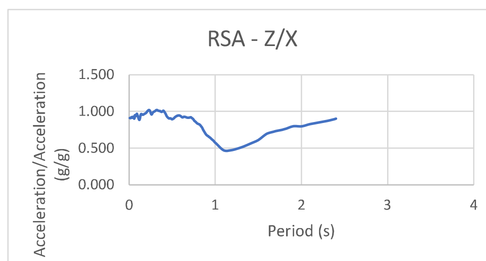

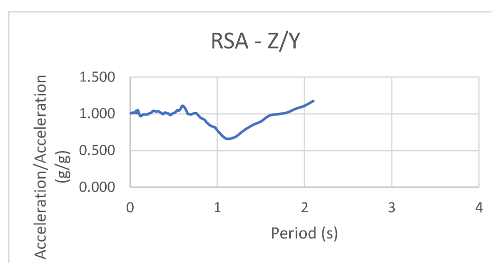

Max UD (g)	0.466228
Per Max UD (s)	0.40
Max UD/EW (g)	1.021
Per Max UD/EW (s)	0.32
Max UD/NS (g)	1.174
Per Max UD/NS (s)	2.10

RSA - X		RSA - Y		MAX(X, Y)	
PGA =	0.196	PGA =	0.177	PGA =	0.196
Ss =	0.406	Ss =	0.402	Ss =	0.406
S1 =	0.386	S1 =	0.287	S1 =	0.386